



This work is protected by copyright and other intellectual property rights and duplication or sale of all or part is not permitted, except that material may be duplicated by you for research, private study, criticism/review or educational purposes. Electronic or print copies are for your own personal, non-commercial use and shall not be passed to any other individual. No quotation may be published without proper acknowledgement. For any other use, or to quote extensively from the work, permission must be obtained from the copyright holder/s.

DOUBLE BEAM AMMONIA MASER
OPERATED
WITH AN OPEN RESONATOR

by

ABDUL-RAHMAN M. AL-JUMAILY

B.Sc.

A thesis submitted to the University of Keele
for the Degree of Doctor of Philosophy

Department of Physics
University of Keele
Staffordshire

July 1979

UNIVERSITY
OF KEELE



IMAGING SERVICES NORTH

Boston Spa, Wetherby
West Yorkshire, LS23 7BQ
www.bl.uk

The following has been redacted from this digital copy of the original thesis, at the request of the awarding university:

Appendix 2, pages 86-87

TO: NESSREN

ACKNOWLEDGEMENTS

The author would like to express his grateful thanks to:

Dr. D.C. Lainé for his guidance and enthusiastic encouragement throughout this work.

Dr. D.E. Dugdale for his many helpful discussions.

Professor W. Fuller for the provision of experimental facilities.

Mr. G. Dudley and the technical staff of the Physics Department -

Mr. G. Marsh, Mr. M. Wallace, Mr. E.J.T. Greasley - for the construction of the vacuum chambers and the other maser components, and for their continued assistance throughout the experimental work.

Mr. M.G. Davies and Mr. B.J. Minshull of the Electronics Workshop for their continuous assistance.

Mr. H. Wardell and the staff of the University Workshop for the machining of the cavity mirrors.

Mr. M. Daniels for the preparation of the photographs reproduced in this thesis.

Mr. F. Rowerth and Mr. C.B. Harrison for their invaluable assistance.

Mrs. K.B. Merifield for typing this thesis.

Mr. G. Yassin, Mrs. L. Hope, Dr. D.H.H. Al-Amiedy, and other colleagues in the Physics Department for many useful discussions.

The University of Baghdad and the College of Education for provision of the study leave from 1975-1979.

His parents, brothers Shaker, Abdul-Wahab, and sisters Samera, Fardos Fawzeyi and Makarm for their continuous and sustained assistance over three years.

ABSTRACT

The construction of a double beam ammonia maser employing an open resonator of advanced design is described. The operation of this maser as an oscillator permitted a strong oscillation to be obtained which has led to the observation of several novel phenomena. These include a biharmonic effect with a beat frequency of a few kilohertz which has remained as an unsolved problem since the original observations in 1964; injection priming of a pulsed ammonia-beam maser oscillator and oscillation of the weak ammonia inversion line $J=K=1$. Also the operation of the maser as a spectrometer has permitted a study of the weak field Stark effect and a beating of beats phenomenon by operation of the cavity in the TEM_{101} mode.

Other experimental work of a general nature is also described, including a comparison between effuser-diaphragm and nozzle-skimmer combinations and the oscillation amplitude characteristics of the inversion lines of ammonia $J=K=1,2,3$ with TEM_{001} and TEM_{101} open cavity modes.

CONTENTS

page

ACKNOWLEDGEMENTS

ABSTRACT

CHAPTER ONE

THE MASER

1.1	General Introduction	1
1.2	The Ammonia Molecule	5
1.3	Theory of the Hyperfine Structure of Ammonia	9
1.4	State Separated Molecular Beams	13
1.5	The Simple Cavity Theory	16
1.6	Oscillation Conditions	17

CHAPTER TWO

THE MASER SYSTEM DESIGN

2.1	The Open Cavity	19
2.1.1	Cavity mirrors	19
2.1.2	The frame for the interferometer mirrors	20
2.1.3	Microwave coupling to the cavity	21
2.1.4	Cavity tuning mechanisms	22
2.1.5	Tuning the cavity	23
2.1.6	Identification of cavity modes	25
2.2	Detection System	26
2.3	State Separator	27
2.4	Theory of the Transverse Ladder Separator	29
2.5	Tapered Transverse State Separator Design	31
2.6	The Vacuum Chambers	32
2.7	Maser Vacuum Supply	33
2.8	The Ammonia Supply	35
2.9	Nozzle and Skimmer Design	36
2.10	The Skimmer and State Design	36
2.11	The Mechanical and Electrical Lead-Throughs	37

<u>CHAPTER THREE</u>	THE MASER AS A SPECTROMETER	
3.1	Introduction	38
3.2	The First Spectrometer	39
3.3	Hyperfine Structure of Ammonia Inversion Lines $J=K=1,2,3$	41
3.4	High Intensity Molecular Beam	44
3.5	Experimental Comparison of Effuser-Diaphragm and Nozzle-Skimmer Combinations	48
3.6	The Stark Effect for Ammonia	51
3.7	Observation of the Stark Effect in the $J=K=1$ Inversion Transition of Ammonia	56
3.8	Operation of the Maser with TEM_{101} Cavity Mode	58
3.9	Observation of a Beating of Beats Effect in Both Naturally and Artificially Split Spectral Line	60
<u>CHAPTER FOUR</u>	THE MASER AS AN OSCILLATOR	
4.1	The Oscillation Frequency	63
4.2	The Oscillation Amplitude Characteristics (the $J=K=1,2,3$ Lines of $^{14}NH_3$)	67
4.3	Oscillation in the Next Higher Order Cavity Mode (TEM_{101})	72
4.4	Biharmonic Oscillation in a Disc Resonator Maser	73
4.5	The Experimental Investigation of the Onset of Oscillation	77
<u>CHAPTER FIVE</u>	SUGGESTIONS FOR FURTHER WORK	81

APPENDIX ONE

84

Measurement of the Cavity Quality Factor

APPENDIX TWO

86

Injection Priming of a Pulsed Molecular Beam Maser
Oscillator

(D.C. Lainé and A.M. Al-Jumaily, Electronics Letters,
Vol. 15, No. 1, pp. 21)

APPENDIX THREE

88

Biharmonic Operation of a Molecular Beam Maser
Employing a Quasi-Optical Flat Disc Resonator

(A.M. Al-Jumaily and D.C. Lainé, Actes du "Optique
hertzienne et dielectriques", Lille, June 27-30, 1979)

REFERENCES

92

CHAPTER ONE

THE MASER

1.1 General Introduction

All the active quantum electronic devices - maser amplifiers and oscillators, depend upon the phenomenon of stimulated emission; the emission of radiation from atoms or molecules induced by a signal field, and coherent with that field. The principle of stimulated emission is often attributed to Einstein (1917) since it is suggested by his thermodynamic arguments concerning the interactions between electromagnetic waves and a quantum-mechanical system. However, this idea did not take practical shape until the successful operation in 1954 by Gordon, Zeiger and Townes, of a device called a MASER which is an acronym for "microwave amplification by stimulated emission of radiation", based on the principle of stimulated emission.

The molecular beam maser has three component parts: gas source, state selector and a region in which the interaction occurs between state selected molecules and radiation. The gas source is required to produce an intense and highly collimated molecular beam. The sources employed in the molecular beam maser are either of the effusive (crinkle foil, klystron grid and multichannel) or nozzle types. The multichannel effusers have been more widely used than the thin wall orifice because of the favourable ratio of forward beam intensity to total gas flow. However, single hole nozzles of small diameter (0.3mm or below) have now in general replaced the effusive type to form intense molecular beams in masers. With them the possibility of dynamic cooling occurs, with an associated enhancement of molecular populations in low-lying rotational states.

The maser requires that the population of the ensemble of molecules be changed in such a way that, for the states involved in the transition, there are more molecules in an upper energy state than in the lower state. This situation is commonly referred to as an inverted population or as an ensemble of molecules with a negative temperature. There are a number of important consequences of this non-equilibrium situation. Consider an ensemble of molecules in which a population inversion occurs. When resonant radiation is passed through the molecules, net emission takes place because there are more molecules in the upper level to be stimulated to emit photons than there are in the lower level to absorb them. However unless some way of maintaining the inverted population could be achieved, thermalising processes would allow only a short life-time of the inverted population. Weber suggested in 1953 a method of obtaining inverted populations to realize an amplifying device which relied on the sudden reversal of either a magnetic or an electric field, applied to the molecules of a volume of gas. This suggestion has never been realized experimentally. Instead, a very successful method has been employed, but which only works for a beam of molecules rather than a simple volume of gas. This method to create a population excess in an upper energy state is that of electrostatic state selection, which may be effected by a variety of electrostatic devices. Since most molecular beam masers employ cylindrical cavities as the interaction region between molecules and radiation field, a cylindrical separating system is usually used in which the electric field gradients have approximate radial symmetry. An electric quadrupole system having longitudinal electrodes with approximately hyperbolic cross-sections was used in the first beam maser operation (Gordon et al., 1954). Ring and bifilar helix types of state selector were later proposed by Krupnov (1959) and investigated by Basov and

Zuev (1961) and Mednikov and Parygin (1963) and others. A crossed-wire focuser was operated by Lainé and Sweeting (1971a) for anti-maser operation. A Stern-Gerlach electric field deflector operated by Hope (1978) has permitted a molecular beam system to be operated either as a maser or anti-maser depending upon the position of the cavity relative to the beam axis. A number of electrostatic state separator systems have been devised to produce plane beams of molecules in conjunction with open cavities, for example by Krupnov (1959), Marcuse (1962), Becker (1963), Krupnov and Skvortsov (1964c) and Takami and Shimuzu (1966).

The region in which the interaction occurs between the state selected molecules and radiation usually takes the form of a resonator cavity, which is one of the most important components of a maser. The closed cavity may be either cylindrical or rectangular; the cylindrical type was used in the first maser in 1954. Two types of modes may exist in a cavity of this type: transverse electric and transverse magnetic. There are several drawbacks to the use of closed cavities, especially for molecular beam maser spectroscopy. These include the small tuning range, difficulties of use as Stark cell and the low intensity of the beam due to the small holes at the cavity entrance, especially at higher frequencies. Many of these constraints are lifted by the use of open resonators. Open resonators were first proposed for beam maser operation by Dicke (1958) and Prokhorov (1958) and first used in an ammonia maser of the parallel disc resonator type by Barchukov et al. (1963). Disc resonators possess many desirable properties; high quality factor, large frontal area to admit the beam, easily evacuated and are readily mechanically tunable over a wide frequency range. In addition, a disc resonator can easily be adapted for Stark studies (Krupnov and Skvortsov, 1964b). The confocal resonator

type has been used in a molecular beam maser oscillator (Marcuse, 1962, Valentin et al., 1978), and a conical rooftop in the ammonia maser (Lainé and Smart, 1971).

The choice of molecules for molecular beam maser operation depends primarily upon the possession of a Stark effect suitable for electrostatic selection of energy levels for population inversion to take place. It also depends upon the strength of the transitions which must be large enough to allow detection of the stimulated emission output, and, if desired, to produce maser oscillation. Various molecules have been used successfully for beam maser spectroscopy and for the operation of molecular beam maser oscillators. These have been reviewed recently in *Advances in Electronics and Electron Physics* (Lainé, 1975) and *International Review of Science* (Dymanus, 1976). The success of ammonia as a working substance in a molecular beam maser is due to the strong Stark effect and to the large population of molecules in the inversion states.

The operation of the first maser which marked the beginning of a new field of study in physics, proved to be very useful in quantum electronics research and in particular as a spectroscopic tool. The Keele maser group, which includes the author, has been pursuing a continuing series of investigations. Since 1966 this group has published some fifty communications, two of which include the writer of this thesis.

The thesis has been organized into five chapters. In Chapter One the working medium of the maser, ammonia in this case, with a discussion of state selection and the interaction region are presented.

In Chapter Two the design and construction of the maser is described, and some design considerations discussed in the light of theory, are also presented in this chapter.

Chapter Three gives details of the experimental and theoretical considerations for the formation of high intensity molecular beams, for the Stark effect, and for the operation of a maser with a higher order cavity mode. A brief description of the first maser system used as a spectrometer for some investigations at the beginning of the project is also included (the experimental work, described in this thesis, is based on two different designs of maser systems).

Chapter Four details the experimental investigation of the oscillation characteristics ($J=K=1, 2$ and 3) when the maser oscillator is operated with TEM_{001} and TEM_{101} cavity modes, with particular reference to new observations of maser oscillation behaviour in these modes.

Chapter Five outlines suggestions for further studies, which are based upon observations of particular effects discovered during the progress of work with the open resonator system investigated.

1.2 The Ammonia Molecule

The ammonia molecule is of the symmetrical top type. The three atoms of hydrogen form a triangle ($r_{HH} = 1.014 \text{ \AA}$), and the nitrogen atom occupies a position above or below the hydrogen's plane.

Fig. 1.1 shows the geometrical structure of this molecule. The Z-axis is the molecular axis of symmetry and the origin of the coordinate system is taken as the centre of gravity. A number of different oscillatory and rotational motions are possible.

The electronic spectrum of a molecule is caused by the orbital motion of electrons; transitions between electronic levels fall into the optical frequency region. For thermal equilibrium at room temperature,

$$h\nu \gg kT$$

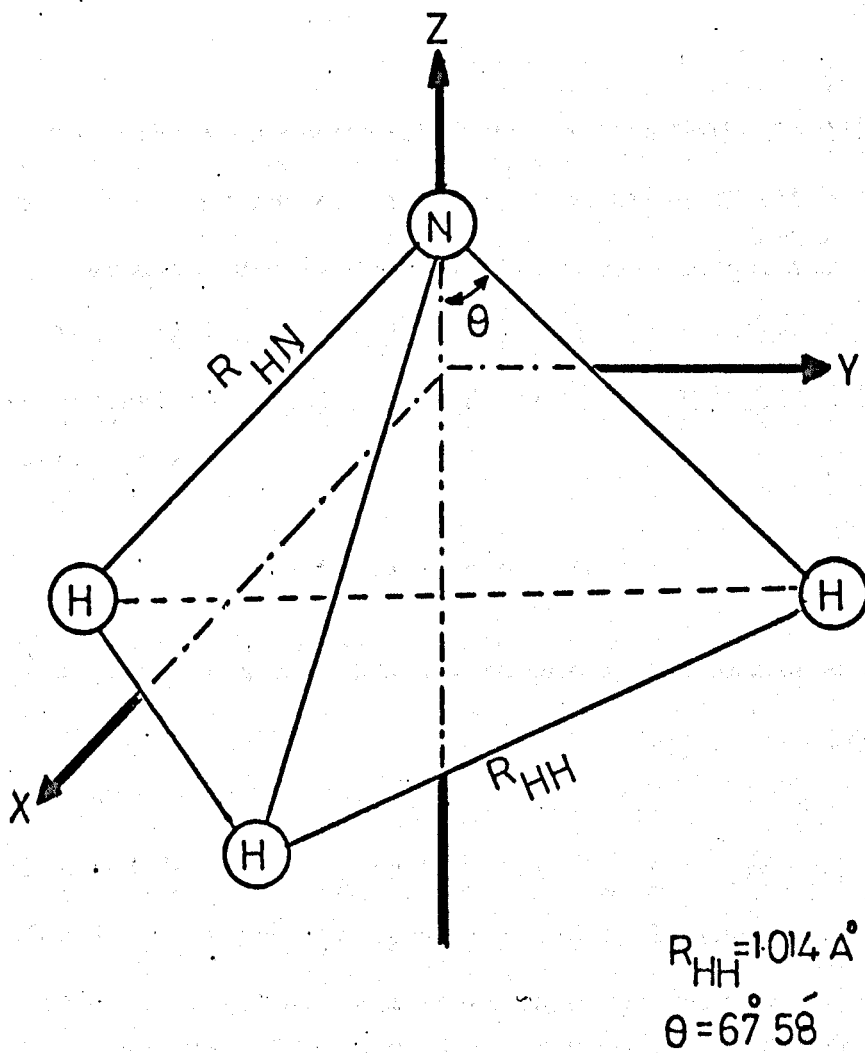


Fig.1.1 Geometrical structure of an ammonia molecule

and so the population of excited electron levels is very small.

The vibration spectrum of the ammonia molecule lies in the infrared range, and consequently the population of vibrational states above the ground state is quite small at room temperature.

The rotational energy levels of ammonia (since ammonia is of the symmetrical top type) may be described by the following equation (Oraevskii, 1964)

$$E_{JK} = hBJ(J+1) + h(A-B)K^2 \quad 1.2$$

where J is the rotational quantum number of the molecule and K is a second rotational quantum number which is equal to the projection of J along the axis of symmetry of the molecule. A and B are rotational constants and depend on I_A or I_B , where I_A is the moment of inertia of the molecule about the symmetry axis and I_B is the moment of inertia of the molecule about the axis that is perpendicular to the symmetry axis and passes through the centre of mass of the molecule,

$$A = \frac{h}{8\pi^2 I_A} \quad B = \frac{h}{8\pi^2 I_B} \quad 1.3$$

For ammonia molecules, $A = 189$ GHz and $B = 298$ GHz.

Transitions between rotational energy levels are governed by the selection rules:

$$\Delta J = 0, \pm 1 \quad \Delta K = 0 \quad 1.4$$

The transition frequencies between rotational energy levels are determined by the selection rules (1.4) and are given by

$$\nu_{JK} = \frac{1}{h}(E_{J+1,K} - E_{J,K}) = 2B(J+1) \quad 1.5$$

Therefore, from Eq. 1.5, the rotational transition frequencies lie in

the submillimeter wavelength range.

The ammonia spectrum has fine structure caused by inversion splitting of the energy levels. The splitting originates from the fact that the nitrogen atom can be found on two different sides of the plane of the hydrogen atoms. On each side of the plane the nitrogen atom may have a stable equilibrium position. The potential energy of the molecule as a function of the distance between the nitrogen atom and the plane of the hydrogen atoms, has the form of a symmetrical curve with two minima, as shown in Fig. 1.2b. Stable positions of a molecule are divided by a potential barrier with finite height. The nitrogen atom can oscillate about the equilibrium positions and the oscillation frequencies are identical since the potential energy function of the molecule is symmetrical with respect to the plane of hydrogen atoms. Since the potential barrier dividing the positions of equilibrium is not very high, owing to the tunnel effect the nitrogen atom can penetrate the potential hill from one side of the hydrogen atom's plane to the other (inversion). Thus the oscillations of the nitrogen atom on either side of the hydrogen atom's plane are not independent of each other. Therefore, in this case the energy levels of an ammonia molecule are split into two sublevels. The splitting is termed inversion splitting. The amount of the splitting of the vibrational levels, and the frequency of the inversion line is very sensitive to changes of the height and width of the potential barrier, and in turn its shape will be a function of the molecular rotational state. The rotation of the molecule about the axis of symmetry will cause the hydrogen atoms to move outwards and thus reduce the height of the potential barrier and increase the inversion frequency. On the other hand, rotation about the axis perpendicular to the molecular axis causes a decrease in the inversion frequency. The transition that gives rise

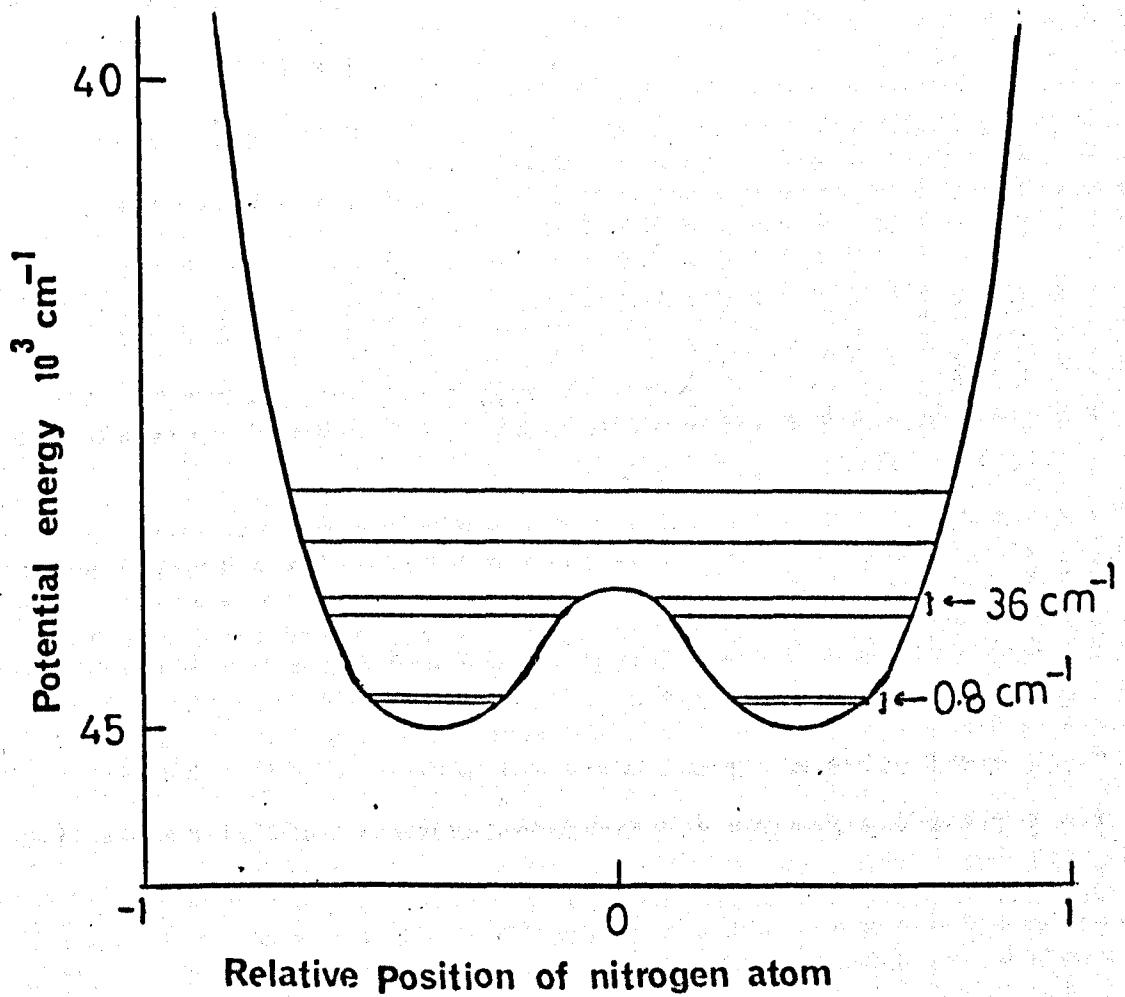
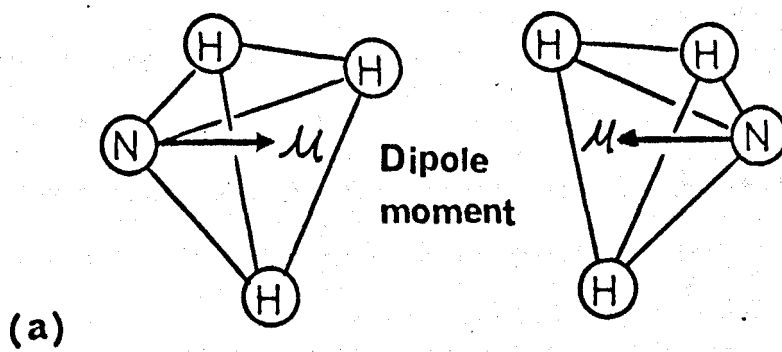


Fig.1.2.b. Potential curve for ammonia molecules showing energy level

to inversion is the one between the two levels of the split vibrational ground state. Thus with each rotational state, there is associated a finite splitting, which is characterized by three quantum numbers; the total angular momentum J , the projection of the total angular momentum on a space axis M_J , and the projection of J on the symmetry axis K . The dependence upon the rotational quantum numbers J and K of the inversion splitting, is given by Oraevskii (1964),

$$h\nu_{inv} = h\{v_0 \exp[aJ(J+1) + bK^2 + cJ^2(J+1)^2 + dJ(J+1)K^2 + eK^4] + \Delta\nu\} \quad 1.6$$

where $v_0 = 23.785$ GHz

$$b = 8.88986 \times 10^{-3}$$

$$-d = 1.7845 \times 10^{-6}$$

$$-a = 6.36996 \times 10^{-3}$$

$$c = 8.6922 \times 10^{-7}$$

$$e = 5.3075 \times 10^{-7}$$

$$\Delta\nu = \begin{cases} 3.5 \times 10^{-4} J(J+1) [J(J+1) - 2] [J(J+1) - 6] & \text{for } K = 3 \\ 0 & \text{for } K \neq 3 \end{cases}$$

The pure inversion spectrum of ammonia is obtained from this equation and lies at $\lambda \approx 12.5$ mm.

The spectral lines of ammonia, in this part of the spectrum are relatively intense; first, the dipole moment is quite large (1.47 debye); secondly, the rotational constants of ammonia are sufficiently large to allow suitable energy separations between rotational energy levels.

The matrix element μ_{12} of the dipole moment for the inversion transition is given by Townes and Schawlow (1955) as:

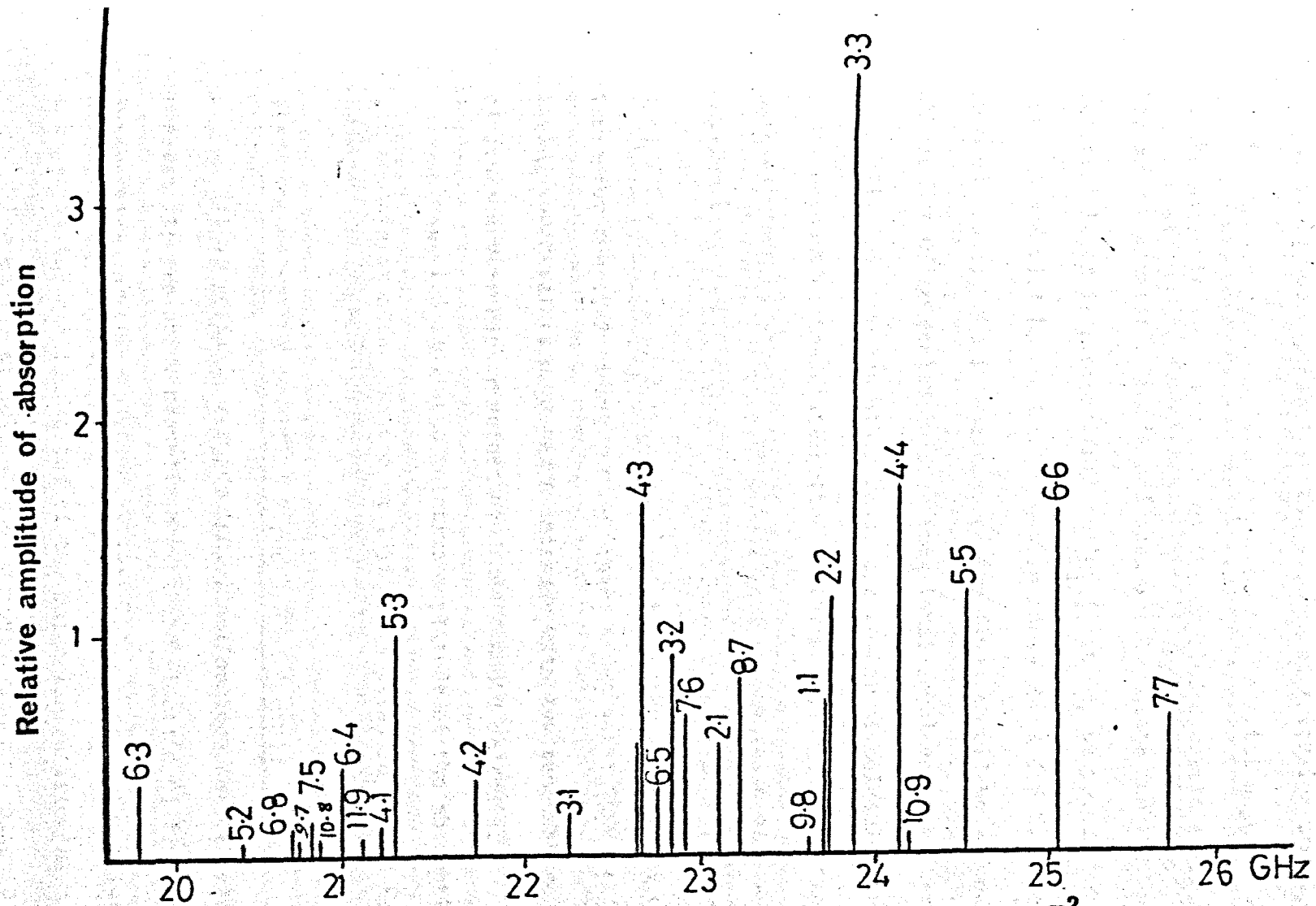


Fig.1.3 Ammonia inversion spectrum, temperature 195°K, pressure 5×10^{-2} mm Hg

(after Good, 1947)

$$\mu_{12} = \mu_0 \frac{KM_J}{J(J+1)} \quad 1.7$$

where μ_0 is the permanent dipole moment pictured in Fig. 1.2a, which the molecule would possess in the absence of inversion and M_J is the quantum number governing the component of the total angular momentum of the molecule along the axis of the applied electric field.

The matrix element is maximised when $J = K$. Since the intensity of spectral lines is proportional to $|\mu_{12}|^2$ it may be noted that lines where $J = K$ will be more intense than those where $J \neq K$. According to Good (1946), the intensities of the lines should be a function of the number of molecules in each rotational level and their transition probabilities. On the other hand, the number of molecules in a given level depends on the distribution of thermal energies and the statistical weights. The statistical weights depend on the value of J and the nuclear spin of the hydrogen atoms (James et al., 1948). For this case levels for $K = 3, 6, 9$ etc. will have twice the statistical weight of those for $K = 1, 2, 4$ etc. Good, 1946, shows the intensities of lines having lower values of J and K increase with low temperature, and that of lines having higher values of J and K would decrease.

Fig. 1.3 shows the relative amplitude of the absorption spectrum for ammonia at a temperature of 195K and a pressure 5×10^{-2} torr.

1.3 Theory of the Hyperfine Structure of Ammonia

It is possible for any individual nucleus in the molecule to possess its own spin, magnetic moment and electric quadrupole moment. Interactions of these with the rotational energy of the molecule cause changes in the quantum states of the molecular rotation as a whole.

The energy of molecules of ammonia with an isotope of nitrogen N^{14} possess a well developed hyperfine structure, caused by different

intramolecular interactions. When the hyperfine interactions are taken into account, the energy levels of various transitions of the molecule should be characterized by the quantum numbers J , I_N , I , F and F_1 where J is the vector of total rotational angular momentum of the molecule excluding nuclear spins, I_N is the spin vector of the nitrogen nucleus, I is the vector of total spin of the three hydrogen nuclei. Since magnetic interactions (which arise from the interaction of magnetic moments of nuclei in the molecule with each other and with the magnetic field induced by molecular rotation) are much smaller than the nitrogen quadrupole coupling energy (which originate from the interaction of quadrupole electric moment of nitrogen nuclei with the intramolecular electric field). The nitrogen spin I_N first couples to J to give F_1 . The hydrogen nuclei can then be numbered according to their positions relative to the chosen molecular axes (I_i where $i = 1, 2, 3$ spin of the i^{th} hydrogen nucleus) and couple together to give a resultant I , which in turn couples to F_1 to give the total angular momentum of the molecule F (Gunther-Mohr et al., 1954). Fig. 1.4 shows the coupling scheme, referred to the laboratory axis. Z is the fixed direction in the laboratory, z is the axis coinciding with the molecular symmetry axis, and K is the projection of J on the molecular symmetry axis. Thus the coupling scheme is

$$F_1 = J + I_N, \quad I = I_1 + I_2 + I_3, \quad F = F_1 + I \quad 1.8$$

The orientation of the nitrogen nucleus and the ammonia molecule can be characterized by independent quantum numbers, M_{I_N} the projection of the nitrogen spin on the Z axis and M_J the projection of moment of rotation of the molecule on the Z axis. However, a calculation of the interaction leads to the fact that these two quantum numbers are not

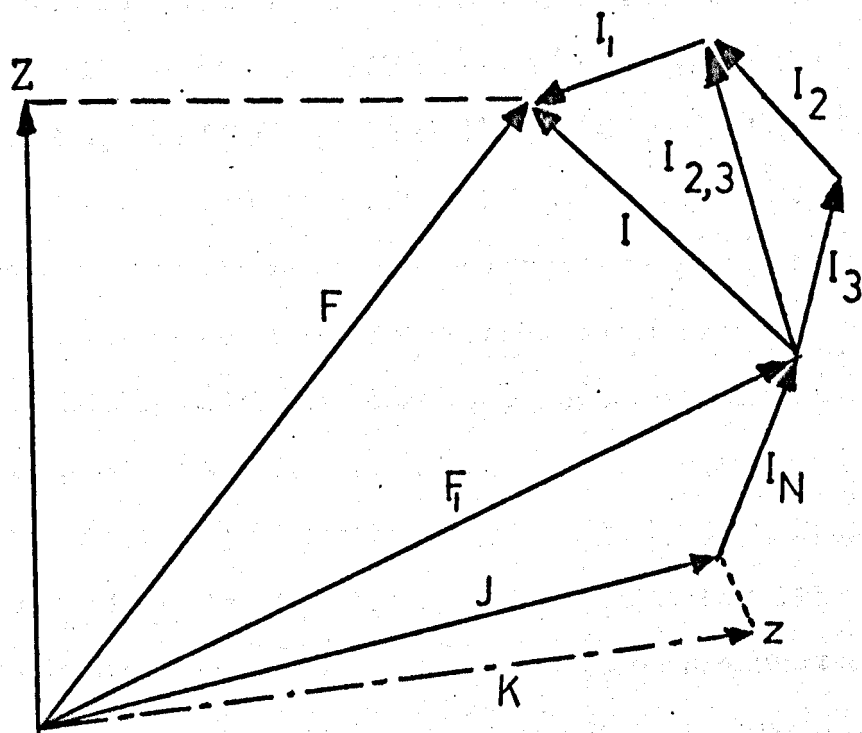


Fig:1.4 NH_3 Molecular coupling scheme

preserved, so instead it is necessary to introduce another quantum number, M_{F_1} , which is the projection of F_1 onto the Z axis.

In 1955 Gordon used a high-resolution microwave spectrometer with a total resolution width at half maximum of 7 kHz. With this narrow linewidth, the magnetic hyperfine structure caused by the orientation of the spins of hydrogen nuclei was resolved and fitted to the theoretical data within an error of 1 kHz. It was found that with a high-resolution spectrometer, the quadrupole coupling constant (eqQ) under the effect of centrifugal distortion was larger for the lower inversion state by 0.01% than for the upper inversion state and the sign of this constant was directly measured to be negative. A theoretical treatment of the magnetic interactions by Gordon was made which was different from the theoretical analysis of Gunther-Mohr et al. and extended to include evaluation of the mutual spin-spin interaction of the hydrogen nuclei. Gordon combined his result with those of Gunther-Mohr et al., and gave the final form of the complete hyperfine energy as follows:

$$\begin{aligned}
 W_{JKF_1} = & - \langle eqQ \rangle \left[1 - \frac{3K^2}{J(J+1)} \right] \Omega_1(J, I_N) \\
 & + \left[a + \frac{(b-a)K^2}{J(J+1)} \right] (I_N \cdot J) + \left[A + \frac{cK^2}{J(J+1)} \right] \frac{(I \cdot F_1)(F_1 \cdot J)}{F_1(F_1+1)} \\
 & + 2g_H g_N \mu_o^2 \left\langle \frac{1 - 1.5 \sin^2 \theta}{r_{NH}^3} \right\rangle \frac{(F_1 \cdot I) \Omega_2(J, I_N)}{F_1(F_1+1)} \\
 & \times \left[1 - \frac{3K^2}{J(J+1)} \right] \\
 & - 0.25 (g_N \mu_o^2) \langle r_{HH}^{-3} \rangle \frac{\phi(F_1, I) \phi(J, F_1)}{F_1(F_1+1)} \\
 & \times \left[1 - \frac{3K^2}{J(J+1)} \right] - \delta_{K_1} (-1)^{J+V} 2f
 \end{aligned}$$

1.9

where

$$2f = \left\langle \frac{1.5 \sin^2 \theta}{r_{HH}} \right\rangle^2 g_H g_N \mu_o^2 \frac{(F_1 \cdot I) \Omega_2(J, I_N)}{F_1(F_1+1)} + \frac{(I \cdot F_1)(F_1 \cdot J)}{F_1(F_1+1)}$$

$$\Omega_1(J, I_N) = \frac{3(I_N \cdot J)^2 + 1.5(I_N \cdot J) - I_N(I_N + 1)J(J+1)}{(2J-1)(2J+3)2I_N(2I_N-1)}$$

$$\Omega_2(J, I_N) = \frac{3(I_N \cdot J)^2 + 2J(J+1)(I_N \cdot J)}{(2J-1)(2J+3)}$$

where $V = 0$ for the lower inversion state and $V = 1$ for the upper state.

θ is the angle shown in Fig. 1.5.

$$A = -17.9 \pm 0.5 \text{ kHz}$$

$$B = -14.1 \pm 0.3 \text{ kHz}$$

$$c = -2.0 \pm 0 \text{ kHz}$$

$$a = 6.66 \pm 0.2 \text{ kHz}$$

$$b = 6.66 \pm 0.2 \text{ kHz}$$

The quadrupole coupling constant is given by

$$(\text{eqQ})_{AV} = 4089[1 + 7.7 \times 10^{-5}[J(J+1)K^2]] \pm 1.5 \text{ kHz}$$

where $(\text{eqQ})_{AV}$ is the average of the quadrupole constant for the upper and lower inversion levels. This was chosen by Gordon to provide a best fit to both his data and that of Gunther-Mohr. But for low J and K lines he gave a better formula, which however, does not agree well at high J and K with the result of Gunther-Mohr. The formula is

$$(\text{eqQ})_{AV} = -4092.4[1 + 5 \times 10^{-5}J(J+1)] \pm 1.5 \text{ kHz}$$

This equation is valid so long as the quadrupole energy term is large compared with magnetic terms.

Equation 1.9 can be used to express the energy levels of a given rotational state (J, K) in terms of five adjustable parameters,

each of which determines the type and strength of interaction

(Kukolich, 1967):

$$(1) \quad -eQq \left[1 - \frac{3K^2}{J(J+1)} \right] = \text{strength of the quadrupole coupling}$$

$$(2) \quad \left[a + \frac{(b-a)K^2}{J(J+1)} \right] = \text{strength of the magnetic } I_N \cdot J \text{ coupling}$$

$$(3) \quad \left[A + \frac{cK^2}{J(J+1)} + \delta_{K_1} (-1)^{J+V} B \right] = \text{strength of the } I \cdot J \text{ coupling}$$

$$(4) \quad D_1 \left[1 - \frac{3K^2}{J(J+1)} \right] - D_2 \delta_{K_1} (-1)^{J+V} = \text{strength of the hydrogen-nitrogen spin-spin interaction}$$

$$(5) \quad -\frac{1}{4} D_3 \left[1 - \frac{3K^2}{J(J+1)} \right] = \text{strength of the hydrogen-hydrogen spin-spin interaction}$$

where

$$D_1 = g_H g_N \mu_o^2 \frac{1 - 1.5 \sin^2 \theta}{r_{NH}^3}$$

$$D_2 = g_H g_N \mu_o \frac{1.5 \sin^2 \theta}{r_{NH}^3}$$

$$D_3 = (g_H \mu_o)^2 r_{HH}^{-3}$$

1.4 State Separated Molecular Beams

Consider first a gas in thermal equilibrium which is irradiated by microwaves at the frequency of one of the transitions of the gas molecules. An absorption of energy invariably takes place. There will be molecules in both the higher and lower energy state of the transition, and the microwaves will excite transitions both up and down with equal probability. The total rate of upward transitions will, however, be slightly larger than the rate of downward transitions, since the Boltzmann distribution gives the lower state a population larger than the upper.

For molecular beam maser operation, it is necessary to increase the number of molecules in the upper level relative to that in the lower level of a pair of energy states between which transitions take place.

It is well known that molecules which possess a large electric dipole moment can be readily deflected by the use of non-uniform electric fields with a gradient perpendicular to the molecular beam axis. In the case of ammonia molecules, as a result of their inversion, there is no average dipole moment (Fig. 1.2a). But in the presence of an electric field, however, the inversion is partially quenched and an average dipole moment appears. Neglecting hyperfine effects, the energies of the inversion states may be written as (Gordon, 1955):

$$W = W_0 \mp \left[\left(\frac{h\nu_0}{2} \right)^2 + \left(\frac{\mu M K E}{J(J+1)} \right)^2 \right]^{\frac{1}{2}} \quad 1.10$$

where W_0 is the average energy of the upper and lower inversion levels, ν_0 is the inversion frequency in zero electric field, μ is the permanent dipole moment the molecule would have if the inversion did not occur, E is the magnitude of the electric field, M is the projection of J on the direction of the field, and h is Planck's constant.

In a uniform field, no force acts on the molecule, but in a non-uniform electric field for which $E < 3 \text{ kV mm}^{-1}$, the molecule is acted upon in the direction of the field gradient (y -axis) by the force

$$F_y = - \frac{\partial W}{\partial y} = \mp \frac{\left(\frac{\mu M K}{(J+1)J} \right)^2 E \frac{\partial E}{\partial y}}{\left[\left(\frac{h\nu_0}{2} \right)^2 + \left(\frac{\mu M K E}{(J+1)J} \right)^2 \right]^{\frac{1}{2}}} \quad 1.11$$

The sign of the force is negative (i.e. towards low electric flux density) for ammonia molecules in the upper inversion level, and positive (towards high electric flux density) for those in the lower level.

The behaviour of the energy in an electric field is shown in Fig. 1.5, for $J=K=3$. It should be noted that molecules in the $M = 0$ level are not deflected by an electric field, but that levels for $M \neq 0$ will have different energies. The magnitude of the separating force is proportional to M^2 at low values of the field. At high field where $\frac{\mu_0 MK}{J(J+1)} \gg \frac{h\nu_0}{2}$ the separating force is proportional to M , and the Stark effect is linear.

Some molecular trajectories passing through a region of non-uniform electric field are shown in Fig. 1.6. Consider a molecule travelling in the x,y plane, which enters the region ABCD at the origin O with an initial velocity v . Let the electric field present in the region be in the x -direction, but which increases from zero on the x -axis to a maximum value E_{\max} at the edges AB, CD of the region. If the molecule is in the lower inversion level with $M \neq 0$, then it will experience a force in the y -direction which accelerates it away from the x -axis and will follow a trajectory such as that labelled L or L'. If, on the other hand, it is in the upper state and $M \neq 0$, the force will be towards the x -axis and it will follow trajectories such as \bar{U} , \bar{U} , $\bar{\bar{U}}$.

The net effect of F_y will also depend on the time spent by the molecule in the region and hence on its initial x -component of velocity v_x . If v_x is small and/or M is large, the molecule may make several oscillations about the x -axis (trajectory $\bar{\bar{U}}$). If v_x is large and/or M is small, the molecule may still be diverging from the x -axis, when it leaves the region (trajectory U). If v_x is in between, then the molecule will follow the trajectory \bar{U} .

The focusing criterion is therefore

$$\frac{mV_y^2}{2} < \Delta W \equiv \frac{mv_c^2}{2} \quad 1.12$$

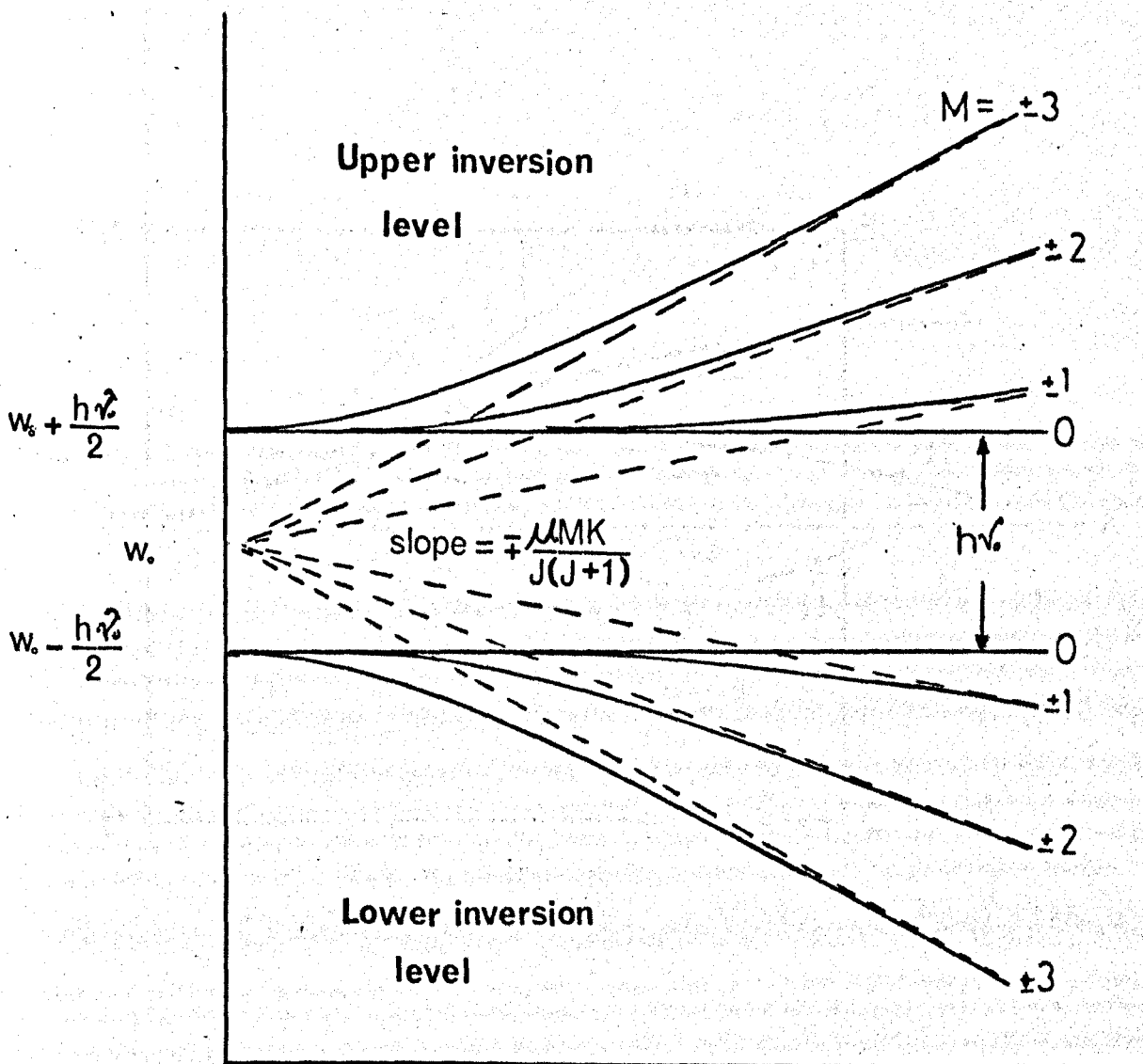


Fig.1.5 Stark effect for the $J=K=3$ inversion transition of ammonia

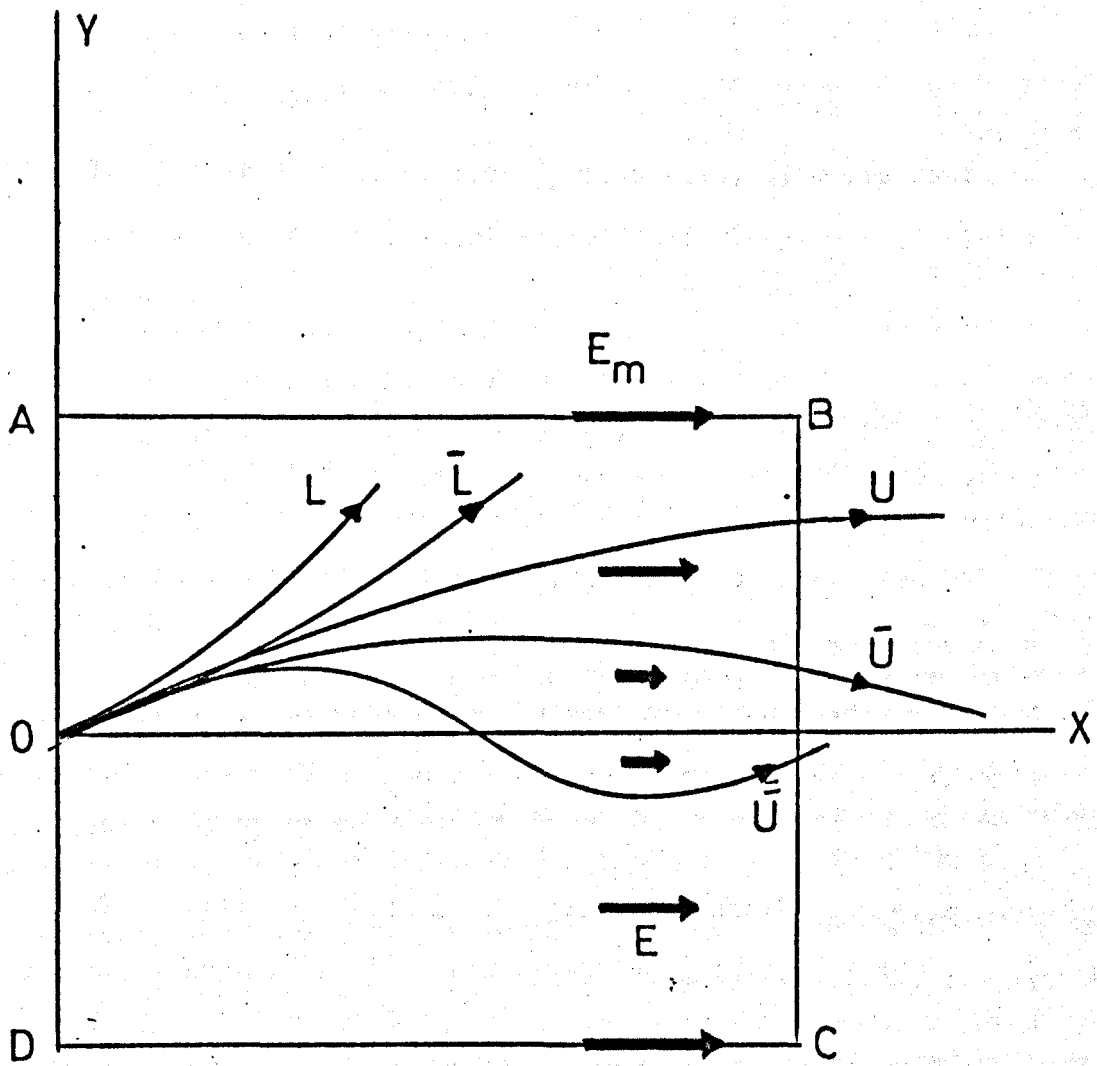


Fig.1-6 Molecular trajectories through a region of non-uniform electric field

where m is the molecular mass and v_c is the critical transverse velocity and ΔW the Stark energy.

1.5 The Simple Cavity Theory

The Fabry-Perot cavity has been described by Schawlow and Townes (1958) on the basis of closed resonators. The resonant frequencies of a closed rectangular cavity of dimensions 2ℓ , $2a$ and $2a$ are given by

$$v_{rsq} = \frac{c}{4} \left[\left(\frac{q}{\ell}\right)^2 + \left(\frac{r}{a}\right)^2 + \left(\frac{s}{a}\right)^2 \right]^{\frac{1}{2}} \quad 1.13$$

where c is the speed of light and q , r and s are integers. In an open cavity with square mirrors of dimensions $2a \times 2a$, separated by a distance of 2ℓ (Fig. 1.7), it is expected that the same resonant modes will be supported, but that only those modes which have low values of the integer r and s should be evident owing to the large diffraction losses for non-axial modes.

The electromagnetic field amplitude distribution over one of the mirrors, taken as the x,y plane and shown in Fig. 1.7a, is given by

$$A = A_0 \sin(\pi r x/a) \sin(\pi s y/a) \quad 1.14$$

The modes predicted by Schawlow and Townes are usually designated the $TEM_{r-1,s-1,q}$ modes, so that the lowest order mode is the TEM_{00q} .

It is possible to write functions analogous to those of Equations 1.13 and 1.14 for an open cavity with circular mirrors. The frequency determining equation is the same as that for TEM_{mnq} modes of a cylindrical cavity:

$$v_{mnq} = \frac{c}{2} \left[\left(\frac{q}{\ell}\right)^2 + \left(\frac{2x_{mn}}{\pi a}\right)^2 \right]^{\frac{1}{2}} \quad 1.15$$

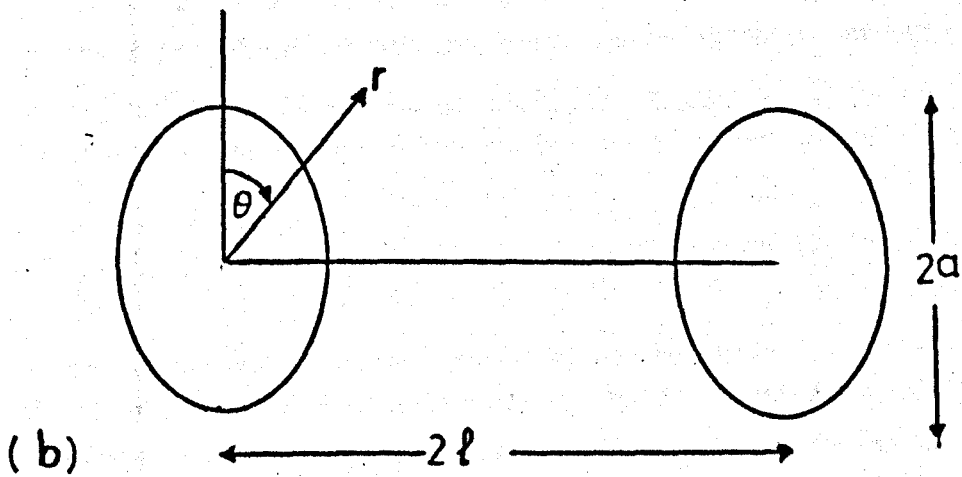
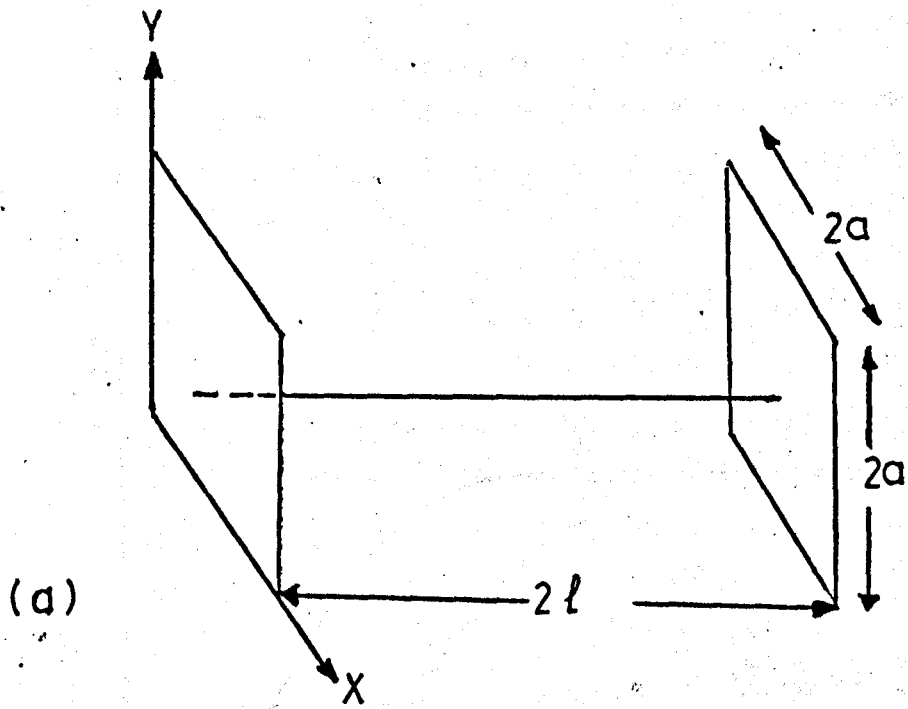


Fig.1.7 Diagrams showing open resonators (a) with square mirrors and (b) with circular mirrors

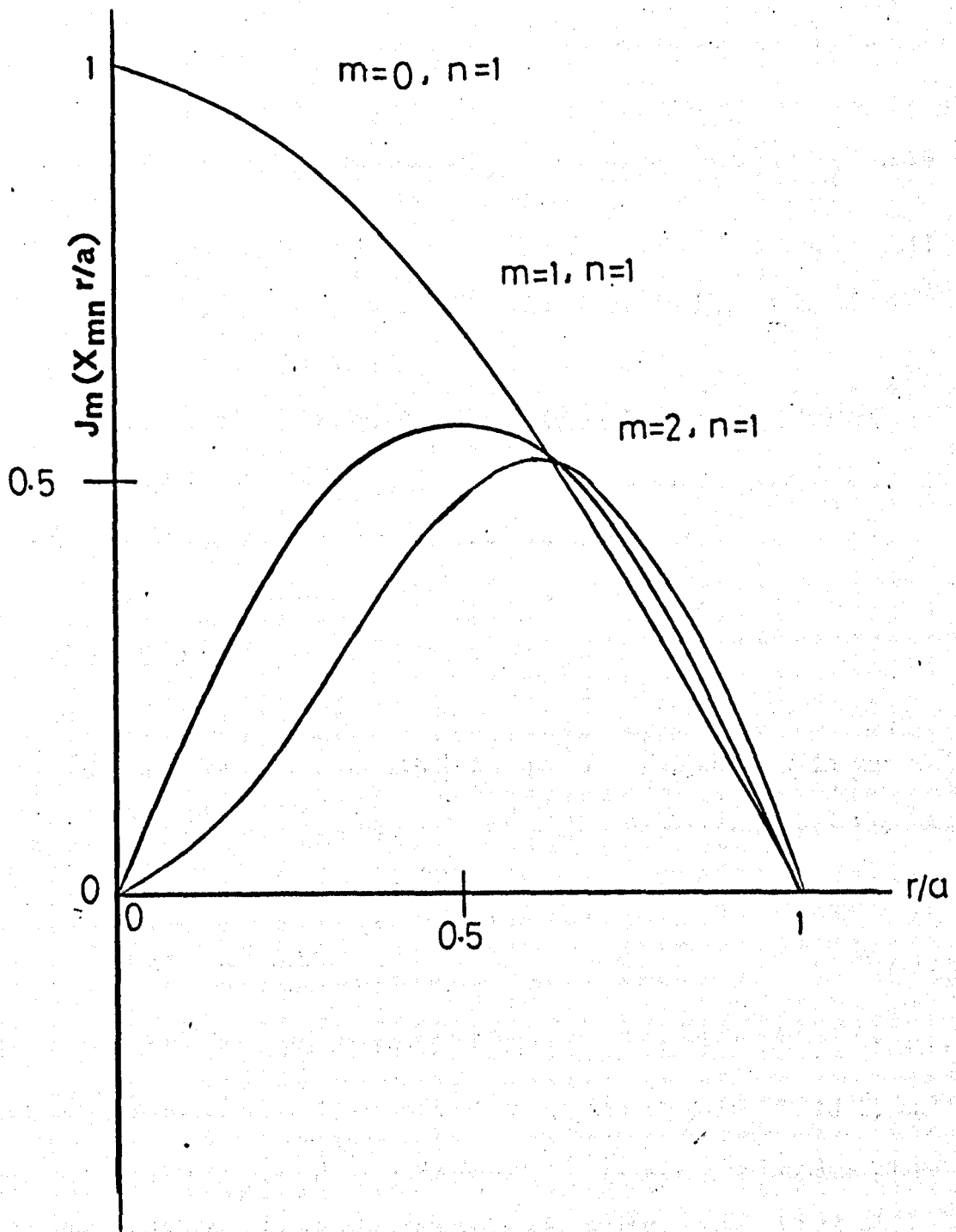


Fig-1-8 The Bessel function $J_m(X_{mn} r/a)$ drawn for three values of m and n , and for values of r in the range $0 \leq r \leq a$ after Smart, 1973

where χ_{mn} is the n^{th} root of the m^{th} order Bessel function of the first kind, J_m . The field amplitude distribution over a mirror, with the origin of coordinates r, θ at its centre as shown in Fig. 1.7b, is

$$A = A_0 J_m(\chi_{mn} r/a) \cos(m\theta) \quad 1.16$$

The scaling factor $\chi_{mn} r/a$ allows the n^{th} zero of the function to fall at the edge, $r = a$, of the mirror. This is shown in Fig. 1.8, where amplitude is plotted against r/a .

The modes of the Fabry-Perot cavity with circular mirrors are usually designated the $TEM_{m,n-1,q}$ and the lowest order mode TEM_{00q} . The TEM_{001} mode is the one usually used in the maser.

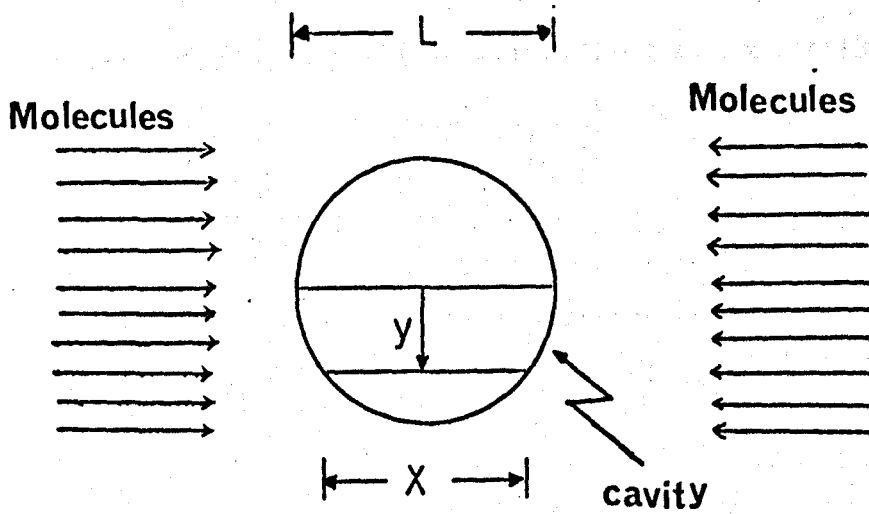
1.6 Oscillation Conditions

A beam of molecules of flux density N (molecules per second) passes through a cavity of length L in the time $\frac{L}{v}$, where v is the velocity of the molecule. The microwave power emitted, with low power excitation and no saturation, is (Shimoda et al., 1956)

$$\Delta P = \frac{N v_0 E^2 \mu_{12}^2 L^2 \pi^2}{h v^2} \quad 1.17$$

where v_0 is the frequency of the transition, μ_{12} is the matrix element of the component of the dipole moment along the electric field E , and h is Planck's constant. This equation holds if all N molecules pass along the symmetry axis of the Fabry-Perot cavity.

As illustrated in Fig. 1.9, most molecules travel a distance shorter than L in the circular mirror cavity. The power emitted of incident molecules per unit height of the cavity is given by (De Lucia, 1969):



$$x(y) = 2 \left[\left(\frac{L}{2} \right)^2 - y^2 \right]^{1/2}$$

Fig-1-9 Path of molecules through cavity

$$\Delta\bar{P} = \frac{\bar{N}v_o E^2 \mu_{12}^2 \pi^2}{h v^2} (L^2 - 4y^2) \quad 1.18$$

where \bar{N} is the number of incident molecules per unit height, or $\bar{N}L = N$, and $\chi(y) = 2[(\frac{L}{2})^2 - y^2]^{\frac{1}{2}}$. Integration of Eqn. 1.18 gives the result

$$\Delta P = \frac{2Nv_o E^2 \mu_{12}^2 \pi^2 L^2}{3 h v^2} \quad 1.19$$

From the definition of cavity quality factor,

$$Q = \frac{2\pi v_o W}{\Delta P} \quad 1.20$$

where W is the energy stored in the cavity. The electric field may be expressed in terms of the energy in the cavity by (assuming a uniform field distribution) using

$$E^2 = \frac{8\pi W}{V} \quad 1.21$$

where V is its active volume.

From Eqns. 1.21, 1.20, 1.19,

$$N_{\min} = \frac{3Vhv^2}{8\pi^2 \mu_{12} Q L^2} \quad 1.22$$

where N_{\min} is the threshold flux for oscillation, if the power emitted from the molecular beam exceeds the power loss from the cavity, then the system becomes self-excited and an oscillation builds up.

CHAPTER TWO

THE MASER SYSTEM DESIGN

2.1 The Open Cavity

2.1.1 Cavity mirrors

Open resonators with circular mirrors were first used in an ammonia molecular beam maser at 24 GHz (Barchukov et al., 1963) with λ spacing between plates of 200mm diameter. A Q value of 7000 was obtained. Krupnov and Skvortsov (1964) operated a Fabry-Perot maser using the CH_2O molecule at a frequency of 72,838 Mc. Their cavity consisted of two flat brass discs 65mm in diameter, with a separation between the mirrors of $\lambda/2$ ($\lambda = 4\text{mm}$). The quality factor Q was 2000 for the lowest order mode. Lainé and Smart (1971) again using ammonia, with $\lambda/2$ ($\lambda = 12.5\text{mm}$) spacing between plates of copper 150mm diameter, obtained a Q value of 2500 for the lowest order mode. Krupnov et al. (1964) and Lainé et al. (1971) observed a line splitting on account of the longitudinal Doppler effect. However with this particular cavity mode no oscillation was obtained.

A cavity of high quality factor with a long time flight of molecules through it, is very important for the successful operation of a molecular beam maser (see Section 1.5). On the other hand, the value of the quality factor strongly depends on the parallelism of the mirrors, the cleanliness of their surfaces (Barchukov and Prokhorov, 1961), and on their diameter. If the distance between the plates is held constant, there is no optimum value for diameter; the larger the diameter the higher the quality factor (Fox and Li, 1960).

Smart (1973) machined the surface of two pairs of mirrors in two different ways, one diamond-turned and the other surface-ground, to

determine whether there was any difference in the flatness of the surface. He found no significant difference for either flatness or quality factor.

Discs of copper 225mm in diameter, 12mm thick, were chosen for the present work. The reasons for this choice were: first, it is somewhat simpler to machine the surface of a metal mirror in a disc shape by diamond-turning; secondly, the quality factor is proportional to the disc diameter (Fox and Li, 1960), and the greater the diameter the greater the transit time for molecules passing through the microwave field region.

The diamond-turning lathe was allowed to run for four hours before starting the work, in order to allow its temperature to stabilize. A fine cut of the mirror surface was made to remove only 1.5×10^{-2} mm of metal, so that pressure on the surface was minimal. In this way a flatness of $\pm 3 \times 10^{-4}$ mm was achieved. The disc flatness was measured by reflection fringes formed between the mirror surface and a glass optical flat, using sodium light.

2.1.2 The frame for the interferometer mirrors

The circular mirrors (Section 2.1.1) were housed in a strong brass frame which bolted firmly into the main vacuum chamber. The frame consisted of two vertical plates (250 × 250mm, 6mm thick), bolted with 50 × 250mm, 6mm thick brass plate as a baseboard. The two vertical plates were separated by four brass rods 7cm in length. These spacing rods may be exchanged for rods of different length in order to operate the cavity with different mirror separations. In the present work the cavity operated at $\lambda/2$ mirror separation only.

One of the mirrors was bolted directly to the three-armed frame, which in turn was bolted to the front plate. This comprised the

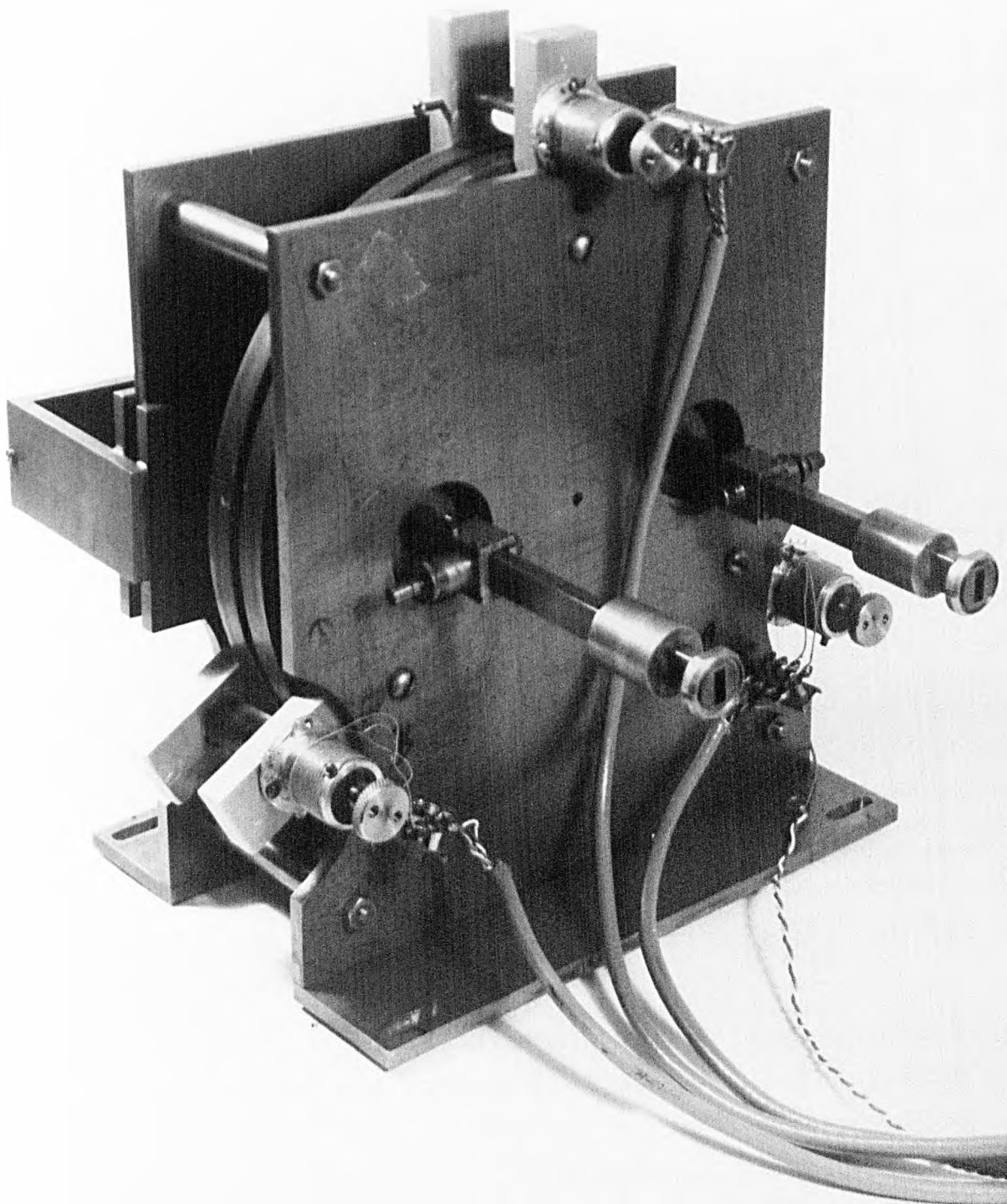


FIG. 2.1 VIEW OF THE OPEN CAVITY SHOWING THE TUNING MICROMETERS, THERMAL TUNING BARRELS AND COUPLING WAVEGUIDES

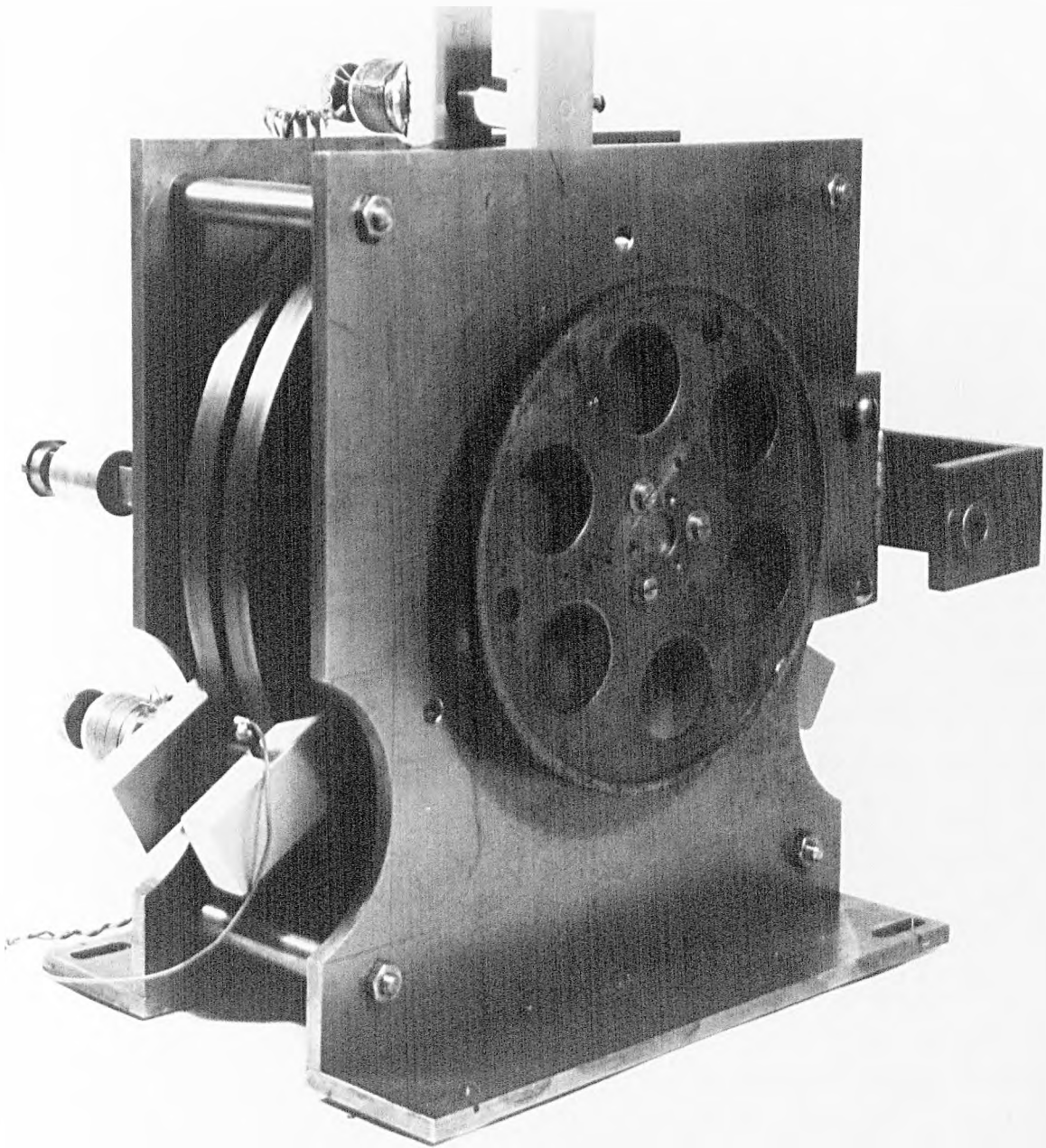


FIG. 2.2 VIEW OF THE OPEN CAVITY SHOWING THE GEAR USED FOR FINE MECHANICAL TUNING

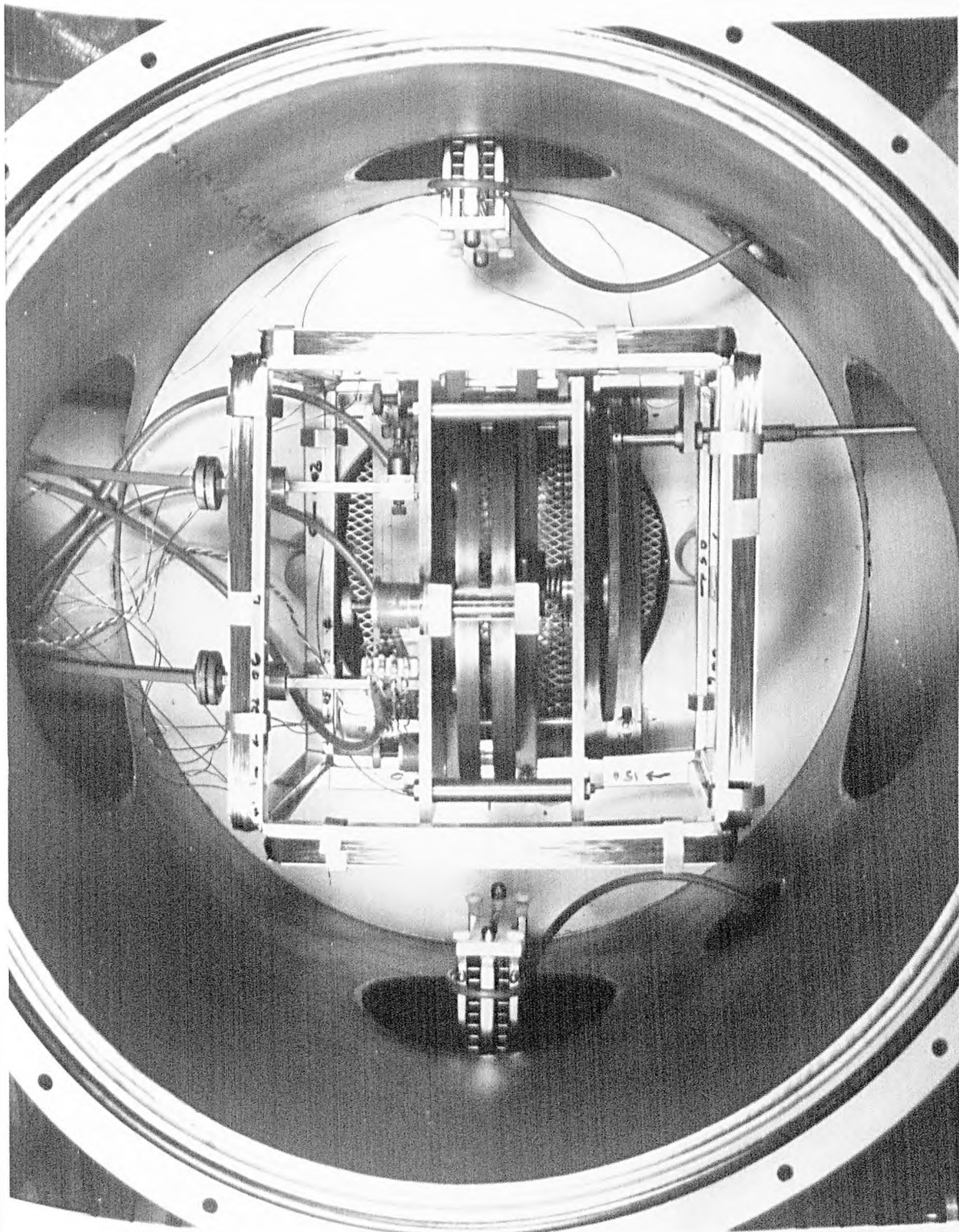


FIG. 2.3

VIEW OF THE MAIN VACUUM CHAMBER FROM ABOVE
SHOWING CAVITY AND STATE SEPARATOR IN POSITION

coupling mirror, which carried the two coupling holes. Two holes 40mm diameter, 112.5mm apart, were drilled through the front vertical plate, to allow the waveguides to pass through and reach the coupling mirror.

The second mirror, used for tuning, was also bolted to a three-armed frame (both three-armed frames were of the same dimensions). Each arm carried a 6mm length glass rod which passed forward through the front arm, from the three-armed frame which carried the coupling mirror, into one of the three micrometer assemblies. The three micrometer assemblies are described in Section 2.1.4. A spring device pressed the tuning mirror at the centre of the three-armed frame. This three-armed frame and its associated tuning mirror were insulated in order that the cavity could be used for work with a weak Stark field. This facility was used during the investigations of the Stark effect on the $J=1, K=1$ ammonia immersion line, described in Section 3.7. Two views of the cavity are shown in Figs. 2.1 and 2.2.

Fig. 2.3 shows the cavity in the main chamber supported on and bolted to four supporting pieces of brass 10mm high, which in turn were bolted to the floor of the main chamber. This figure also shows the two waveguides which couple with the cavity.

2.1.3 Microwave coupling to the cavity

Krupnov and Skvortsov (1964b) using a formaldehyde beam maser, tested three types of microwave coupling to the Fabry-Perot cavity. In one case coupling was effected by coupling waveguides to the side of the cavity with their broad sides parallel to the planes of the mirrors. Another type of coupling employed a single waveguide opening into the cavity at the centre of the mirror. The third coupling was achieved by means of two waveguides whose ends opened into the cavity. The latter was found to be better than the two other types.

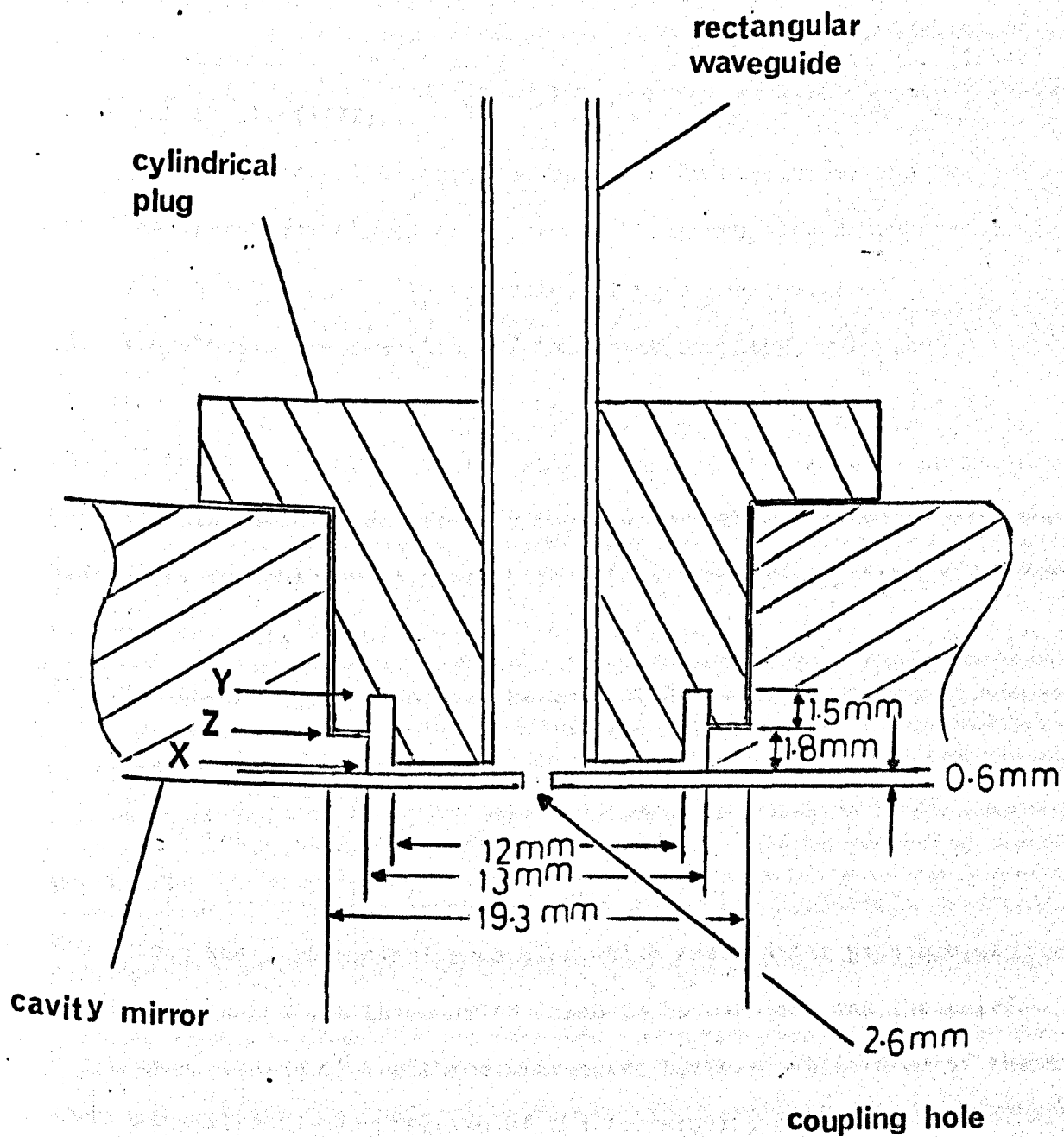


Fig-2.4 Cross-section of the choke coupling between waveguide and coupling mirror

In the present work the microwaves are coupled to the cavity through two holes placed symmetrically on the horizontal diameter of the coupling mirror with a separation equal to the mirror radius (112.5mm). The holes were 26mm in diameter with a 0.6mm diaphragm. This was similar to the coupling scheme used by Krupnov et al. (1964b) and Lainé et al. (1971).

The mechanical arrangement between the waveguides and the coupling mirror was chosen as a form of choke coupling based on the design frequently used with waveguide flanges (Harvey, 1963). Fig. 2.4 shows a cross-section of the choke coupling, only the difference is the join between the two components should be on the plane X where the current in the wall of the quarter-wave choke is zero. However this would have left only the diaphragm thickness to support the waveguide, so that the join was placed in a compromise position, halfway up the choke wall at the Z-plane. This mechanical coupling is similar to the mechanical coupling used by Smart (1973).

2.1.4 Cavity tuning mechanisms

In the cavity design there were three tuning mechanisms. The first was mechanical tuning by means of the three micrometer screws. The second was a mechanical mechanism which enabled the pressure of the spring behind the three-armed frame to be changed, and the third was thermal tuning of the three micrometer barrels. All three of these mechanisms altered the position of the rear-tuning mirror.

Each micrometer assembly consisted of an aluminium barrel carrying a stainless steel micrometer screw. The aluminium barrel was partially insulated thermally from the cavity by a mica washer. Coarse mechanical adjustment of the position and tilt angle of the mirror, was made by these three screws before the chamber was sealed and air pumped out.

The second mechanical tuning method was used to tune the cavity from outside the vacuum chamber after sealing and evacuation. This comprised a finely-threaded plug, screwed into the rear plate of the cavity frame, which supported the centre pressure spring. The plug was bolted to a large gear wheel 150mm in diameter, which meshed with a small pinion (15mm diameter) turned by $\frac{1}{4}$ inch Edwards rotary shaft vacuum seal. By turning the shaft from outside the vacuum chamber, the plug could be screwed into or out of the frame and the spring compressed or decompressed. In this way the pressure on the three-armed frame could be changed, causing it to bend and move the tuning mirror which itself remained absolutely flat and parallel to the coupling mirror. Not only did this mechanism provide fine tuning, but it also gave a very wide tuning range of about ± 70 Mc. This facility was used extensively during the investigations of the higher cavity mode (TEM_{101}), described in Section 4.6.

The need for a method of making fine tuning adjustments when the cavity was under vacuum, was met by heating the aluminium micrometer barrels. This tuning method made use of the differential thermal expansion between the aluminium barrels and the stainless steel of the micrometer screws. The barrel heaters were bifilar wound with a heater coil of glass-covered Eureka wire and a sensor coil of 40 gauge enamelled copper wire. The change of temperature of a barrel was detected by the change in resistance of its sensor winding. The electronic control equipment used was capable of holding the temperature of the barrel stable to $\pm .02^{\circ}\text{C}$.

2.1.5 Tuning the cavity

The cavity design tuning mechanisms are described in Section 2.1.4. A procedure was found whereby the cavity could be adjusted to resonate

in a particular mode as follows. A small steel post was machined to be slightly smaller in width than a free-space half wavelength corresponding to the particular inversion line of ammonia used. By inserting it between the mirrors at different points and by making suitable adjustments to three cavity micrometers, the mirrors were made parallel with a separation almost equal to an integral number of free-space half wavelengths.

Microwave power from a frequency swept klystron was then passed into the cavity via one coupling waveguide, and crystal video detection equipment was attached to the other waveguide. In this way, a display of power transmitted through the cavity was obtained.

The three micrometers were advanced by equal increments until a cavity resonance was observed on the display. As soon as the lowest order mode was located (see Section 1.4), the matching stubs were adjusted for maximum transmission so that further tuning of the cavity could be carried out using a strong transmitted microwave signal.

By using the second mechanical tuning method only, the cavity tuning range of about ± 70 Mc was obtained without significant effect on the mirror parallelism. Therefore, the cavity resonances from lowest mode to higher mode (TEM_{101}) with a given ammonia inversion line, were obtained without a readjustment to the cavity micrometers. The frequency separation between TEM_{001} and TEM_{101} modes was 28 MHz.

Initial tuning to the cavity as described above was usually carried out on the laboratory bench. In order that the cavity should resonate at the maser frequency after it had been placed in the maser vacuum chamber and the chamber pumped out, it was tuned to a frequency slightly higher than that of the maser by an experimentally determined amount. This not only allowed for the change in dielectric constant when the chamber was evacuated, but also for the effect of atmospheric

pressure on the vacuum seals of the coupling waveguide, which tended to strain the cavity and alter its tuning.

2.1.6 Identification of cavity modes

Checcacci and Scheggi (1965) used a perturbation method to investigate the field distribution inside the cavity. Their method is as follows. A small perturbing object is placed in the field between the mirrors, and the power it absorbs is measured by the reduction in the power transmitted or reflected by the cavity.

As the object is moved about inside the resonator, the power it absorbs is proportional to the intensity of the microwave field.

Krupnov et al. (1965) used the perturbation method to identify resonance modes by observing the number and positions of the electromagnetic field maxima, by a half-wave dipole ($\approx 2\text{mm}$ long) made of copper wire cemented to a hair stretched across a frame. In the present work this method was used at 12.5mm wavelength to identify the mode resonances of the Fabry-Perot cavity.

A small piece of copper wire held parallel to the electric field vector in the cavity was used as the perturbing object.

This was cemented to a thin thread stretched horizontally across the cavity between the mirrors, parallel to their surface. With a klystron as the signal source, the output signal was detected by crystal video detection, and a resonance curve was observed on the oscilloscope screen. The drop in signal amplitude on the oscilloscope indicated the amount of power absorbed which in turn was approximately proportional to the microwave field intensity in the vicinity of the wire.

It was found that the crystal video detection scheme needed to be sensitive to very small changes in the microwave power transmitted through the cavity, and accurate positioning of the thread parallel to

the mirror surfaces was needed to map the field intensity accurately. For these reasons, the perturbation method was only used as a qualitative indicator of the resonant mode (or modes) in the cavity.

The fundamental mode (TEM_{001}) and the TEM_{101} mode were readily identified by this method, for a mirror separation of $\lambda/2$.

2.2 Detection System

After the completion of the initial setting up procedure of the Fabry-Perot cavity tuning using the simplest method of microwave detection (crystal video), the maser was operated in transmission with a single klystron superheterodyne detection system. The exciting signal was one of the two sidebands produced by amplitude modulation of a portion of the local oscillator power.

The superheterodyne detection circuit is shown in Figs. 2.5 and 2.6, and the description of its operation which follows refers to Fig. 2.5.

Microwave power from the klystron (OKI type 24V10A) passed via a 6dB directional coupler, an attenuator, and an isolator to the circulator A, and thence to the modulator crystal B (IN26A). The impedance of this crystal was modulated at 30 MHz by an R.F. generator so that 30 MHz sidebands were impressed on the power reflected from it. The frequency of the klystron was such that one of these sidebands occurred at the frequency of the maser transition. The reflected and sideband signals passed via the circulator to the cavity input port C. Since the cavity was tuned to the maser transition frequency, only the sideband at this frequency entered the cavity and provided the stimulation signal for the maser.

Power from the klystron also passed via an attenuator and circulator D to the cavity output port E. Since the cavity was not

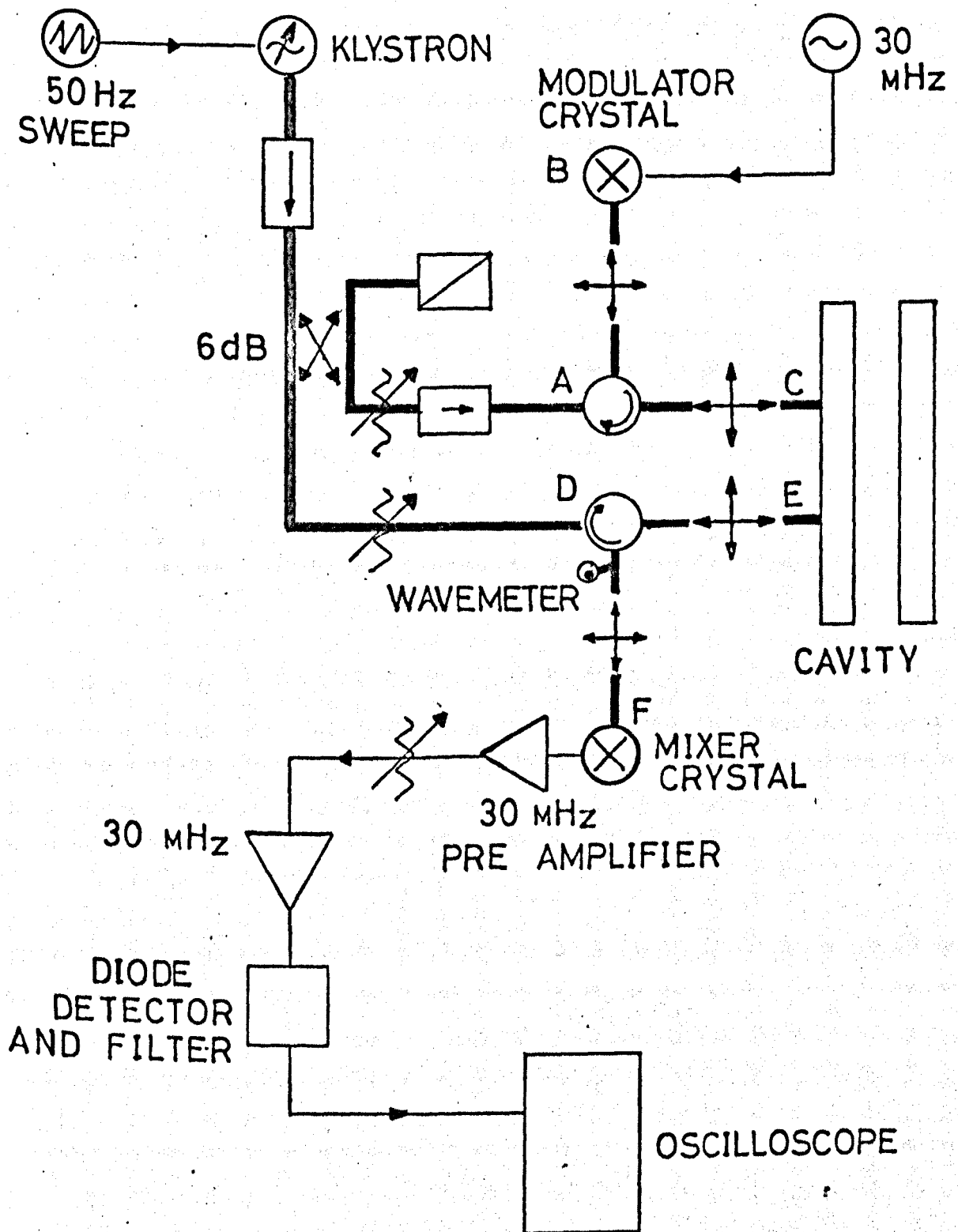


FIG. 2.5 THE TRANSMISSION DETECTION CIRCUIT.

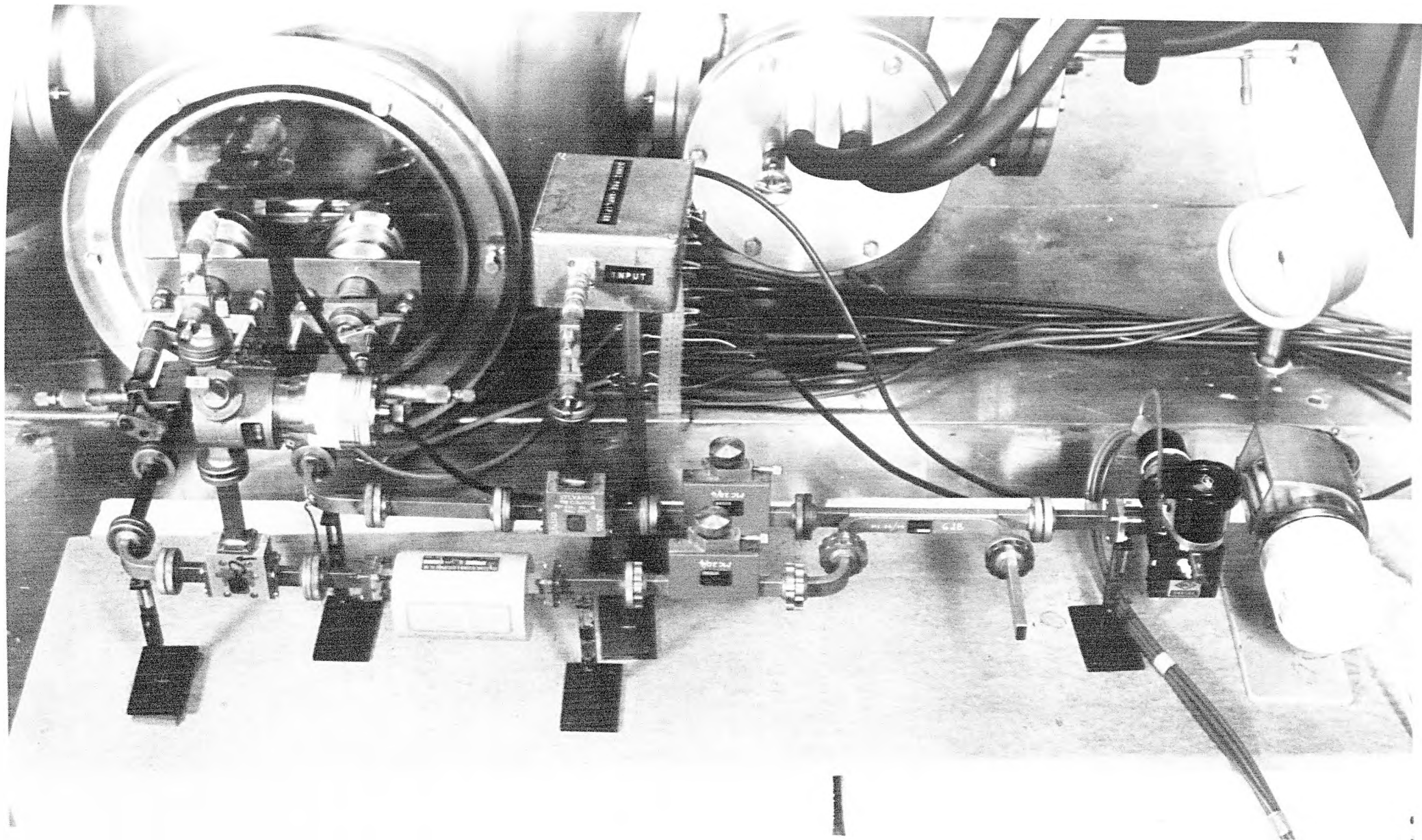


FIG. 2.6 MICROWAVE BRIDGE

tuned to the klystron frequency, most of this power was reflected by the cavity coupling iris and arrived via the circulator D at the mixer crystal F (1N26A). It provided the L.O. power for the mixer. At the same time, a signal from the maser was coupled out of the cavity at port E and also appeared at the mixer crystal. The output from the mixer was a signal at 30 MHz whose amplitude was proportional to the amplitude of the maser signal.

The 30 MHz signal was amplified by the two I.F. amplifiers. It was detected by the diode detector and filtered by an R.C. filter before being displayed on the oscilloscope (Telequipment type D53). If the diode were to have a linear characteristic, this display would be proportional to the maser signal amplitude. With a 50 Hz sawtooth sweep applied to the klystron reflector the stimulating signal was frequency swept through the maser transition, enabling all four modes of display, spectroscopic mode, molecular ringing, zero beats and I.F. bandpass display, which were all used and will be described in the following chapters.

2.3 State Separator

The terms "state separator" and "focuser" are used in the literature on focusing systems for molecular beams to describe the same type of device. Such a device captures and focuses molecules in certain quantum states, hence the term "focuser". The same device usually defocuses other quantum states and is therefore also known as a "state separator".

A number of separator systems to produce planar (flat) beams of molecules for open resonators have been used. Krupnov (1959) proposed a state separator consisting of two planes of rods, arranged circumferentially around a Fabry-Perot cavity with plane parallel

mirrors, and charged alternately to positive and negative potentials. The gas nozzles were arranged to shoot radial molecular beams between the two planes of electrodes towards the centre of the cavity.

Marcuse (1962) used two closely spaced planes of radially arranged rods with a semi-confocal cavity. The gas nozzles and the geometry of electrodes were similar to those of Krupnov (1959).

The transverse ladder type of state selector, where a flat beam of molecules passes over the separator in a direction perpendicular to the electrodes, has been used by Krupnov and Skvortsov (1964c), in a 4mm formaldehyde maser. The longitudinal ladder type where the flat beam of molecules passed over the separator in the direction of the electrodes, has been used in a radio frequency formaldehyde maser by Takami and Shimizu (1966). Becker (1963) compared transverse and longitudinal ladder types and found no difference in their focusing effect.

Helmer et al. (1960) showed that a state separator of non-uniform cross-section is preferable to a uniform one. If A_1 and A_2 are the entrance and exit cross-section areas of the state separator respectively, and Ω_1 and Ω_2 are the solid angles of capture occupied by the molecular trajectories, averaged over A_1 and A_2 , then

$$A_1 \Omega_1 = A_2 \Omega_2$$

2.1

Thus a separator whose exit area is larger than its entrance area narrows the angular spread of the molecular trajectories.

The results from the experimental work by Becker (1963) shows the tapered transverse ladder state separator requires less beam flux than the parallel one to reach oscillation threshold at the same voltage. This advantage of the tapered state separator was supported by Smart (1973).

The tapered transverse ladder separator was chosen for the present investigation, not only from qualitative considerations of efficiency, but also because of its simple construction.

The electrode assemblies can be made as two units whose relative positions can be easily altered. The tapered state separator design is discussed in Section 2.5.

2.4 Theory of the Transverse Ladder Separator

In Section 1.3 it was seen that the force which acts on a molecule perpendicular to its line of flight, is proportional to $E\partial E/\partial y$ (or $\partial E^2/\partial y$) in the region of quadratic Stark interaction.

A theoretical expression for $\partial E^2/\partial y$ was calculated by Becker (1963) after an experimental investigation of the potential distribution for one half of a transverse ladder separator, made from plates with rounded corners in an electrolytic tank. Fig. 2.7a shows the electrodes with diameter a , equally spaced by the distance d . In the region $y > 0$, suppose E_x and E_y represent the electric field components in the directions of the x-axis and y-axis respectively. The electric field in this region is certainly periodic with period $2d$. In this case the effective force on a molecule passing near the electrode is proportional to the average value of $\partial E^2/\partial y$ defined by

$$\frac{\partial E^2}{\partial y} = \frac{1}{2d} \int_0^{2d} \frac{\partial E^2(x)}{\partial y} \partial x \quad 2.2$$

The electric field components E_x and E_y are given by

Becker

$$E_x = E_1 \exp(-\pi y/d) \sin(\pi x/d) + E_3 \exp(-3\pi y/d) \sin(3\pi x/d) + \dots \quad 2.3$$

$$E_y = E_1 \exp(-\pi y/d) \cos(\pi x/d) + E_3 \exp(-3\pi y/d) \cos(3\pi x/d) + \dots \quad 2.4$$

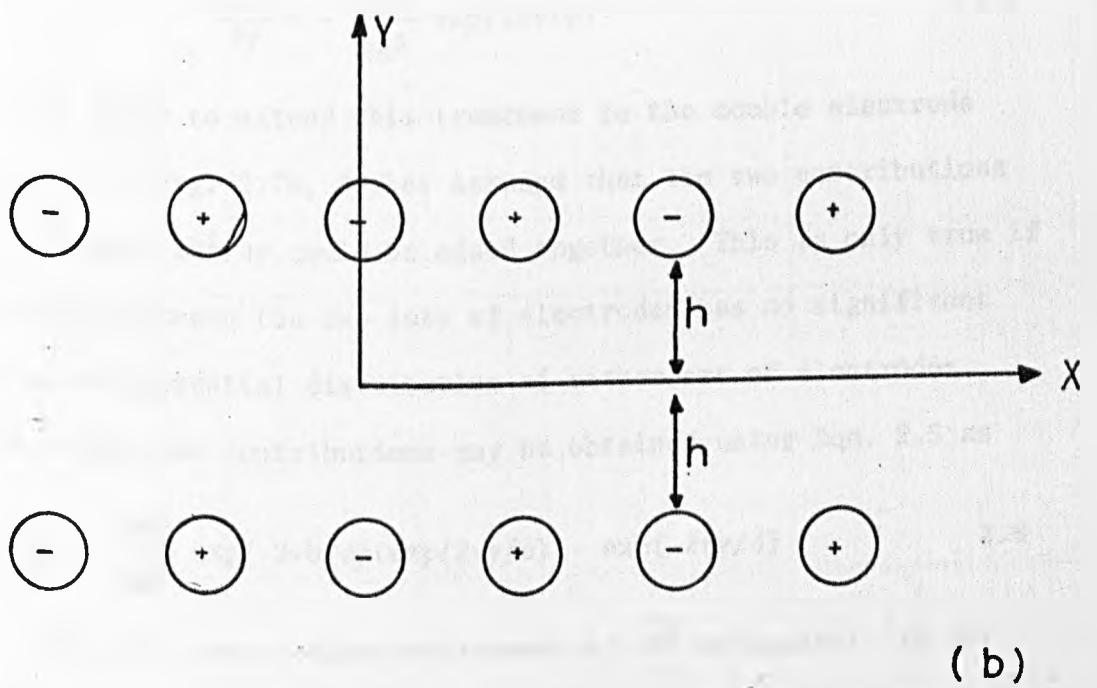
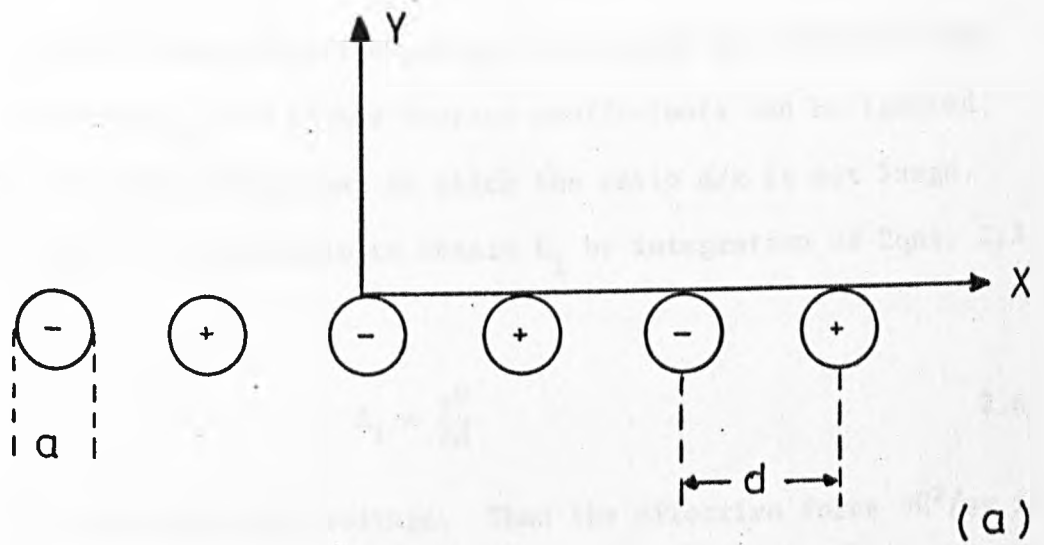


Fig-2-7(a) Model for one transversal ladder electrode assembly

(b) Model for the transverse ladder separator

Substituting Eqns. 2.3 and 2.4 in 2.2 gives

$$\overline{\frac{\partial E^2}{\partial y}} = -(2\pi/d)E_1^2 \exp(-2\pi y/d) - (6\pi/d)E_3^2 \exp(-6\pi y/d) \quad 2.5$$

Becker found from the measured potential distribution the terms involving E_3 and higher Fourier coefficients can be ignored for an electrode arrangement in which the ratio d/a is not large. In this case it is possible to obtain E_1 by integration of Eqns. 2.3, 2.4:

$$E_1 = \frac{\pi V}{2d} \quad 2.6$$

where V is the electrode voltage. Then the effective force $\partial E^2/\partial y$ is

$$\frac{\partial E^2}{\partial y} = -\frac{\pi^3 V^2}{2d^3} \exp(2\pi y/d) \quad 2.7$$

In order to extend this treatment to the double electrode arrangement of Fig. 2.7b, Becker assumed that the two contributions to the averaged $\partial E^2/\partial y$ could be added together. This is only true if the distance between the two sets of electrodes has no significant effect on the potential distribution of either set of electrodes. The sum of the two contributions may be obtained using Eqn. 2.5 as

$$\frac{\partial E^2}{\partial y} = \frac{\pi^3 V^2}{2d^3} \exp(-2\pi h/d) \{ \exp(2\pi y/d) - \exp(-2\pi y/d) \} \quad 2.8$$

Fig. 2.8 shows calculated curves of $\overline{\partial E^2/\partial y}$ against y/h for four values of h . These curves are of considerable design interest. For large h/d , the focusing effect is concentrated near the plane of the electrodes and little or no force is exerted on a molecule travelling through the central region of the separator. Such a separating system would allow a large number of molecules in the lower state to pass through it without removing them from the molecular beam. However, a separator with $h < d/2$ does have an effect on molecules travelling close to its centre plane.

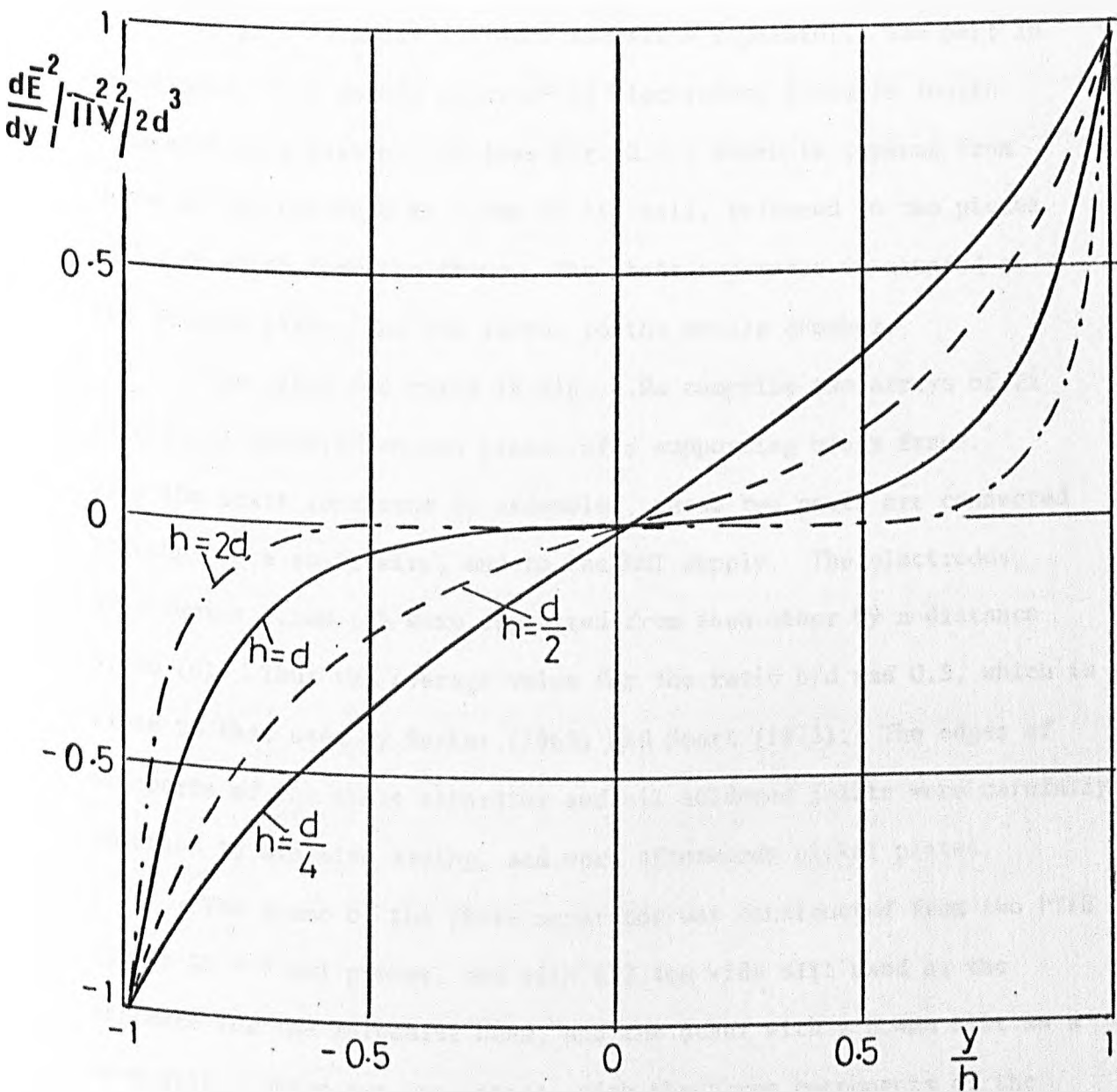


Fig. 2.8 Relative focusing force plotted for four geometries
(after Becker, 1963)

2.5 Tapered Transverse Ladder State Separator Design

The geometry of the electrode structure for both state separators used in the present work are identical.

Fig. 2.9a shows a dismantled state separator. The part in the middle, is a double array of 22 electrodes, 8.6cm in length separated by a distance $2h$ (see Fig. 2.7), which is tapered from 0.8mm at its entrance to 4.8mm at its exit, soldered to two pieces of brass which form the frame. The state separator is mounted on the skimmer plate, and the latter to the nozzle chamber.

The other two parts in Fig. 2.9a comprise two arrays of 21 electrodes soldered on two pieces of a supporting brass frame. When the state separator is assembled, these two parts are connected together by a small wire, and to the EHT supply. The electrodes, of diameter 1.6mm (t) were separated from each other by a distance 3.2mm (d). Thus the average value for the ratio h/d was 0.5, which is close to that used by Becker (1963) and Smart (1973). The edges of all parts of the state separator and all soldered joints were carefully smoothed to minimise arcing, and were afterwards nickel plated.

The frame of the state separator was constructed from two PTFE (105 × 35 × 7 mm) pieces, one with a 2.4mm wide slit used as the entrance for the molecular beam, and the other with a 6.4mm slit as a beam exit. These two insulators, with the three components of the electrode system, were assembled to give the double ladder state separator shown in Fig. 2.9b. The slit widths in the PTFE insulators were made equal to the separation of two planes of the state separator electrodes (taken from centre to centre) at points of entrance and exit of the molecular beam, in order to scatter all molecules whose trajectory outside the state separator is close to the electrodes (Fig. 2.10). This was important because this region of electric field can focus lower

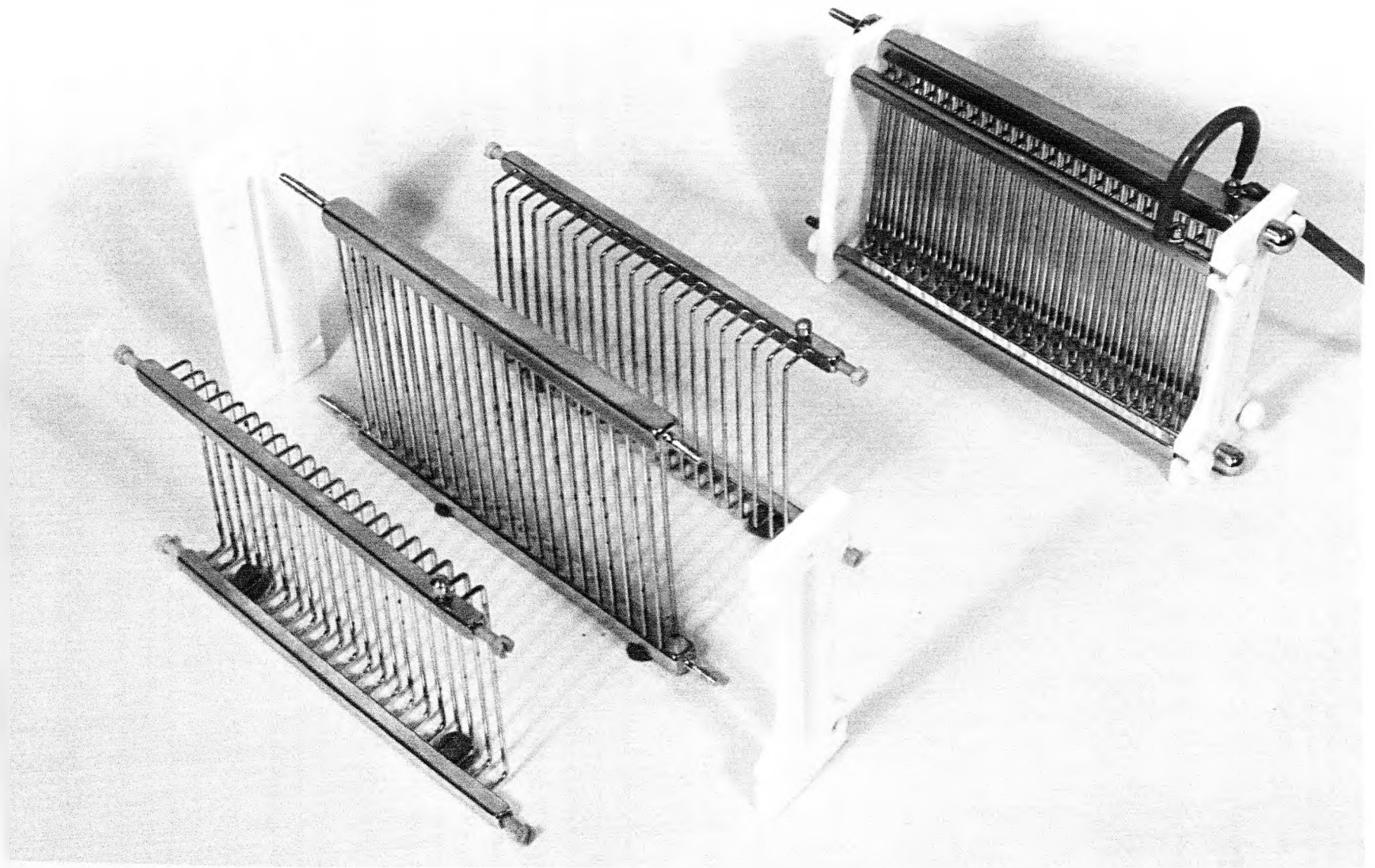


FIG. 2.9 THE STATE SEPARATOR

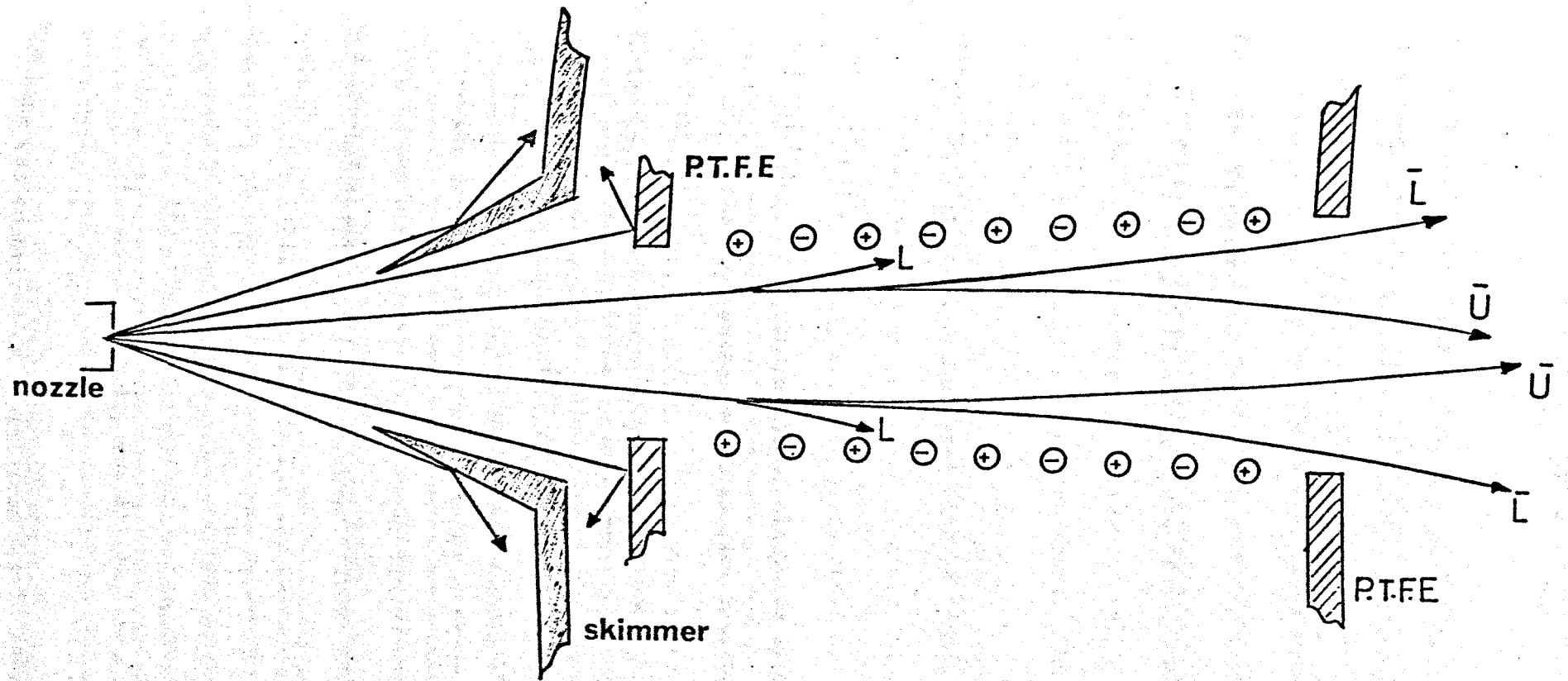


Fig-2-10 Schematic diagram of molecular beam system

state molecules into the microwave cavity (Al-Amiedy and Lainé, 1978). This would clearly be undesirable for achieving a low threshold state separator voltage for maser oscillation.

2.6 The Vacuum Chambers

Figs. 2.11, 2.12 and 2.13 are front, back general view and block diagram of the maser system respectively. Fig. 2.14 shows an engineering drawing of the vacuum chambers. The three vacuum chambers are mounted horizontally on an aluminium bench, constructed from aluminium 'U' channel and covered with an aluminium sheet.

The main chamber consisted of a 42cm high, 50cm internal diameter rolled non-magnetic stainless steel cylinder, with 0.4cm wall thickness. An arrangement of six ports fabricated from stainless steel tubes was used where two of 15.24cm internal diameter mated with the nozzle chamber. Two cylinders of 27cm internal diameter were fitted with 34cm diameter, 2.54cm thick perspex discs, one on the front carried the 'K' band waveguides to the Fabry-Perot microwave cavity, and the electrical lead-throughs for thermal tuning (Section 2.1.4) and to the coils inside the vacuum chamber to produce a known magnetic field in the maser. The other perspex window was mounted on the back and carried the ionization gauge head, pirani gauge and the rotary shaft vacuum seal. Two flanges for the tubes of 6.35cm internal diameter were fitted with perspex discs 13cm diameter, 1cm thick. Each one carried the electrical lead-through to the state separator from the EHT power supply. The top was fitted with a stainless steel lid (57cm diameter, 2.54cm thick) and carried three liquid nitrogen traps. The base was comprised of a stainless steel disc, 50cm outer diameter and 22.86cm internal diameter, which supported a nine inch diffusion pump.

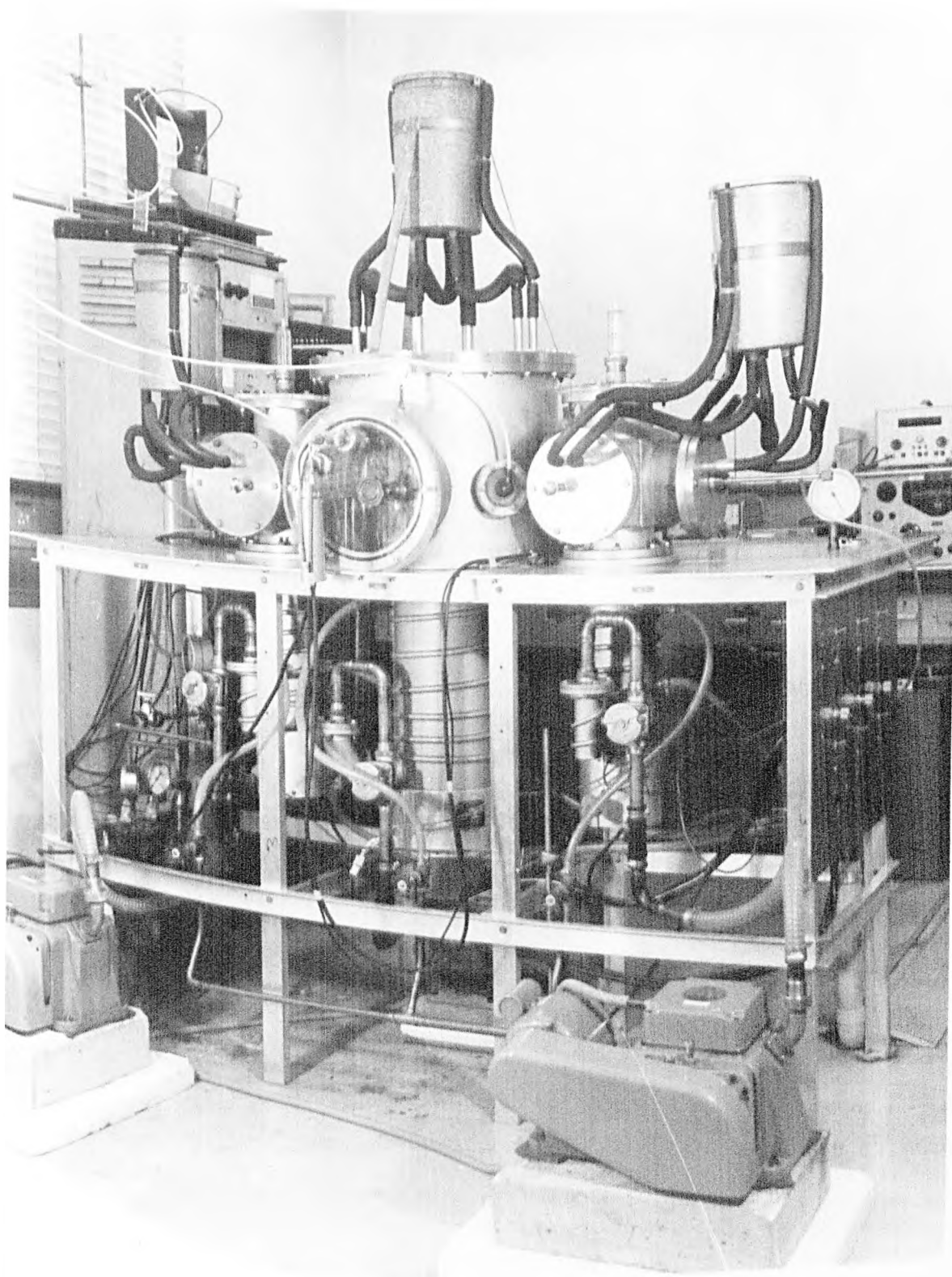


FIG. 2.11 GENERAL VIEW OF THE MASER



FIG. 2.12 GENERAL VIEW OF THE MASER

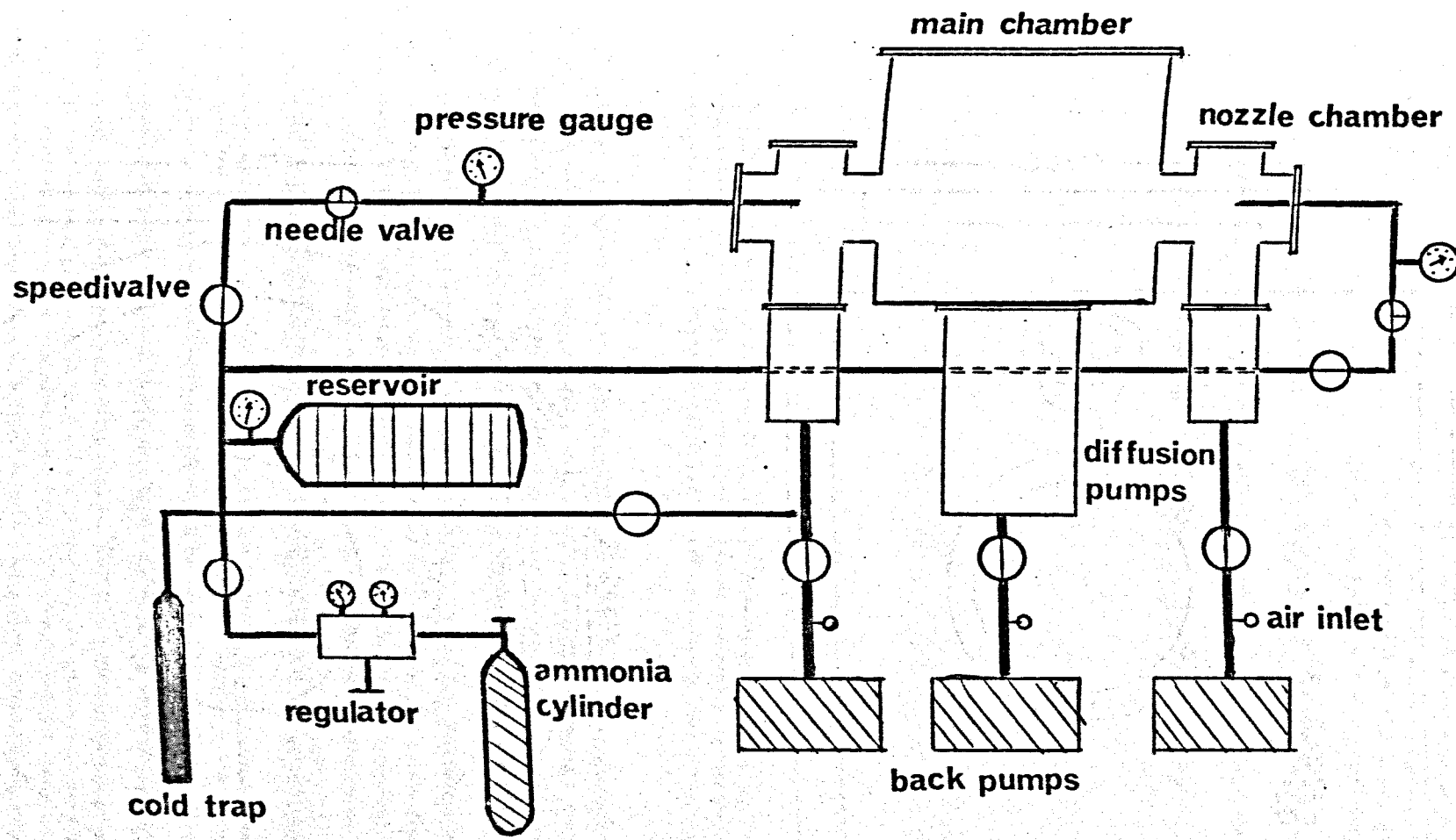


Fig-2-13 Block diagram of maser vacuum assembly and ammonia supply

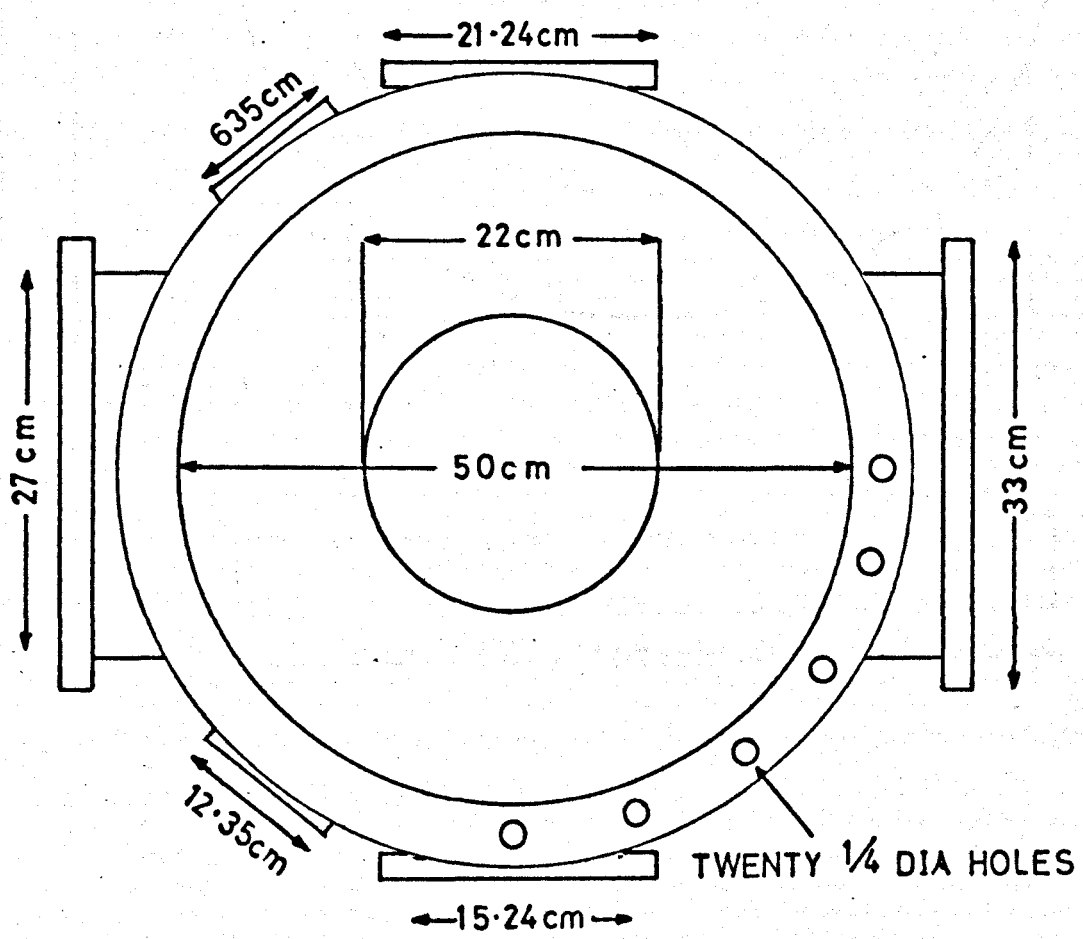
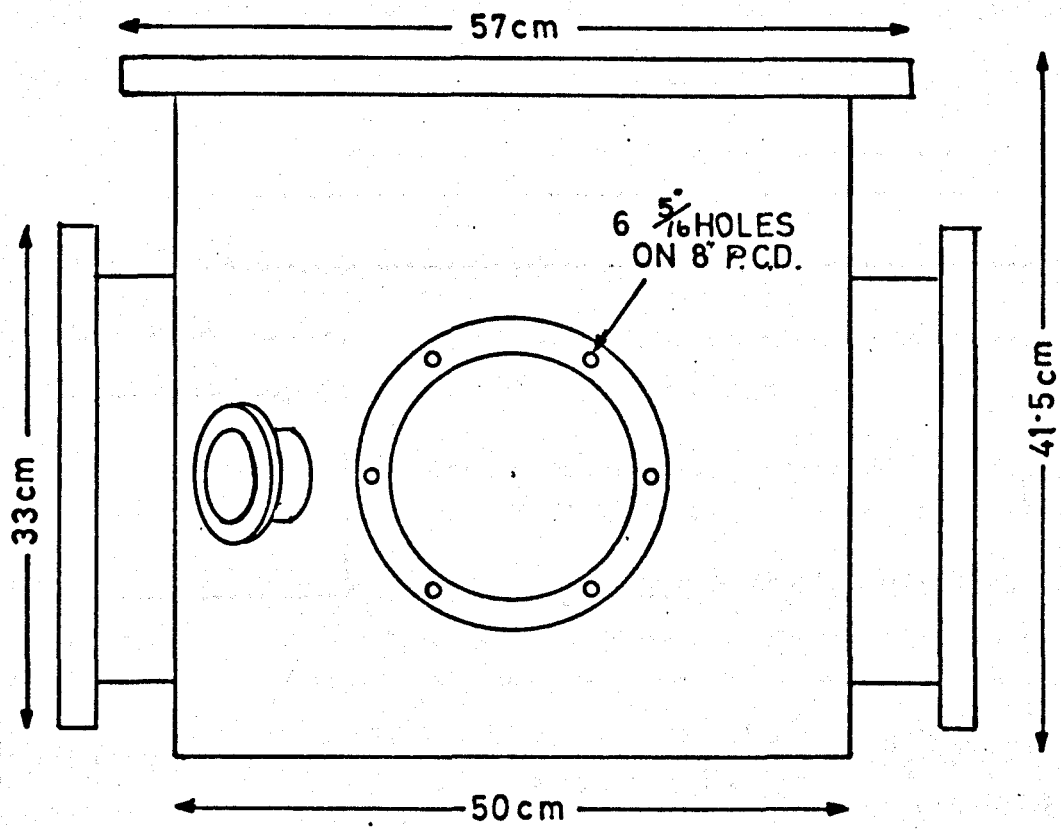


FIG. 2-14 ENGINEERING DRAWING FOR THE MAIN CHAMBER.

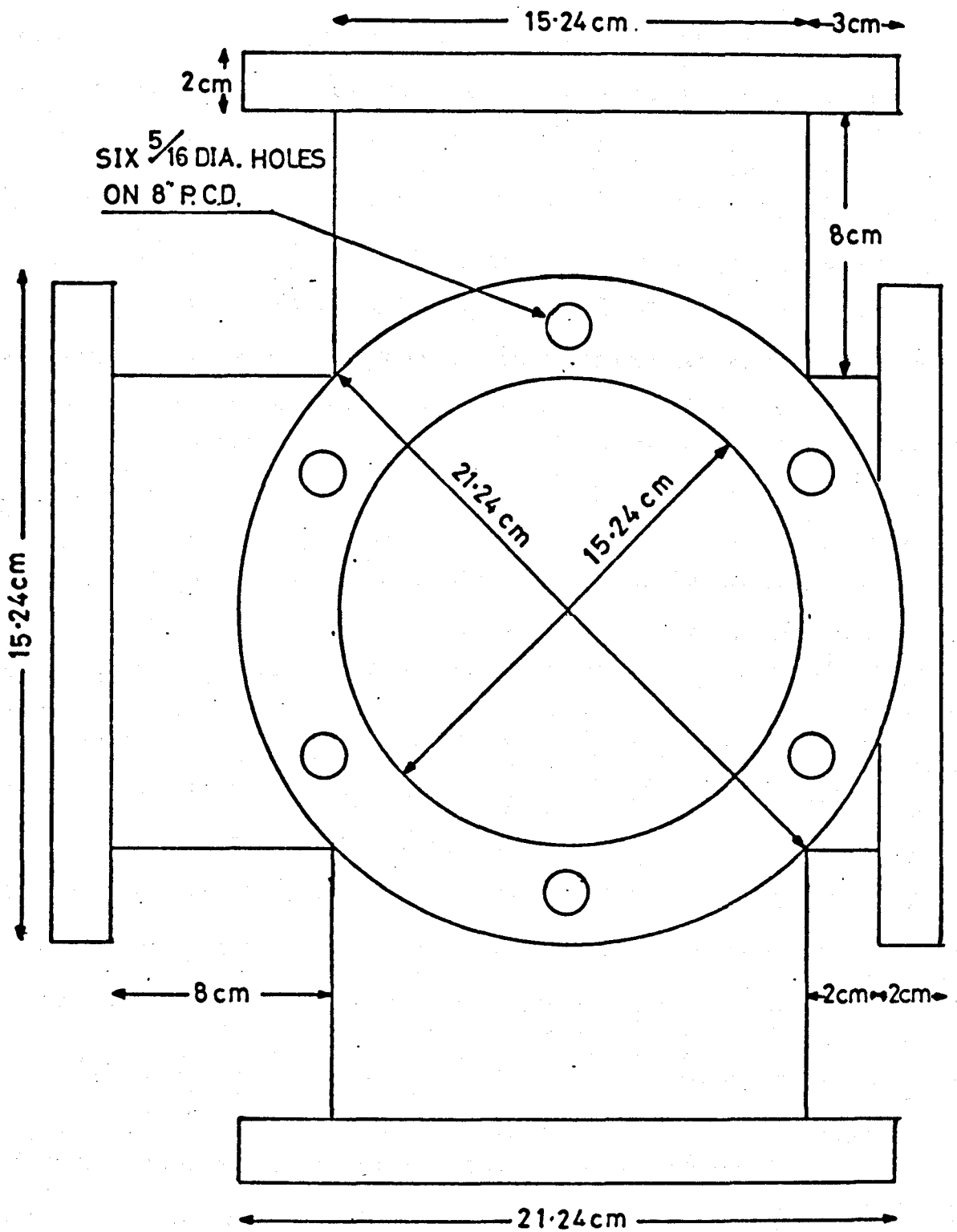


FIG 2-14 ENGINEERING DRAWING FOR THE NOZZLE CHAMBER.

Each nozzle chamber was a six-port arrangement fabricated from stainless steel tubes of 15.24cm internal diameter, 0.4cm wall thick, all joined to a stainless steel box of dimensions 18 × 18 × 18 cm. One port mated with the main chamber, and the opposite port was closed by a stainless steel flange which carried both a liquid nitrogen trap and the ammonia supply to the nozzle. The other two horizontal ports were closed by stainless steel flanges, each of which carried a liquid nitrogen trap and a mechanical lead-through for adjustments to the skimmer width. The top port was fitted with a 34cm diameter, 1.5 thick perspex window which carried an ionization gauge head to monitor the chamber pressure, and the bottom port flanged onto a six inch diffusion pump.

All vacuum connections were sealed with rubber 'O' rings.

2.7 Maser Vacuum Assembly

A three chamber vacuum system was adopted for the double beam ammonia maser, in which the two state separators and the open cavity were situated in a main vacuum chamber, and each nozzle was housed in a smaller chamber (nozzle chamber).

The pumping arrangement is shown in Figs. 2.11 and 2.13. One Metrovac type 093C nine inch diameter diffusion pump was mounted below the main chamber, and a six inch Edwards oil diffusion pump Model F 603, below each nozzle chamber. Each diffusion pump was charged with an appropriate quantity of 704 silicone oil which has a limiting vapour pressure of 10^{-7} torr. The nine inch and the two six inch diffusion pumps were backed by three N.G.N. Model PSR6 rotary pumps. The three rotary pumps were vacuum coupled to the equipment by means of one inch flexible couplings to minimise mechanical vibration.

To further reduce vibration the three pumps were mounted on a concrete bed of dimensions 50 × 35 × 12 cm.

Liquid nitrogen cooled surfaces were provided in each chamber to assist in pumping the ammonia gas by freezing it out as solid ammonia. Three high density polystyrene reservoirs, each of four litres capacity, stored liquid nitrogen outside the vacuum chambers, as shown in Fig. 2.11. A 0.25 inch copper tube carried the liquid nitrogen from the reservoir into the vacuum chamber and back again, thus passed twice through the vacuum flange. An 8cm length of thin walled nickel silver tube was employed as the connection between the copper tube and the vacuum flange, because of its low thermal conductivity. This prevents the 'O' rings from cracking due to repeated cooling cycles. Silver solder was used for all joints subjected to thermal cycling.

The main chamber was fitted with three such traps, connected all with one reservoir. Fig. 2.15a shows the three traps. The middle one was constructed from four copper tubes of two inch diameter connected together by four copper elbows, and the other two from $\frac{1}{2}$ inch copper tube in a coil shape around each state separator, to freeze the ammonia molecules which are deflected out by the state separator. Three traps made from $\frac{1}{2}$ inch diameter copper tube and shaped into coils were fitted into each nozzle chamber (Fig. 2.15b) to freeze the remaining ammonia molecules in the chamber, and thus maintain low pressures in the region between the nozzle and skimmer so as to minimize beam scattering.

The pressure in the main and nozzle chambers were monitored by Edwards IG6G ionization gauge heads operated by Edwards control unit Model ION7. Under normal operating conditions without prior exposure to atmospheric pressure, main chamber pressure of 2×10^{-6} torr could be reached after about two hours of pumping with the diffusion pumps,

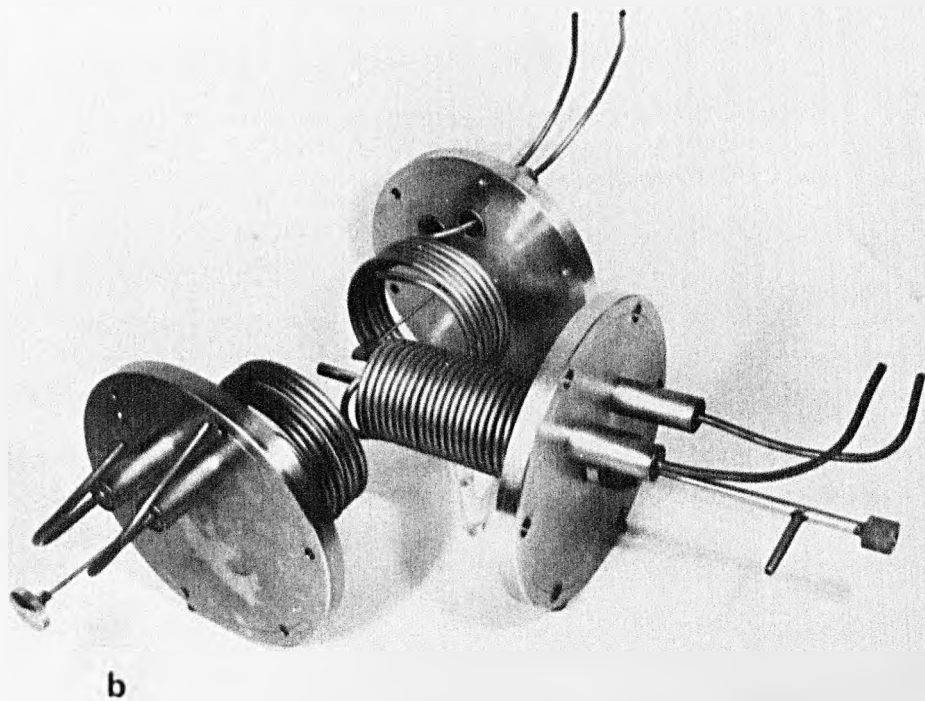
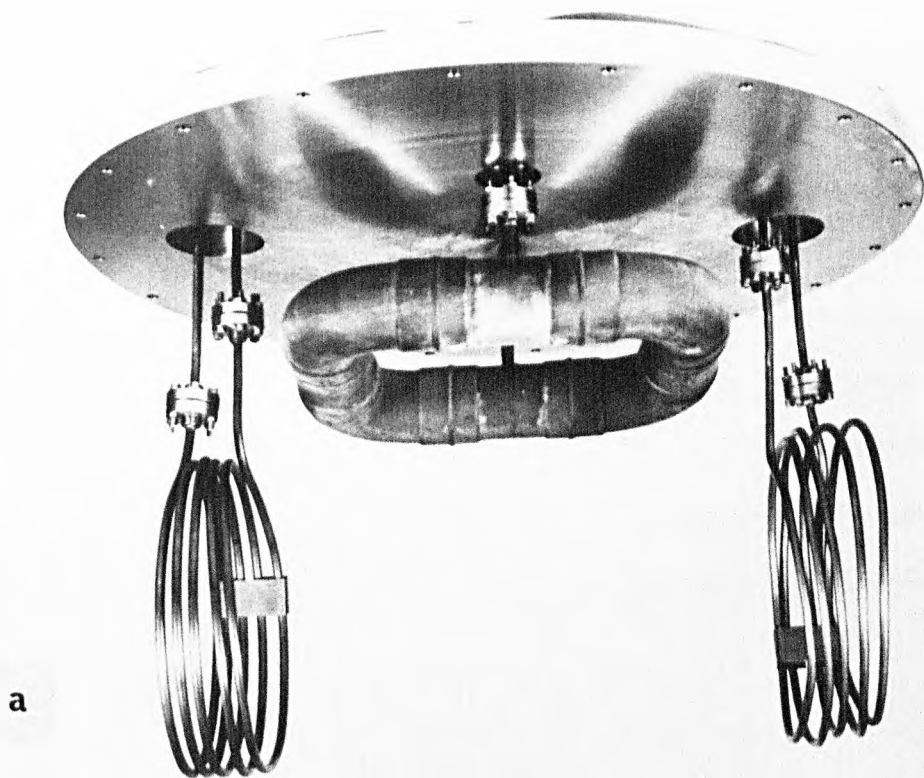


Fig. 2.15 LIQUID NITROGEN TRAPS,
(a) FOR THE MAIN CHAMBER
(b) FOR THE NOZZLE CHAMBER

and 1.5×10^{-5} torr for the two nozzle chambers. However, if the maser and its components had been exposed to the atmospheric pressure for some days it sometimes took as much as ten hours of pumping to reach this pressure. The pressure reduces to 8×10^{-7} torr for the main chamber and 9×10^{-6} torr for the nozzle chambers, when the liquid nitrogen traps are charged. The main chamber rises once more to the nearly constant pressure of 1.5×10^{-6} torr when a molecular beam of ammonia is introduced into the system from both nozzles, even for 760 torr gas pressure behind the nozzle. However, for the nozzle chamber, the pressure rises to 1.5×10^{-4} and 1.5×10^{-5} torr when the nozzle pressure is 760 and 80 torr respectively.

2.8 The Ammonia Supply

Fig. 2.16. shows the arrangement of the ammonia source, control valves, trap, reservoir, and pressure gauges. The source of the ammonia was a lecture size cylinder of anhydrous liquid ammonia which was controlled by a pressure regulator valve adjusted to an output pressure of a little above that of the atmosphere. Purification of the ammonia is carried by freezing it in a trap cooled with liquid nitrogen. Impurity gases which have not condensed are then pumped away using the same N.G.N. PSR6 pump as used to back the diffusion pump. The trap is warmed and the ammonia is allowed to expand into the reservoir. A dial gauge with a range 0 - 760 torr was used to monitor the gas pressure in the reservoir. The flow from the reservoir to each nozzle was controlled by hand valves and a fine needle valve. The needle valves were coupled to the nozzle holders by thick walled polyethylene flexible tubes. The pressures behind the two nozzles were measured by gauges in the range 0 to 760 torr. The block diagram of the ammonia supply is shown in Fig. 2.13.

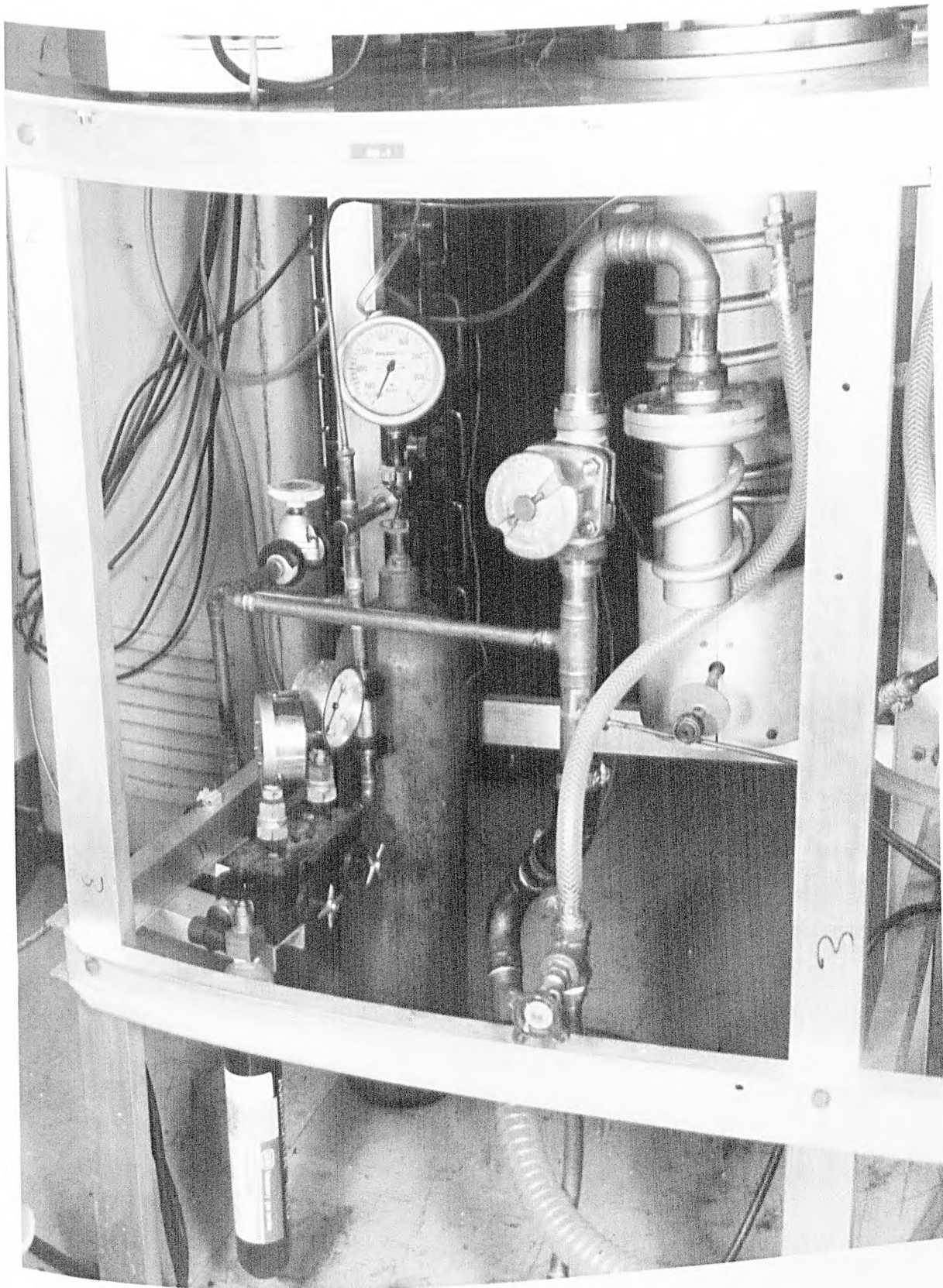


FIG. 2.16 GENERAL VIEW OF THE AMMONIA SUPPLY

2.9 Nozzle and Skimmer Design

The considerations for optimum skimmer design and the nozzle diameter chosen, are discussed with some exploratory experiments in Section 3.4. Here, only the construction of the nozzle and skimmer are described.

The nozzle was constructed from a 380mm long, 10mm diameter, 2mm thick stainless steel tube. One end was fitted with a perspex window sealed by a rubber 'O' ring, and was used for alignment purposes. The other end was machined such that a brass disc 6mm diameter may be soldered into it, into which the nozzle hole was drilled.

The ammonia supply was introduced through a 100mm long stainless steel tube soldered on the side of the nozzle holder tube near the perspex window. The needle valve was coupled to the nozzle holder tube by thick walled flexible polyethylene tube.

The adjustable skimmer, shown in Fig. 2.17, was constructed from two pieces of brass forming the lips, the surfaces of which were ground as sharp as possible and highly polished. Each lip was mounted on a brass strip of dovetail cross-section which fitted into slots made in a stainless steel plate. This design allowed the jaw to slide to and fro with respect to the other jaw. The outside and inside angles of the lip were 45° and 35° respectively.

2.10 The Skimmer and State Separator

The skimmer plate, which closed off the nozzle vacuum chamber from the main chamber, carried the skimmer jaws and also supported the state separator. Slotted holes were provided in the skimmer plate to bolt the state separator onto it.

The skimmer plate was fixed on a 100mm long cylinder, 139mm diameter, which was smaller than the nozzle chamber port to give

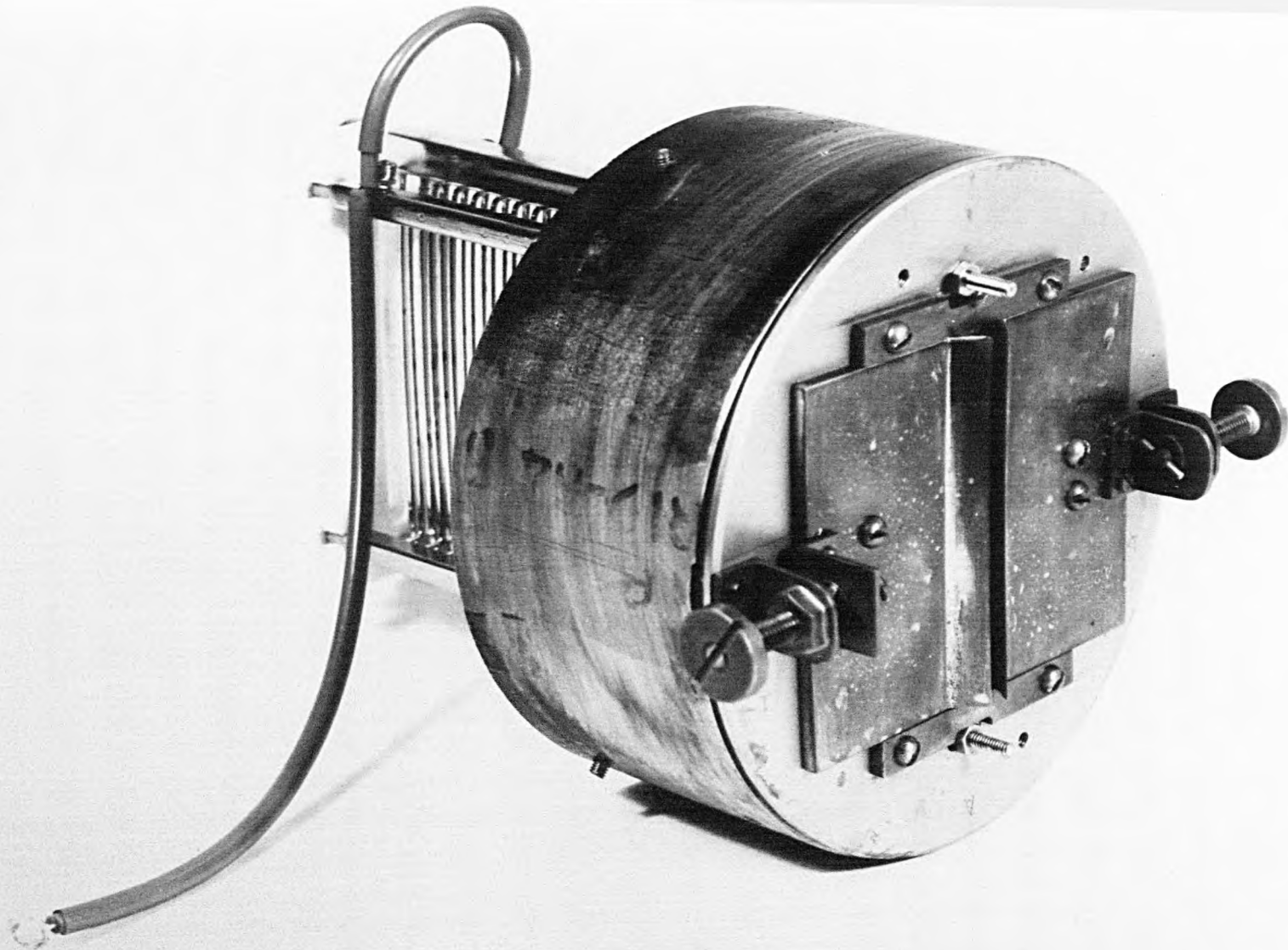


FIG. 2.17 STATE SEPARATOR AND SKIMMER

sufficient clearance for movement in three dimensions for the whole assembly, in order to align it with the centre of the cavity.

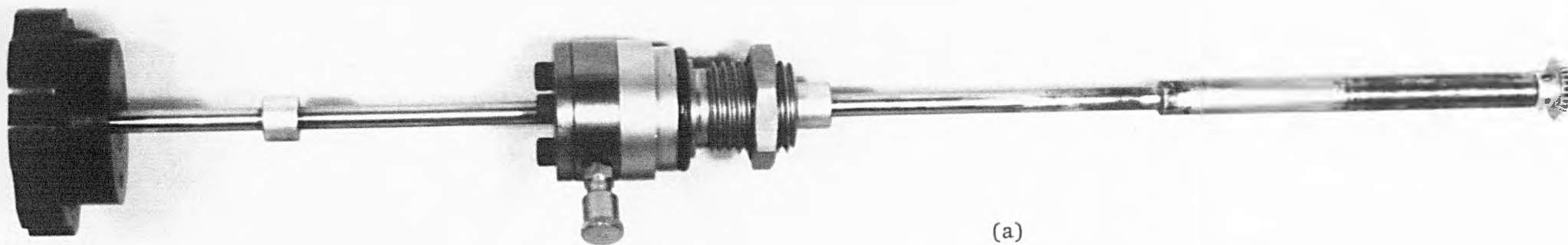
The assembly is shown in Fig. 2.17.

2.11 The Mechanical and Electrical Lead-Throughs

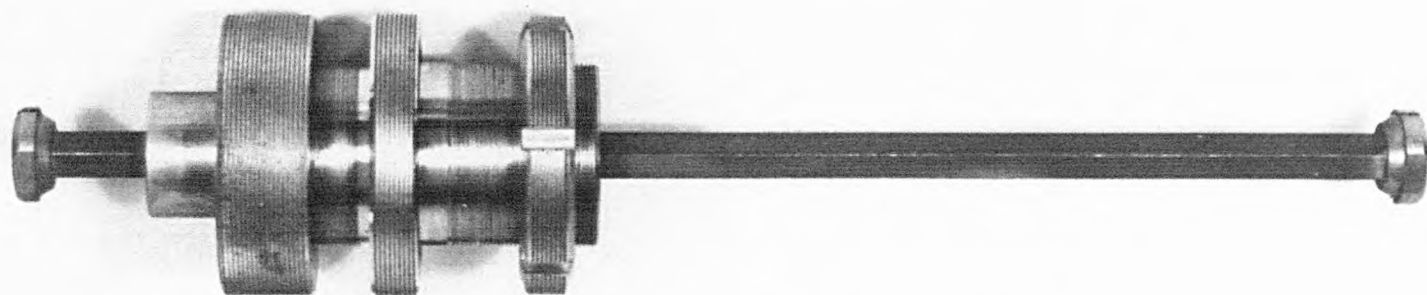
Fig. 2.18 shows two types of the mechanical lead-throughs; (a) is an Edwards rotary shaft vacuum seal used for mechanical cavity tuning and skimmer width adjustment; (b) is a brass unit which provides for a vacuum seal and vacuum chamber access for the pirani and ionization gauge heads, and for the waveguide lead-throughs. The waveguides were fitted with cylindrical barrels where they passed through brass holders and were provided with two pressure-relief mechanisms on each waveguide which were accessible from outside the vacuum chamber. This was necessary since atmospheric pressure on the waveguides could bend the coupling mirror of the cavity, and adversely affect its quality factor.

The electrical supply for the thermal tuning of the open cavity, the voltage between the two mirrors for Stark effect studies, and the current through the coils for magnetic field production within the maser vacuum chamber, were all provided for as follows. A groove of $10 \times 3 \times 0.5$ cm in dimensions was made on the outside face of the perspex window of the front port of the main chamber. The 24 copper pins were threaded through matching holes in the bottom of the groove. The groove with pins in position, filled with araldite epoxy resin, then provided a mechanically strong vacuum seal.

The EHT lead-through for the state separators were treated in the same way. The thermal tuning and the EHT lead-through are shown in Figs. 2.12 and 2.11 respectively.



(a)



(b)

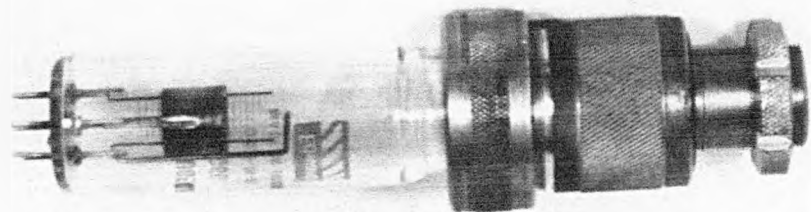


FIG. 2.18

(a) ROTARY VACUUM SEAL

(b) BRASS UNIT SEAL

CHAPTER THREE

THE MASER AS A SPECTROMETER

3.1 Introduction

Two different spectrometer designs have been employed in the experimental work described in this chapter.

At the beginning of the project, the work was concentrated on the improvement of the spectrometer resolution of the first already existing maser system, by changing from effuser-diaphragm to nozzle-skimmer combinations (Section 3.5) to achieve a high intensity molecular beam, and to use the system as an oscillator by reaching the oscillation threshold beam flux for the weaker intensity inversion lines of ammonia relative to $J=K=3$ such as $J=K=1$ and 2 , in a TEM_{001} open cavity mode. However, oscillation was not achieved with the line $J=K=1$, but was successfully obtained with the inversion line $J=K=2$ which oscillated for the first time in this system. But the improvement which resulted from the use of the nozzle-skimmer combination in the system employed as a spectrometer was sufficient for the observation of the weak field Stark effect with the $J=K=1$ inversion line (Section 3.7). Details of this spectrometer are described in the following section.

As a result of the partial success of obtaining maser oscillation with weaker spectral lines than $J=K=3$ in ammonia with this system and limited spectral resolution for Stark spectroscopy, a completely new system was designed, details of which have already been described in Chapter Two. This new maser, again operated with an open resonator, was used as an oscillator (Chapter Four) on the $J=K=1, 2$ and 3 lines of ammonia and in addition could be operated as a spectrometer with improved spectral resolution (Section 3.8 and 3.9).

3.2 The First Spectrometer

The main vacuum chamber was an aluminium bronze casting, in the shape of a rectangular box of dimensions approximately 450 × 200 × 200 mm. The chamber was sealed on the outside surface with Araldite and on the inside surface with silicone varnish. It was fitted with a brass lid, which carried two liquid nitrogen traps, and closed the top of the box. Two ports on the front of the box were closed by brass flanges, one of which carried the two waveguides which coupled with the cavity. On the back of the box one panel was machined flat, and carried electrical and mechanical lead-throughs. All connections were sealed with rubber 'O' rings. All the nitrogen traps were made with a single continuous coil of copper tubing, to which copper plates were attached. One end of the box mated with the nozzle chamber, and the other was closed by a perspex window which carried the electrical lead-throughs to the cavity.

The nozzle chamber was a four-port arrangement constructed from brass tube. One port mated with the main chamber. At the opposite end a smaller port, closed by a flange which carried a mechanical lead-through, enabled longitudinal movement of the nozzle from outside the vacuum chamber. The top of the nozzle chamber was closed by a flange which also carried a liquid nitrogen trap and, in addition, the ammonia supply line to the nozzle.

The pumping arrangement for the two chambers was provided by three Edwards type 203 two inch diameter diffusion pumps; two were mounted below the main chamber, and one below the nozzle chamber, which were charged with silicon 704 oil. Each diffusion pump was backed by a rotary pump; the two for the main chamber were two-stage Metrovac GRD1, but for the nozzle chamber a high speed PSR16 N.G.N. rotary pump was used. The reason for the use of a high speed rotary

pump in the nozzle chamber was because it was only the central part of the molecular beam from the source which was allowed to pass into the main chamber by the skimmer or the diaphragm-slit. If a high speed pump were not to be used scattering of molecules tend to spoil the overall vacuum, and thereby reduce the mean free path of the molecules in the beam.

The pressure in the main chamber was monitored by a combination of a pirani and an ionization gauge. A similar ammonia gas supply and purification arrangement to the one already described in Section 2.8 was used, except that this system operated with only one nozzle.

The transverse ladder state separator used in this system is shown in Fig. 3.1, and was constructed of brass rods and P.T.F.E. insulators. The distance between the electrodes (1.6mm diameter) was 3.2mm, separated by a distance $2h$ (see Section 2.4) which tapered from 1.6mm at its entrance to 4.8mm at its exit. The length of the state separator was 55mm.

Fig. 3.2 shows the cavity which consisted of 150mm diameter copper discs 12mm in thickness, with $\pm 3 \times 10^{-4}$ mm surface flatness (Smart, 1973). The cavity design was similar to that of the cavity described in Chapter Two. The microwave coupling and the cavity tuning mechanisms were also similar to those in Sections 2.1.3 and 2.1.4, thus the cavity tuning (Section 2.1.5) and the mode identification procedure (Section 2.1.6) were carried in the same way. The cavity was supported on and bolted to a rectangular frame, which in turn was bolted to the floor of the main chamber. This frame can be seen below the cavity in Fig. 3.3. This figure also shows the two waveguides which coupled to the cavity and passed through a flange on the front of the main vacuum chamber. A general view of the maser system is shown in Fig. 3.4.

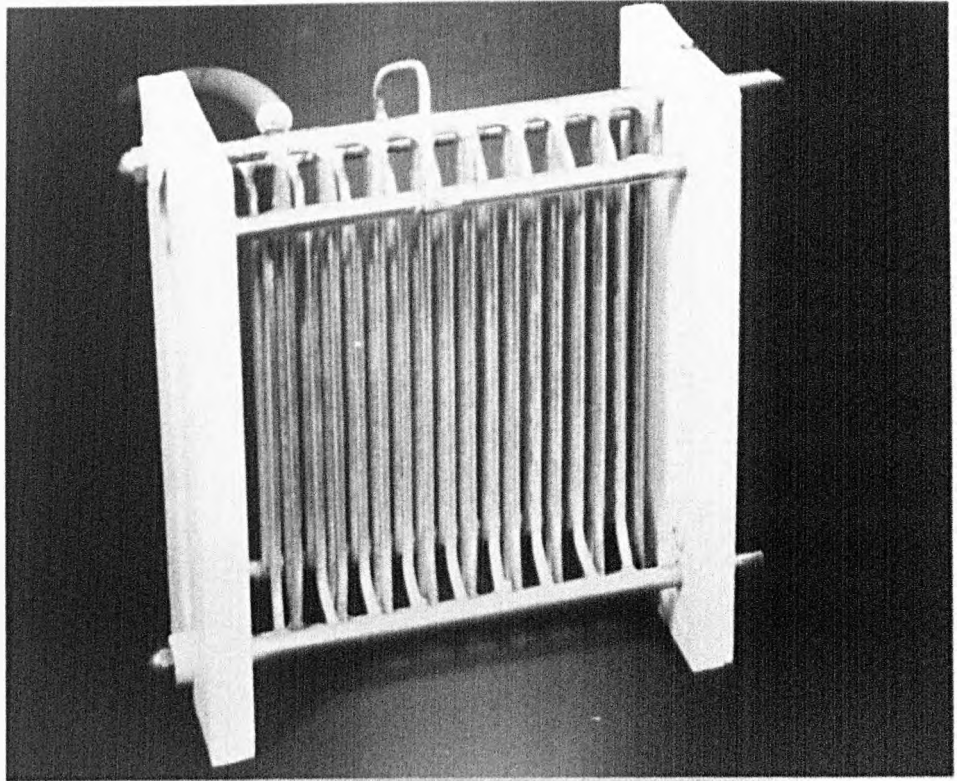


Fig. 3.1 THE STATE SEPARATOR

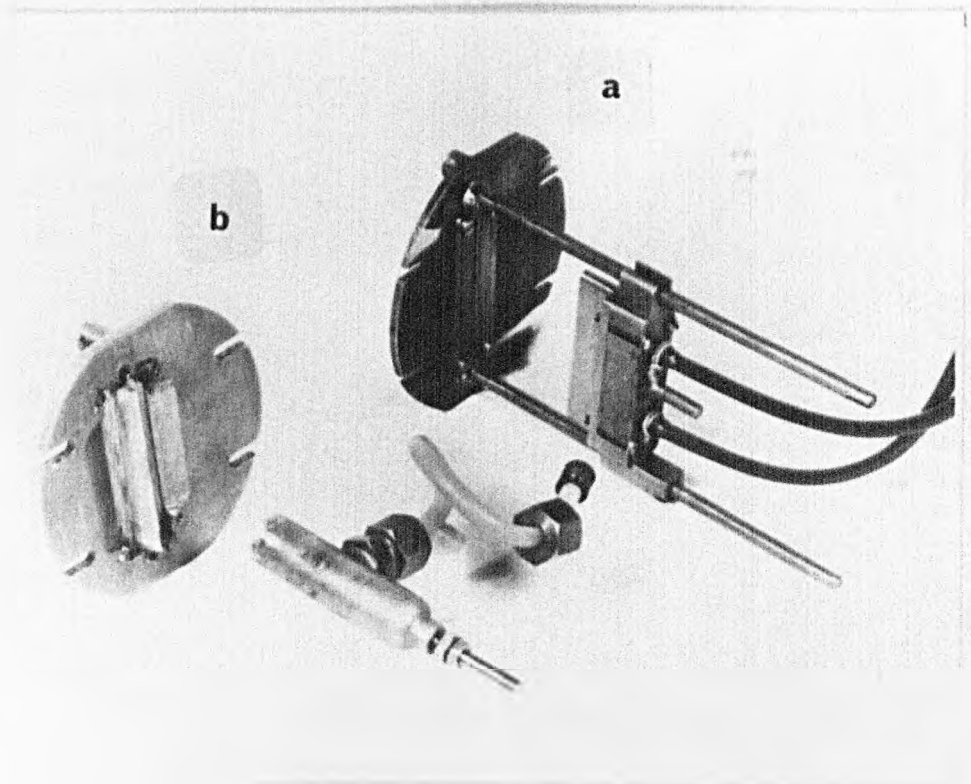


Fig. 3.13 (a) EFFUSER AND DIAPHRAGM
(b) NOZZLE AND SKIMMER

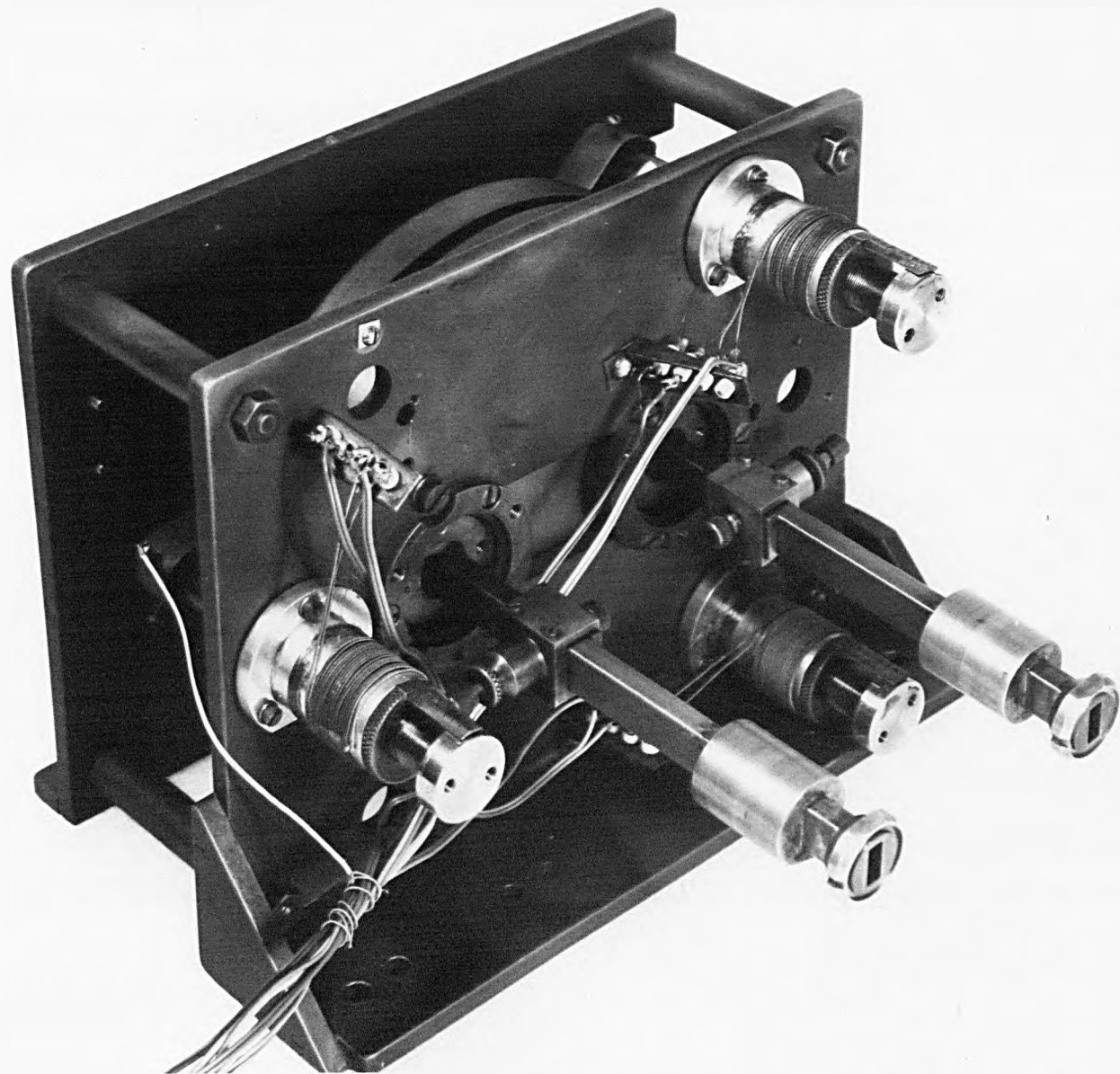


FIG. 3.2 THE CAVITY

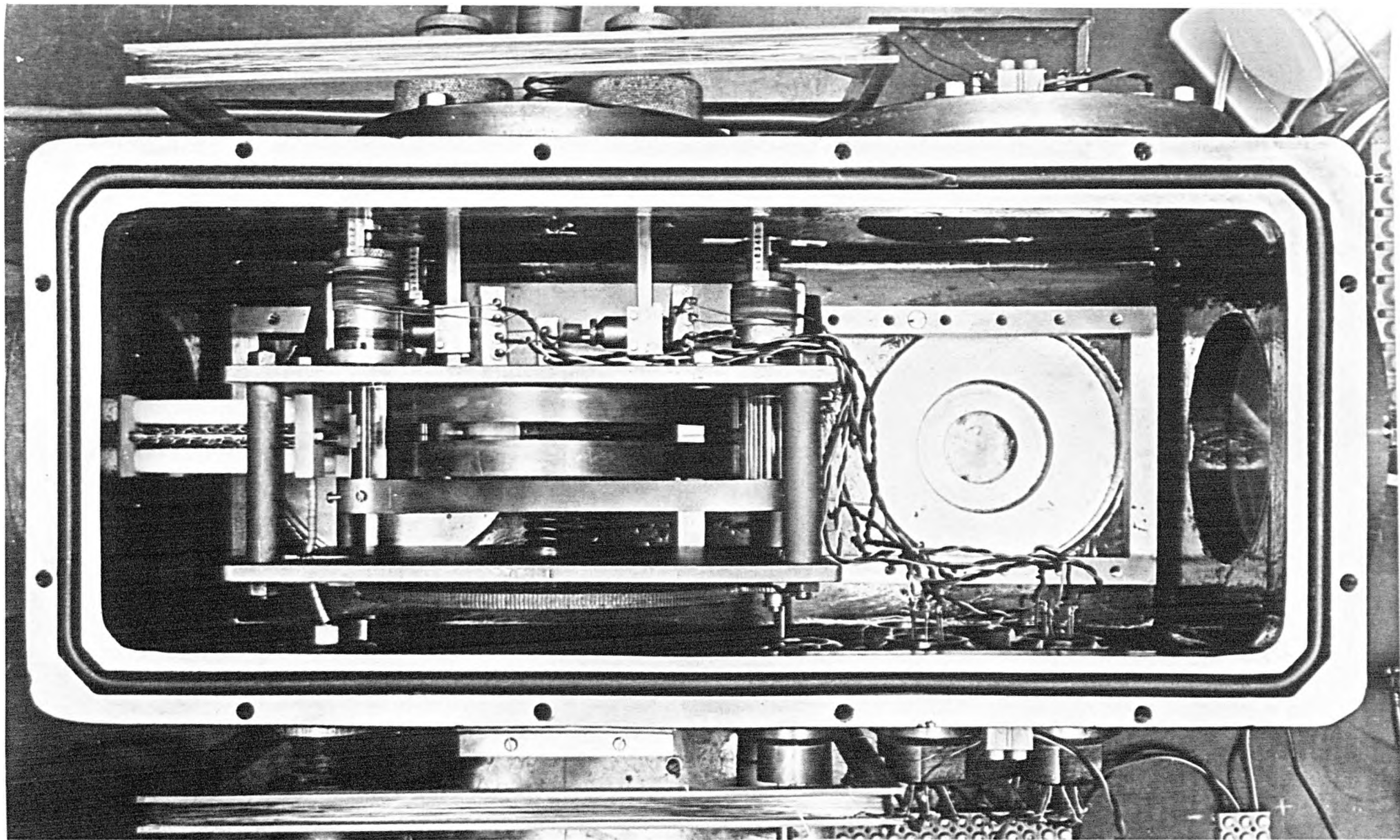


FIG. 3.3 THE MAIN CHAMBER

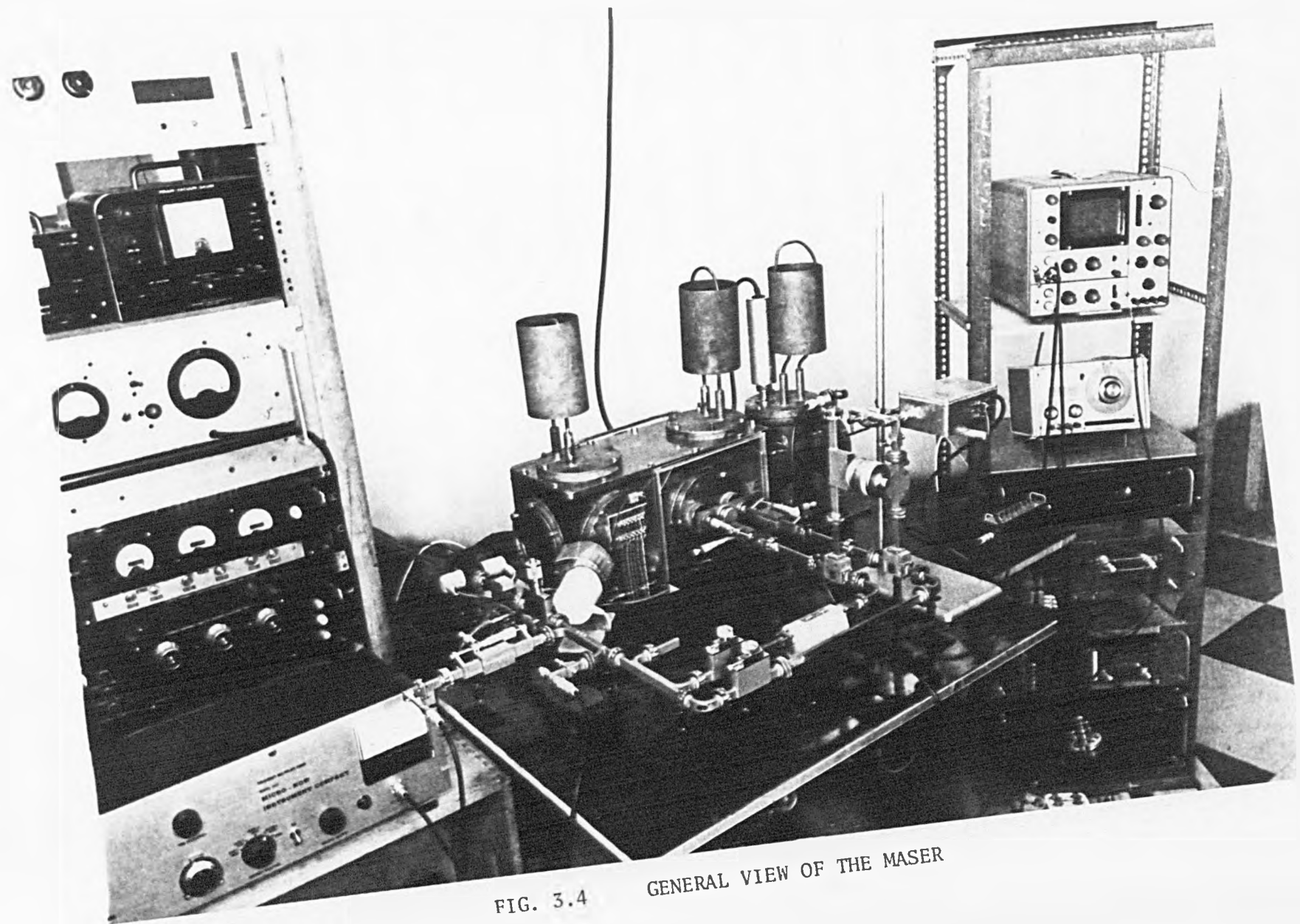


FIG. 3.4 GENERAL VIEW OF THE MASER

3.3 Hyperfine Structure of Ammonia Inversion Lines J=K=1,2,3

The selection rule 1.4 was given for the rotational inversion spectrum, but when $\Delta J = \Delta K$ the pure inversion spectrum of ammonia is obtained (Oraevskii, 1964). As a result of the hyperfine interactions in the molecule, a splitting of the inversion transitions into a number of hyperfine structure components occurs.

From the coupling scheme (Fig. 1.4) $F_1 = I_N + J$, where I_N is the spin vector of the nitrogen nucleus, and J is the vector of the total rotational angular momentum of the molecule. The quantum number F_1 can take values from $I_N + J$ to $|I_N - J|$. Since every value of F_1 corresponds to an energy level, it turns out that the degeneracy of energy levels due to spin orientation of the nitrogen nucleus and the molecule is removed by a factor equal to $(2I_N + 1)(2J + 1)$.

When the hyperfine interactions are taken into account, it is necessary to add the following selection rules to those given in 1.4 for the pure inversion spectrum:

$$\Delta F_1 = 0, \pm 1 \qquad \Delta F = 0, \pm 1 \qquad 3.1$$

Owing to the selection rules, every component of quadrupole hyperfine structure corresponding to a given value of F_1 is split into three times the number of different values taken by F , where it can take values from $F_1 + I$ to $|F_1 - I|$ through one, so that the number of different values of F is equal to the least of the numbers $(2I + 1)$ or $(2F_1 + 1)$. The total spin of the hydrogen nuclei I is equal to $\frac{3}{2}$ when K is a multiple of three, and equal to $\frac{1}{2}$ when K is not a multiple of three (Gordon, 1955). The nuclear spin of the nitrogen I_N is equal to one.

Kukolich (1967), used a two cavity maser spectrometer to measure the hyperfine structures of the $J=K=1, 2, 3$ lines of inversion

transitions of ammonia ($^{14}\text{NH}_3$) to try to explain some discrepancies between the previous theory and measurements. The tables of the results of $J=K=1,2,3$ line frequencies measured and calculated, and deviations are given by Kukolich (1967).

In the case of the inversion transition of ammonia $J=K=1$, $I_N = 1$ and $I = 1/2$, therefore F_1 can take three values and F can take the five values:

F_1	F
0	$1/2$
1	$3/2, 1/2$
2	$3/2, 5/2$

Fig. 3.5 is a schematic diagram of all energy levels, and associated transitions for the $J=K=1$ inversion line of the ammonia molecule. As it is clear from this figure, the main line is composed of eight hyperfine transitions from $\Delta F = 0, \pm 1$ and $\Delta F_1 = 0$, spread over a range of 56 kHz. The quadrupole satellites result from transitions $\Delta F_1 = \pm 1$ and $\Delta F = \pm 1, 0$, and thus there are ten possible transitions, five on each side of the main line (upper and lower frequency side). Two outer quadrupole satellites are approximately 1530 kHz above and below the main line frequency, and three inner quadrupole satellites are approximately 600 kHz above and below the main line frequency.

In the case of the inversion transition of $J=K=2$, F_1 can take three values and F six values:

F_1	F
1	$3/2, 1/2$
2	$5/2, 3/2$
3	$7/2, 5/2$

OUTER QUAD. (2 COMP.)	INNER QUAD. (3 COMP.)	MAINLINE (8 COMP.)	INNER QUAD. (3 COMP.)	OUTER QUAD. (2 COMP.)
$\Delta F_1 = -1$	$\Delta F_1 = +1$	$\Delta F_1 = 0$	$\Delta F_1 = -1$	$\Delta F_1 = +1$
$\Delta F = -1, 0$	$\Delta F = +1, 0$	$\Delta F = -1, 0$	$\Delta F = -1, 0$	$\Delta F = +1, 0$

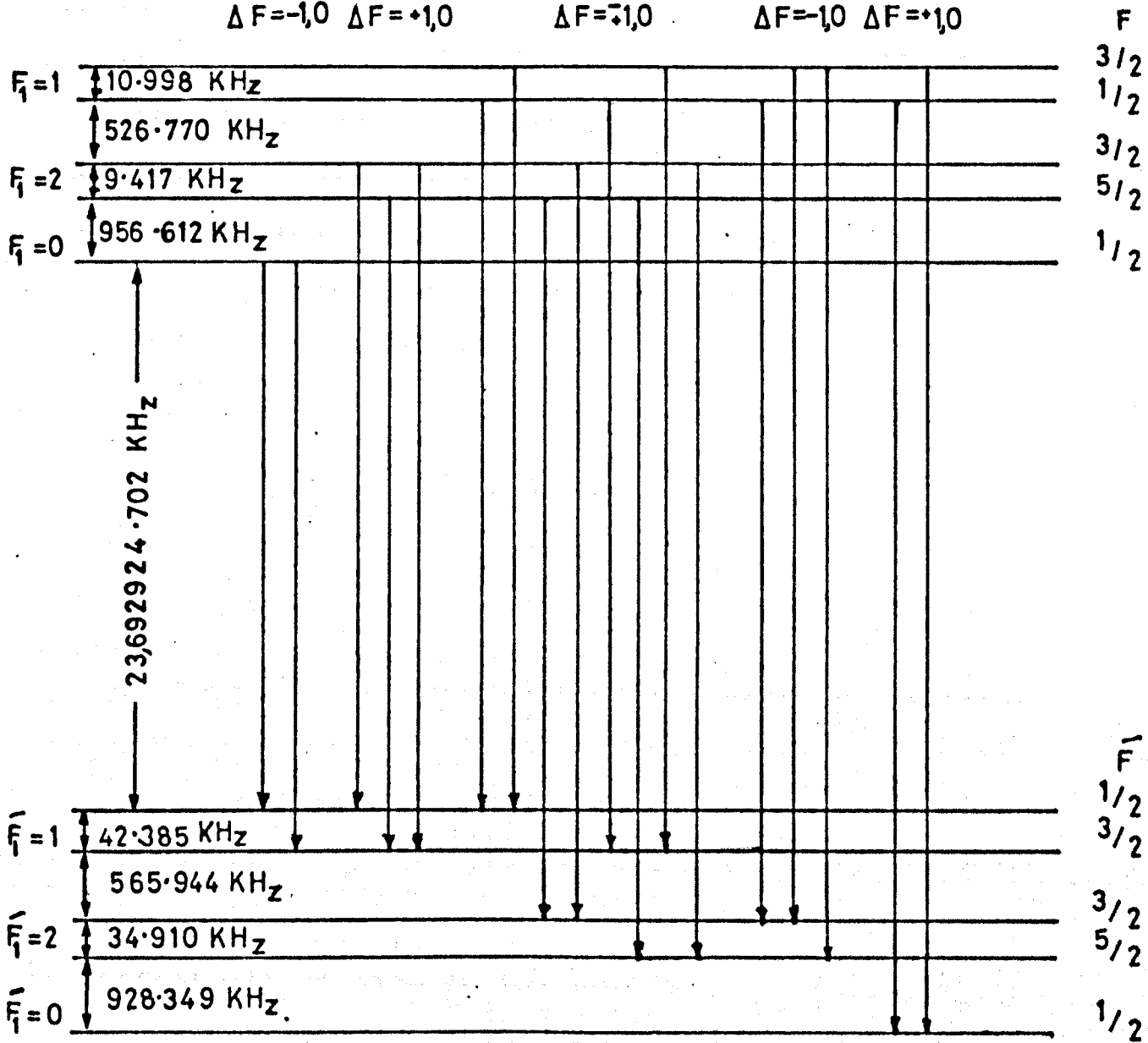


FIG. 3-5 SCHEMATIC DIAGRAM OF ENERGY LEVELS FOR $J=K=1$ INVERSION LINE OF AMMONIA MOLECULE.

For the $J=K=2$ (Fig. 3.6), the main line is composed of six transitions from $\Delta F_1 = \Delta F = 0$, to spread over a range 2 kHz. There are three magnetic satellites, approximately 42 kHz above and below the main line frequency arising from $\Delta F_1 = 0$ and $\Delta F = \pm 1$. Of the six quadrupole satellites on each side of the main line, three outer quadrupole satellites arising from $\Delta F_1 = \pm 1$, $\Delta F = \pm 1, 0$ transitions, are approximately 2058 kHz above and below the main line frequency, and the other three quadrupole lines (inner satellite lines) lie above 1296 kHz from the main line frequency.

In the case of the inversion transition $J=K=3$, $I = 3/2$, then F_1 can take three values and F twelve values:

F_1	F
2	$1/2, 3/2, 5/2, 7/2$
3	$3/2, 5/2, 7/2, 9/2$
4	$5/2, 7/2, 9/2, 11/2$

Fig. 3.7 shows the main line with twelve components from $\Delta F_1 = \Delta F = 0$, spread over the range 2.4 kHz. There are nine magnetic satellites, approximately 65 kHz above and below the main line frequency, which arise from $\Delta F_1 = 0$ and $\Delta F = \pm 1$. On either side of the main line lie the quadrupole satellites, seven components of which for the inner quadrupoles lie approximately 1690 kHz above and below the main line frequency, and arise from $\Delta F_1 = \pm 1$ and $\Delta F = \pm 1, 0$, and the outer quadrupole satellites, also including seven components arising from the selection rules $\Delta F_1 = \pm 1$ and $\Delta F = \pm 1, 0$. These lie about 2320 kHz above and below the main line frequency.

The mean frequency of the peak of the composite main line depends on the ratios of the intensities of the individual components and on their frequencies (Skobeltzyn, 1964). The $J=K=3$ main line

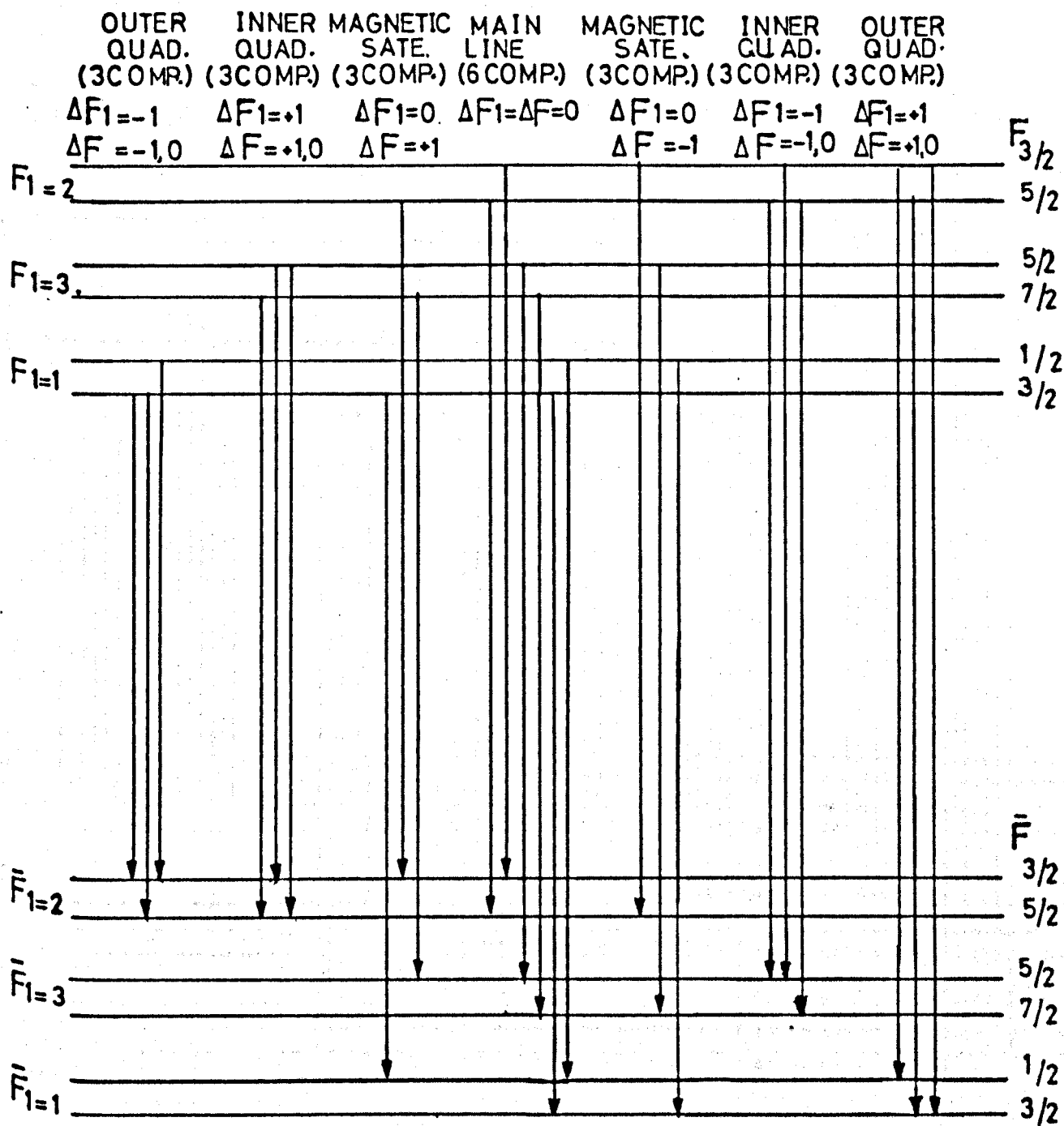


Fig.3.6. Schematic diagram of energy levels for $J=K=2$ inversion line of ammonia molecule.

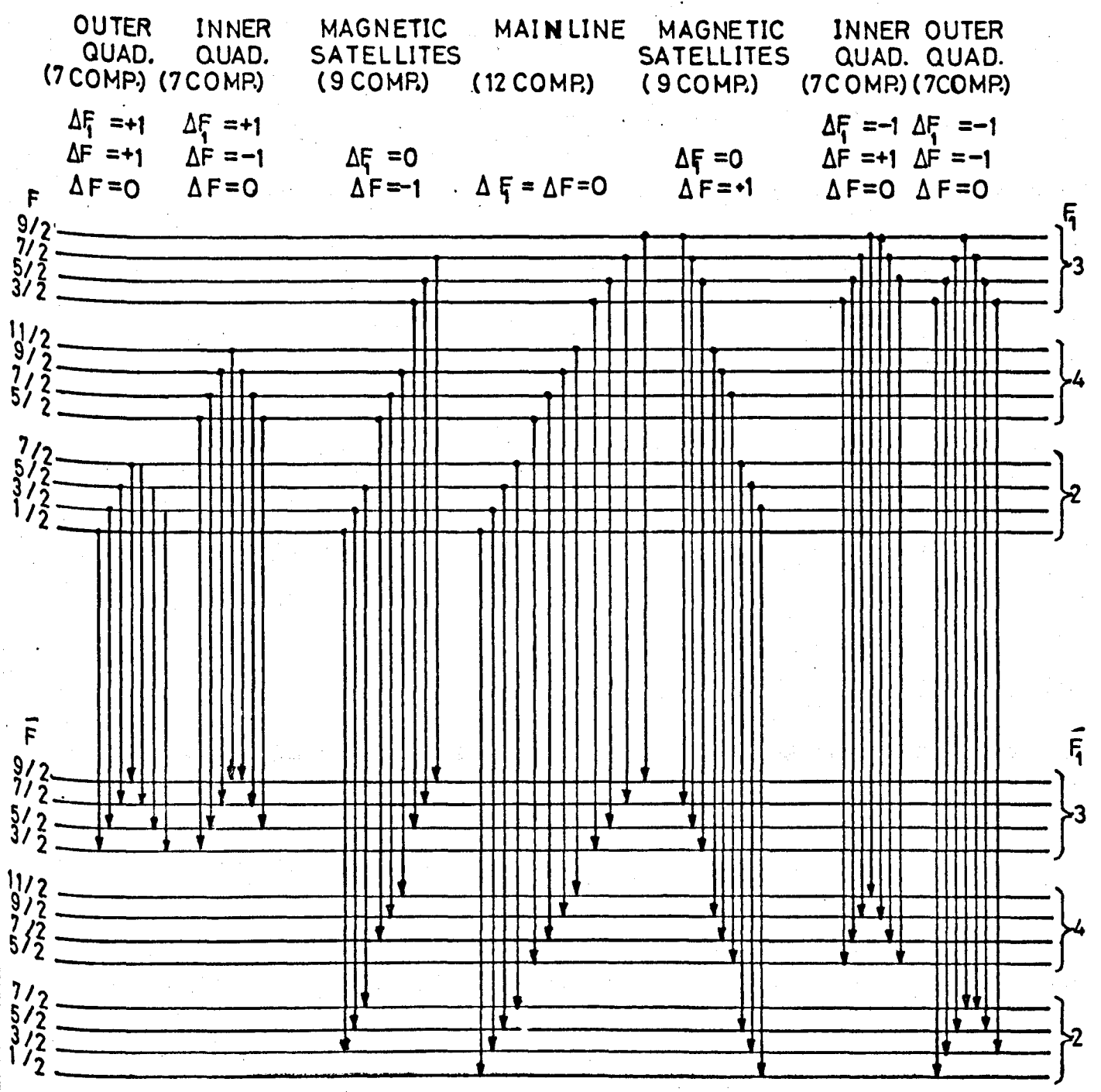


FIG. 3·7 SCHEMATIC DIAGRAM OF ENERGY LEVELS FOR $J = K = 3$
INVERSION LINE OF AMMONIA MOLECULE

frequency is 23 870 129.183 kHz; $J=K=2$: 23 722 633.335 kHz and $J=K=1$: 23 694 495.487 kHz (Kukolich, 1967).

3.4 High Intensity Molecular Beam

The molecular beam source is one of the important basic elements of the molecular beam maser. Increasing the oscillation power of a maser for realizing oscillation on a split spectral line, or for maser spectroscopy with enhanced sensitivity for the detection of weak spectral lines means increasing the number of active molecules entering the cavity (Eqn. 1.22). This number can be enhanced by increasing the total number of molecules directed towards the cavity, for example by increasing either the beam intensity, or the molecular capture angle in the selector system or both.

Johnson (1928) showed that beams of far greater intensity can be produced from a nozzle source rather than the conventional effusive molecular beam source. The graph (Fig. 3.8) of relative intensities measured at the detector against the corresponding source pressures as given by Johnson, shows a linear curve up to a nozzle pressure of about 50 torr, and continues rising up to a maximum intensity at 100 torr. With further increase in nozzle pressure, the beam intensity decreases. The decrease in intensity was attributed to scattering of beam molecules in the region downstream of the nozzle by background gas. Rodebush (1931) noted the possibility of using a nozzle source with collimation (resembling a skimmer) to achieve high beam intensities, but this method was ignored until it was rediscovered later by Kantrowitz and Grey (1951), who made an important suggestion that beam intensities orders of magnitude greater than could be achieved by any effusion technique were possible. The arrangement to exploit this idea is as follows. The beam material emerges through a nozzle from a container in which

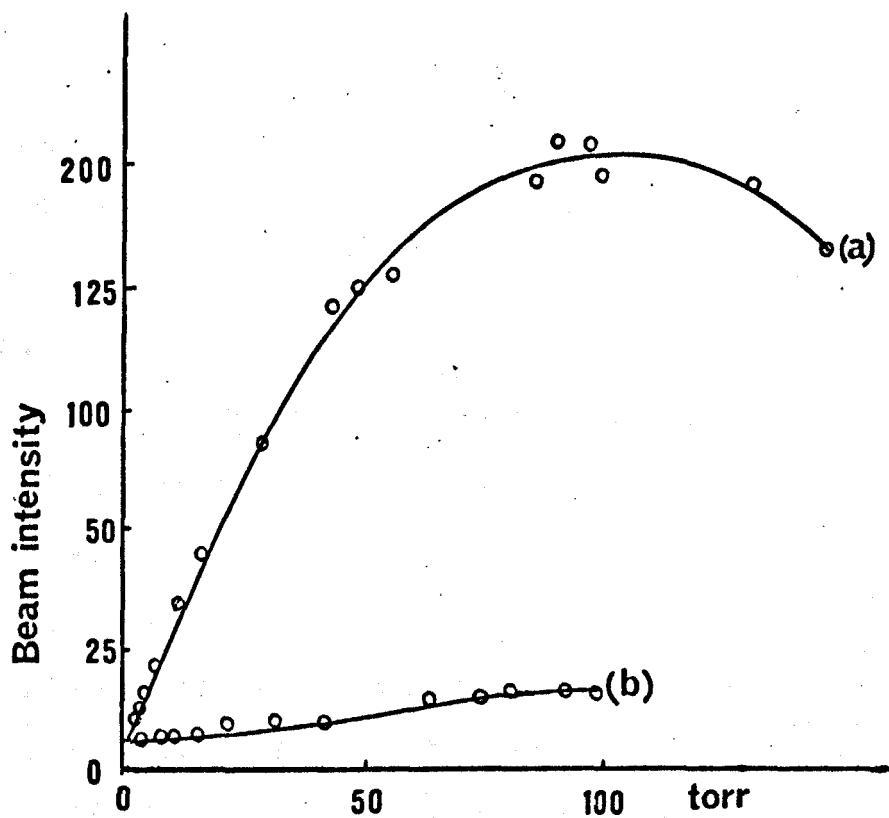


Fig.3.8 Beam intensity as a function of source pressure
 (a) nozzle source, (b) conventional effusive source
 (after Johnson, 1928)

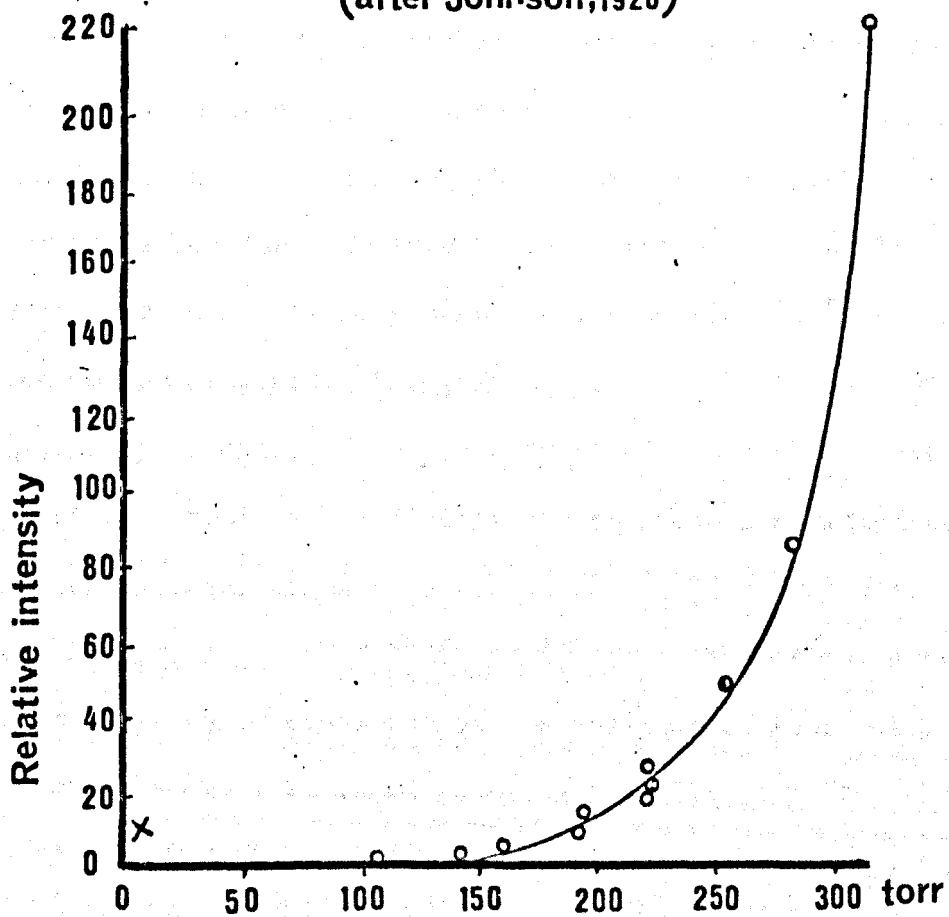


Fig.3.9 Beam intensity as a function of inlet ammonia gas pressure (after Kistiakowsky et al, 1951)

the pressure is of the order $10^2 - 10^3$ torr. The flow is hydrodynamic through this nozzle and a jet of gas expands into the nozzle chamber which strikes a suitably shaped diaphragm called a skimmer, allowing free passage of the central core of the molecular beam, and the remaining gas is pumped away. In the region of the skimmer, the gas flow changes from continuum to molecular, i.e. the collision rate drops very sharply.

A lot of attention has been given by many investigators to this proposal of Kantrowitz et al., including Kistiakowsky and Slichter (1951), Deckers and Fenn (1963), Campargue (1964) and others.

Kistiakowsky et al. (1951) employed a nozzle skimmer combination using ammonia as a test gas. It was found that the maximum intensity obtained exceeded by more than a factor of twenty that which is obtainable from an ordinary effusion system under optimum conditions. Fig. 3.9 represents a typical result obtained for the beam intensity of ammonia gas as a function of the inlet gas pressure. For relatively low gas pressures the beam intensities obtained were small. At higher pressures the intensity of the beam began to rise far more rapidly with respect to the pressure. For pressures above 170 torr a marked gain in the intensity is obtained, especially at a pressure of about 300 torr. The point x on the graph indicates the relative beam intensity expected with a conventional effuser source at the optimum pressure.

Deckers and Fenn (1963) introduced a theoretical expression for beam intensity which comes out of the analysis of Kantrowitz et al. for Mach numbers above three, and assuming no collisions after the skimmer entrance. It was found that

$$I = \frac{S n_0 a M}{[1 + \frac{1}{2}(\gamma-1)M^2]^3} \quad 3.2$$

where I is the total beam flux in molecules per second, S is the area

of skimmer inlet, n_0 is the number density of molecules upstream of the nozzle, a_0 is the speed of sound in the gas upstream of the nozzle, γ is the specific heat ratio ($\gamma = \frac{C_p}{C_v}$) and M is the Mach number at the skimmer entrance (the Mach number is: the ratio of flow velocity to the local velocity of sound).

Fig. 3.10 shows the variation of beam intensity with the nozzle pressure for two different skimmer shapes and the theoretical beam intensities. For both skimmers the beam intensity increases with nozzle pressure along the theoretical line at low pressure, but falls below the theoretical line, and reaches a maximum at higher pressure. With a further increase in nozzle pressure the beam intensity falls to reach a minimum, then begins to rise. This indicates that the effect of the skimmer (skimmer interference) is due to molecules reflected from the external skimmer surface. The presence of the skimmer interference was unclear since the first time it was observed by Deckers et al., several explanations were proposed. The arguments centred on the question of whether the scattering of beam molecules took place in front of or within the skimmer. Years later, it was found that scattering can occur at either location depending on the density of the beam approaching the skimmer. Fig. 3.11 shows an illustration of skimmer interference phenomena. Those molecules hitting the external surface are reflected back into the beam, but their density is sufficiently low that collisions with approaching beam molecules are negligible. As the beam density is increased, the density of reflected molecules increases and causes scattering of beam molecules in front of the skimmer. With a further increase in beam density both the reflected and scattered molecules contribute to the density in the scattering region. This region appears to have some of the characteristics of a diffuse shock wave. For still higher jet densities, the flux of jet molecules is sufficiently high to

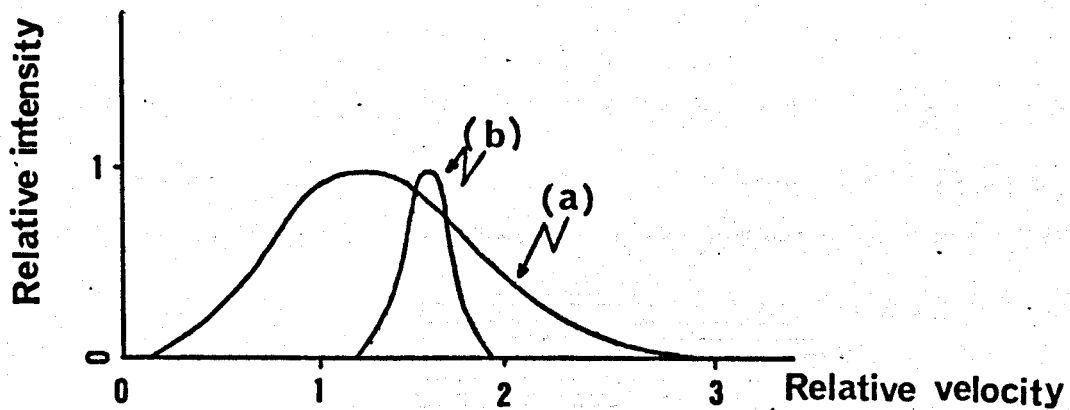


Fig.3-12 Theoretical velocity distribution of (a) effusive and (b) nozzle source (after Anderson et al,1965)

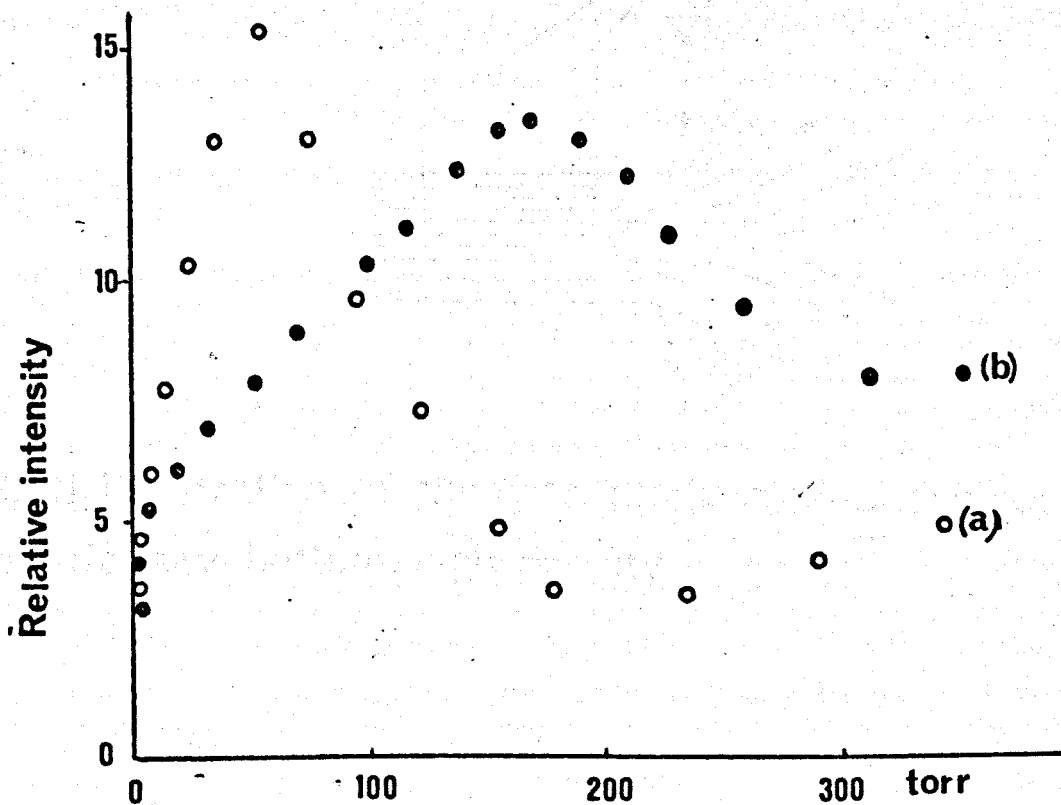


Fig.3-10 Variation of beam intensity with nozzle pressure for two skimmer shapes, (a) open circles (b) closed circles (after Anderson,1972)

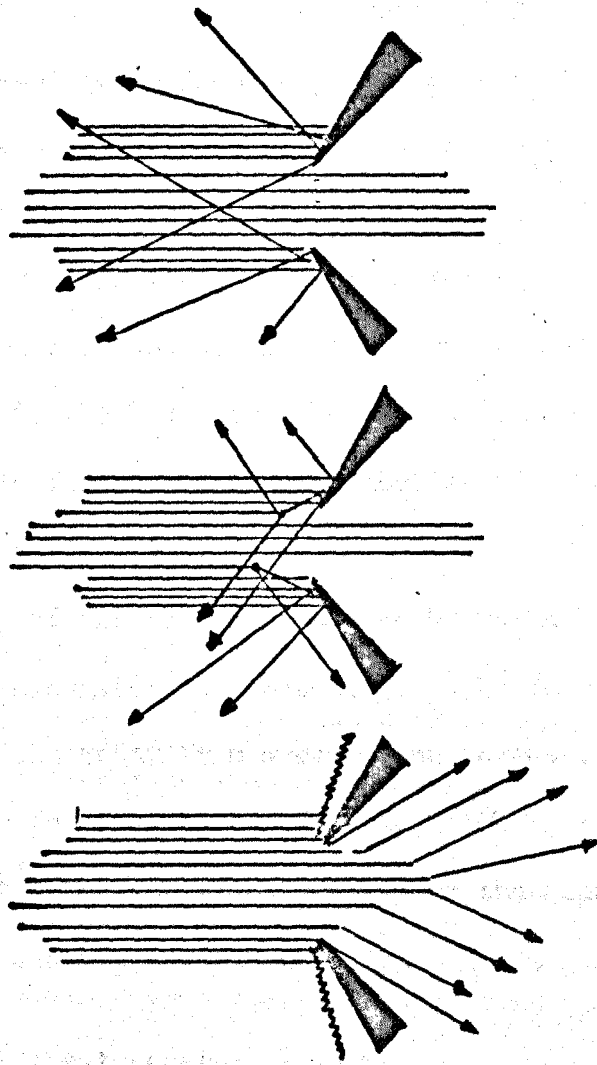


Fig.3.11 Illustration of skimmer interference phenomena.
top: low density. bottom: high density

drive reflected molecules in front of the skimmer. An oblique shock wave is formed along the external walls of the skimmer, and the diffuse shock wave structure in front of the skimmer entrance no longer appears.

By the use of a nozzle type source, according to Kantrowitz et al., most of the random translational and internal energy of the gas is converted into directed mass motion, which provides an initial collimation. This improves the effusion rate and the geometrical profile of the gas flow. Therefore, all the molecules spread within a narrow elliptical profile, mainly along its major axis which is several times the distance between the nozzle source and the skimmer. As a consequence, the molecular velocities in the beam would be partially monochromatized. Fig. 3.12 shows the theoretical velocity distribution of effusive and nozzle sources (Anderson et al. 1965).

The simple theory of the action of nozzle beams is based upon the assumption that the expansion is isentropic. The increase in forward velocity of the beam comes from a reduction in the local enthalpy of the gas. The lowering in temperature, from T_i (initial temperature) to T_f (final temperature), accompanying the expansion is given by (Fluendy and Lawley, 1973):

$$\frac{T_f}{T_i} = [1 + \frac{\gamma-1}{2} M^2]^{-1} \quad 3.3$$

where γ and M have the same meaning as in Equation 3.2. According to Kantrowitz (1951) the temperatures which are attainable by nozzle source expansions are very low ($0.24 \times$ gas supply temperature for the sample design) and it should be possible to attain a molecular beam with a large number of the molecules in the lower rotational states. The population of rotational state in a molecule of symmetric top type is proportional to the Boltzmann factor and the statistical weight of the

energy state (Herzberg, 1947)

$$N_{(J,K)} \sim g_{(J,K)} e^{-(E_{(J,K)}/kT)} \quad 3.4$$

where $E_{J,K}$ is the rotational energy level, $g_{J,K}$ is the statistical weight, k is Boltzmann's constant and T is the absolute temperature.

3.5 Experimental Comparison of Effuser-Diaphragm and Nozzle-Skimmer Combinations

The discussion in Chapter One shows that the ammonia molecular beam formation plays a major role in maser operation through the following factors: beam intensity, molecular velocity distribution and molecular temperature. The discussion of the theoretical and experimental results in Section 3.4 shows the advantages to be gained by the use of a nozzle-skimmer combination in the molecular beam maser from the viewpoint of high intensity, narrow velocity distribution and rotational cooling of the molecules, thus enhancing the population of molecules in low lying rotational states.

The validity of these points was consolidated by the following known results obtained from the ammonia type of molecular beam maser operated with a nozzle-skimmer combination. Firstly, oscillation was secured on the relatively weak $J=3, K=2$ inversion line of ammonia without cryopumping (Maroof and Lainé, 1974); secondly, oscillations on several hyperfine components as well as the main line of the $J=K=1$ inversion line of ammonia were also obtained (Maroof and Lainé, 1976, Lainé and Truman, 1977a). All of these results were realized with a skimmer in the shape of a cone, to produce a cylindrical beam, which subsequently passed through the ring state separator and then on to the cylindrical microwave cavity.

From the foregoing experiments, it seemed reasonable to suppose that if the skimmer was shaped to give a flat rather than a pencil-like beam, then the advantages of the nozzle-skimmer combination could be applied to the open resonator.

The diaphragm plate which closed off the subsidiary vacuum chamber from the main chamber, and carried the diaphragm slit, also supported the state separator and the effuser unit. Two parallel rods on the subsidiary chamber side of the plate carried the effuser unit, and allowed it to slide in a direction perpendicular to the diaphragm slit. Slotted holes were provided in the diaphragm plate for the bolts to secure it to the vacuum chamber port. This provided for the horizontal adjustment of the whole effuser and the state separator, in order to align it with the centre of the cavity.

The effuser unit was of the multichannel type which consisted of a linear array of 33 holes, 1mm in diameter and 10mm in length. A thick walled flexible tube with an appropriate vacuum lead-through supplied ammonia gas to the effuser. The ammonia, after purification by freezing was stored in a 2 litre reservoir, and was used to operate the maser by flowing it through a needle valve, using a pirani gauge to monitor the pressure behind the effuser. Fig. 3.13a shows the effuser unit and the diaphragm.

The nozzle source was constructed by machining a cone into a brass disc, to within about 0.1mm of breaking through. A hole was then made by using a jeweller's drill of the required diameter. Otherwise the arrangement for the nozzle source inside the subsidiary vacuum chamber is exactly as for as the effuser source just described.

The skimmer represented a somewhat more difficult design problem than the nozzle. Because it was to be immersed in a supersonic stream it was necessary to be concerned about the formation of shock waves.

In order to avoid, if possible, a detached shock in front of the slit entrance, it was essential to make the outside angle as acute as possible. A compromise was made by taking 35° for the inner angle, and 45° for the outer angle. Brass was used for the construction of the skimmer and as sharp an edge as possible was obtained by grinding. Such a sharp edge was necessary to ensure that the number of molecules which struck the edge and then scattered was minimal. The inside and outside surfaces of the skimmer were highly polished. Slotted holes were provided in each skimmer lip-holder for the bolts which secured it to the diaphragm plate, which was fixed to the vacuum chamber port. This provided for horizontal movement of the lips, and thereby permitted adjustment of skimmer width. Fig. 3.13b shows the nozzle and the skimmer.

Since the signal-to-noise ratio is an increasing function of the number of active molecules in the cavity, this ratio may be taken as an indicator of the success of machine improvements.

Fig. 3.14 shows the oscilloscope photographs of the maser emission signal for the $J=K=1$ inversion line: (a) when the maser is operated with an effuser-diaphragm combination. Here the two largest intensity components of the eight components of the main line are shown with a signal-to-noise ratio of three. Photograph (b) shows three components of the eight with a signal-to-noise ratio of ten, when the nozzle-skimmer combination was used.

When the effuser was used as the molecular beam source, in combination with a collimating diaphragm, the maser oscillated on the $J=K=3$ inversion line of ammonia only, while oscillation was obtained on the weak inversion line $J=K=2$ also, when the nozzle was used as the molecular beam source in combination with the skimmer.

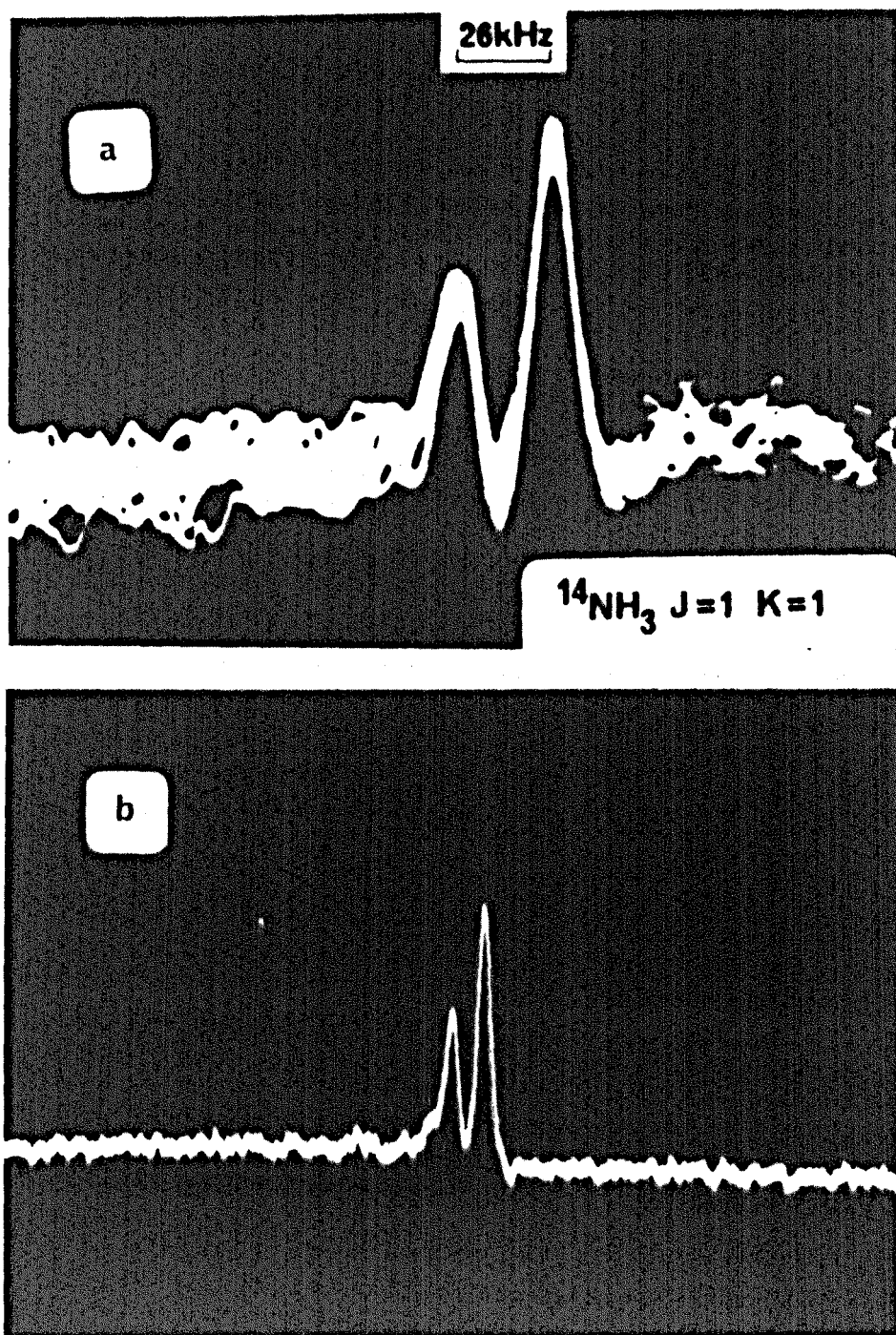


Fig. 3.14 THE J=K=1 INVERSION TRANSITION OF AMMONIA, THE SYSTEM OPERATED WITH
(a) EFFUSER AND DIAPHRAGM
(b) NOZZLE AND SKIMMER

The signal amplitude of the maser was investigated experimentally, and the results have shown that small diameter nozzles were best suited for the ammonia beam maser, which was 0.09mm. With smaller than 0.09mm nozzle diameter, such as 0.05mm, condensation phenomena could be reached (Maroof, 1975); condensation was detrimental to maser operation.

The simultaneous use of two separate nozzles 0.09mm diameter spaced 30mm apart in the same subsidiary chamber, was also investigated. Surprisingly, the single nozzle gave better results than the two nozzles used at the same time. This was attributed to the scattering of molecules from the nozzles by background gas in the subsidiary vacuum chamber.

The best width of the skimmer slit, was found to be 0.8mm for nozzle pressures up to 300 torr. For every change in the skimmer slit it was necessary to open the vacuum system to the atmosphere with attendant readjustments of the distance between nozzle and skimmer, state separator and the cavity. As a result of these difficulties an optimum width for the skimmer slit was difficult to find. Therefore it was necessary for the skimmer width to be adjustable from outside the vacuum chamber during the maser operation in order to find an optimum width. A suitable design is discussed in Section 2.9 in conjunction with the new maser system.

3.6 The Stark Effect for Ammonia

The Stark effect is the change observed in the spectrum of a system subjected to an electric field. The rotational spectrum of a molecule which has an electric dipole moment may be expected to be modified when the molecule is in an electric field, since the field exerts a torque on the molecule and thereby can change its rotational motion.

Stark effects have been investigated by many investigators for different types of molecule. The first Stark measurements in microwave spectroscopy were those of Dakin, Good and Coles (1946) on the linear molecule OCS. The theoretical work by Golden and Wilson (1953) on asymmetric top molecules, showed that the intensities of the $\Delta J = 0$ transitions are proportional to M^2 , whereas those of the $\Delta J = \pm 1$ transitions are proportional to $[(J+1)^2 - M^2]$. An example of the use of the Stark effect in identifying different absorption lines is given by the measurements of Ferguson and Wilson on SOF_2 (1953). Its use in determining dipole moments for several other molecules is illustrated by the paper of Townes et al. (1949).

In 1946 Coles and Good showed that the Stark splitting of ammonia is somewhat of a special case as its dipole moment is not permanent. A detailed theoretical treatment of the Stark splitting produced in ammonia, including quadrupole interactions has been given by Jauch (1947), and, in the particular case of the $J=K=3$ inversion line, has been worked out in detail.

Symmetric top molecules have a component of their electric dipole moment parallel to the angular momentum vector, and thus components which are fixed in direction rather than rotating. Thus for a symmetric top rotating about its symmetry axis, the dipole moment is in the direction of J and its energy in an electric field is $-\mu E \cos \theta$, where μ is the dipole moment of the molecule, and θ is the angle between J and the electric field E . The projection of J on a fixed direction, such as that established by the direction of E , is always an integer M , the magnetic quantum number. Hence the energy might be expected to be $-\mu E \cos \theta = -\mu E (M/J)$. In the more general case of the angular momentum J and a component of the angular momentum K along the symmetry axis, the component of μ along the J direction is

$\mu E/J$. The energy will then be:

$$\Delta W = - \frac{\mu E M K}{J(J+1)} \quad 3.5$$

The change in energy of a symmetric top molecule due to an electric field, is proportional to the first power of μE (first order Stark effect), whereas that for a linear molecule is proportional to the second power of μE (second order Stark effect) (Townes and Schawlow, 1955). The first order Stark effect of symmetric tops is more generally a characteristic of a system with degenerate levels. In the absence of an external field no system can have a dipole moment fixed in direction, unless it is in a degenerate level such as is found in a symmetric top, which has a dipole moment and can interact with the applied electric field. The ammonia molecule is a symmetric top. Its Stark splitting is somewhat of a special case as its dipole moment is not permanent but changes with the inversion frequency, and the first order Stark effect does not occur. Classically the dipole moment of ammonia molecule might be regarded as rapidly reversing in direction because of the inversion, so that its average value in any direction is zero. Therefore, a second rather than first order Stark effect splitting should be applied to the ammonia molecules (Coles and Good, 1946).

When hyperfine structure is present due to a nucleus of spin I (Section 1.3), the total angular momentum of a molecule is given by the quantum number $F = J+I, J+I-1, \dots, |J-I|$ rather than by J . The projection of the angular momentum on the same chosen direction is $M_F = F, F-1, \dots, -F$. Thus the number of Stark components depends on F rather than J , and it may be expected that the energies of Stark components will be rather different from the case with no hyperfine structure.

In the weak field case ($E < E_s$, where $E_s \sim 500V/cm$) the electric field is so small that the Stark energy is less than the hyperfine energy. Expressed otherwise, the precession of the molecule due to the Stark field is so slow and gentle that the interaction between the nucleus and molecule is very little disturbed. The molecular state is satisfactorily specified by the quantum numbers I, J, F and M_F . Each hyperfine line is then split into various components, according to the value of M_F , and this splitting is small compared with the hyperfine splitting.

In the strong field ($E > E_s$) case the Stark energy is much larger than the hyperfine energy. The molecule is precessed so violently by the electric field that the nuclear orientation cannot follow the motion. I and J are said to be decoupled, and the hyperfine structure is radically changed. The quantum number F is no longer good, since the vector sum of I and J is no longer fixed. Appropriate quantum numbers for describing the molecular state are I, J, M_I and M_J , where M_I is the projection of I on the direction of the field and M_J is the projection of J on the direction of the field.

An intermediate field ($E \sim E_s$) case occurs when Stark and hyperfine energies are comparable. In those cases neither M_J nor M_F and F are good quantum numbers. The hyperfine structure causes the Stark pattern for intermediate field values to be quite complicated (Jauch, 1947).

Jauch analyzed the Stark effect of the ammonia inversion spectrum $J=K=3$ by including the quadrupole energy. The Hamiltonian for the system was

$$H = H_o + H_q + H' \tag{3.6}$$

where H_o is the energy for the rotational levels, including the

inversion splitting, H_q is the quadrupole energy and H' is the interaction energy of the electric dipole moment with the external electric field. Dugdale (1976) calculated the effect of a Stark field up to 218V/cm (weak field) on the energy levels of the ammonia inversion rotational state $J=K=1$, including all the hyperfine structure of the inversion spectrum, which was based on the result obtained by Kukolich (1967). From this calculation a coordination of the energy levels as a function of the parameter χ , which is equal to $\mu^2 E^2 / \Delta(J,K)$, was obtained and is shown in Fig. 3.15, where μ is the dipole moment (1.45×10^{-18} e.s.u.), $\Delta(J,K)$ is the energy difference between the upper and lower inversion state and E is the electric field. In this figure the coordination of the energy levels for the upper state (a) and lower state (b), is in a Stark field from 0 to 144.87V/cm. On this graph $E^2 = 954 \times$ number of centimeter divisions (x-axis), and each centimeter is equal to 20 kHz. The y-axis is equal to 10 kHz for each centimeter (energy levels shift).

According to Jauch, the transitions occur with the following selection rules:

(main line)	$\Delta F_1 = 0, \Delta M_F = \mp 1$	} for the case of mutually perpendicular Stark and microwave electric fields
(satellites)	$\Delta F_1 = \mp 1, \Delta M_F = \mp 1$	
3.7		
(main line)	$\Delta F_1 = 0, \Delta M_F = 0$	} for the case of parallel Stark and microwave electric fields
(satellites)	$\Delta F_1 = \mp 1, \Delta M_F = 0$	

It is possible, from Fig. 3.15, to draw a diagram of all energy levels and associated transitions for $\Delta M_F = \mp 1$ or $\Delta M_F = 0$ in any value of electric field, to identify the number of components in the main line and each satellite, as well as their relative frequency separations. Fig. 3.16 shows the energy levels and the possible transitions in the

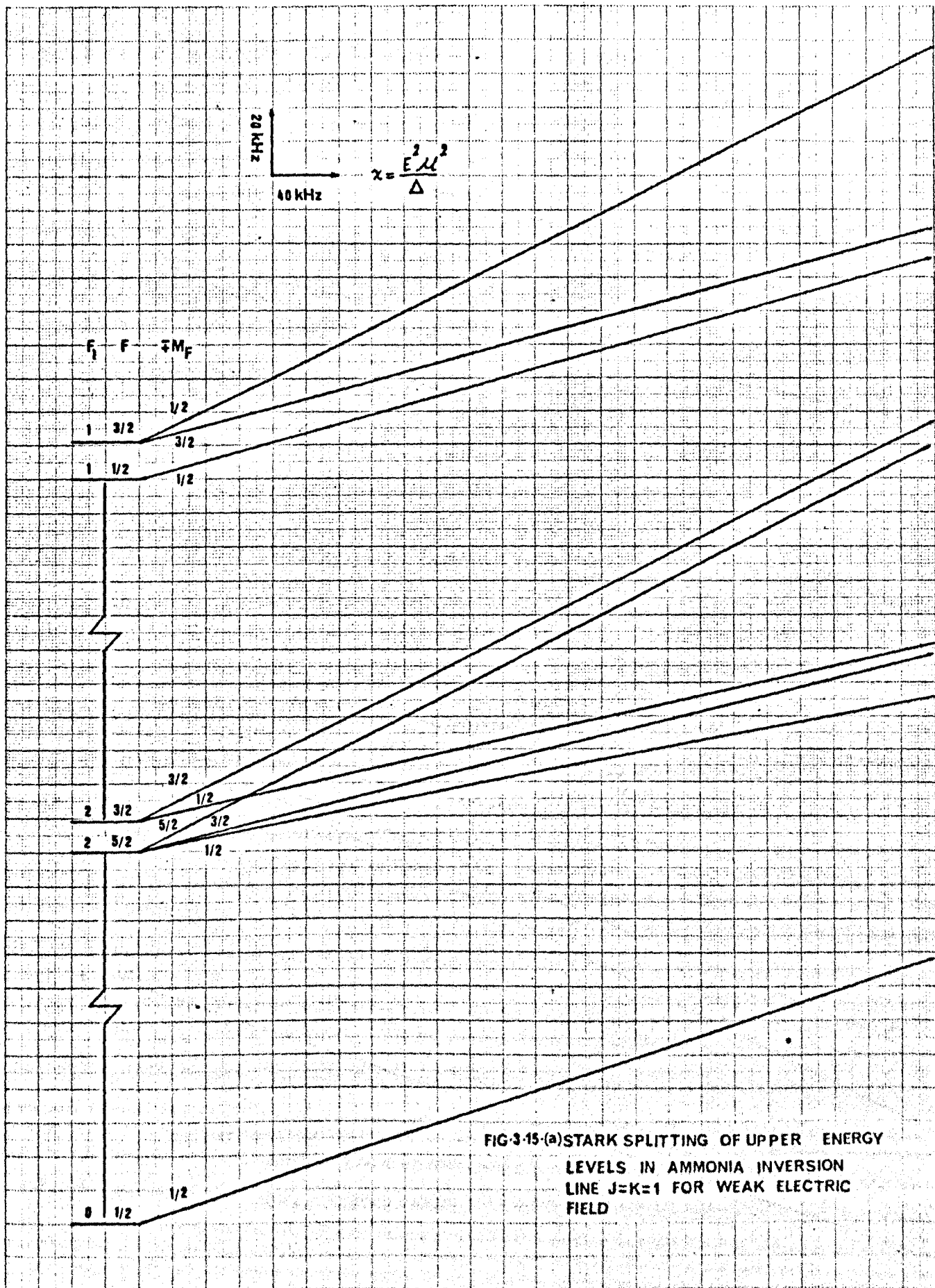
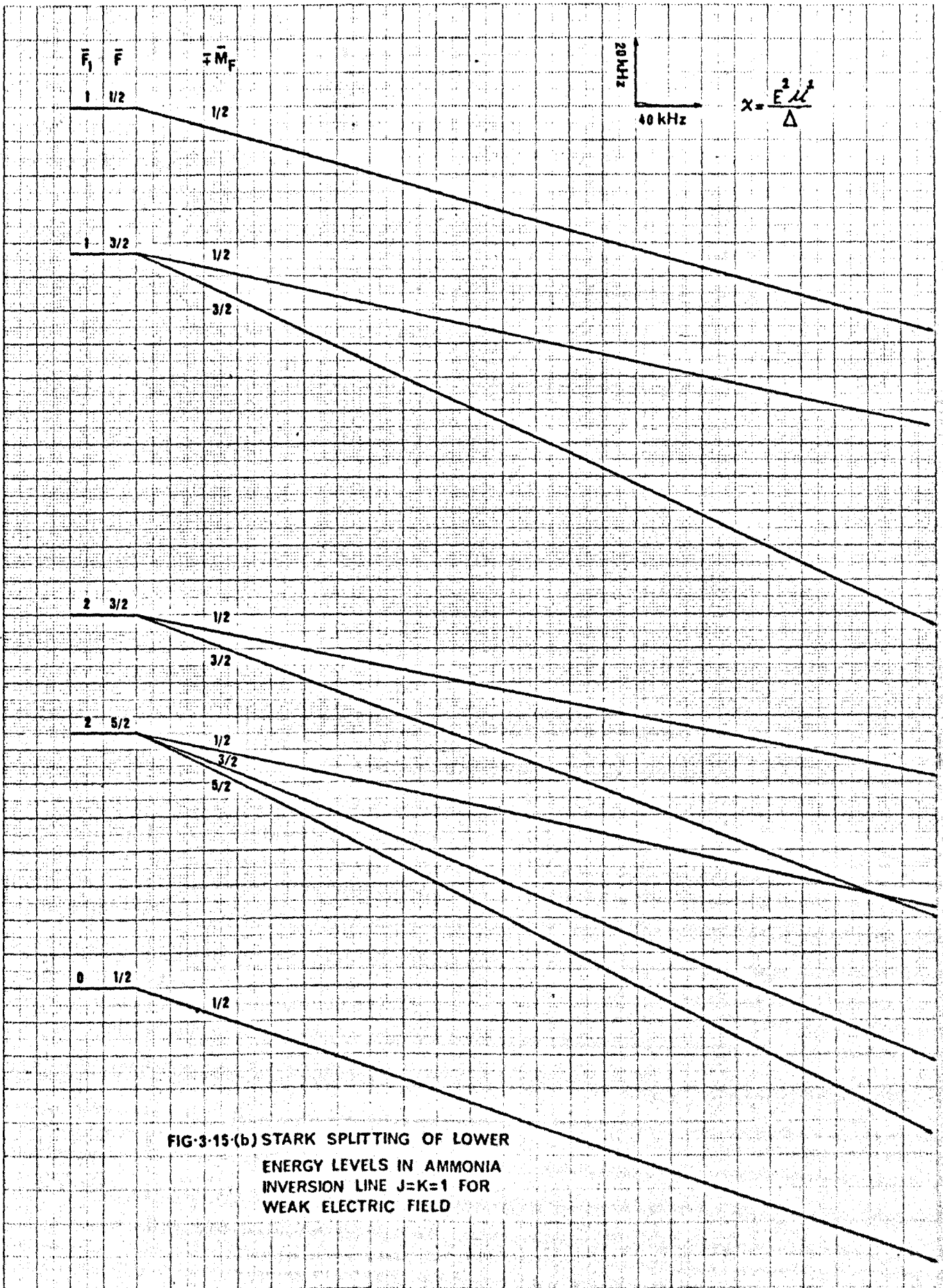


FIG-3-15-(a) STARK SPLITTING OF UPPER ENERGY LEVELS IN AMMONIA INVERSION LINE J=K=1 FOR WEAK ELECTRIC FIELD



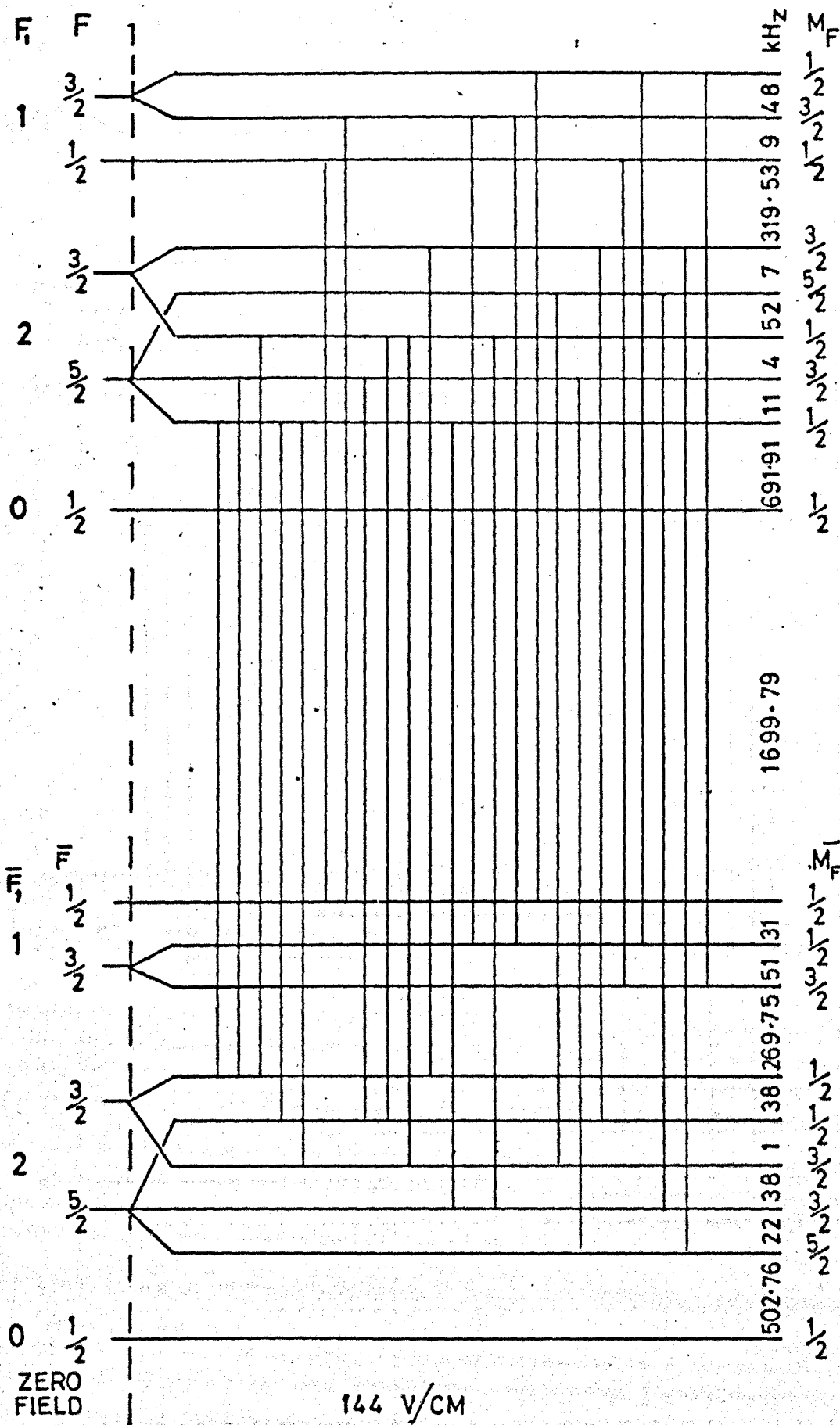


FIG. 3-16 SCHEMATIC DIAGRAM OF ENERGY LEVELS FOR $J=K=1$ INVERSION LINE OF AMMONIA MOLECULE IN WEAK ELECTRIC FIELD (144 V CM) AND $\Delta M = \pm 1$ MAIN LINE TRANSITIONS.

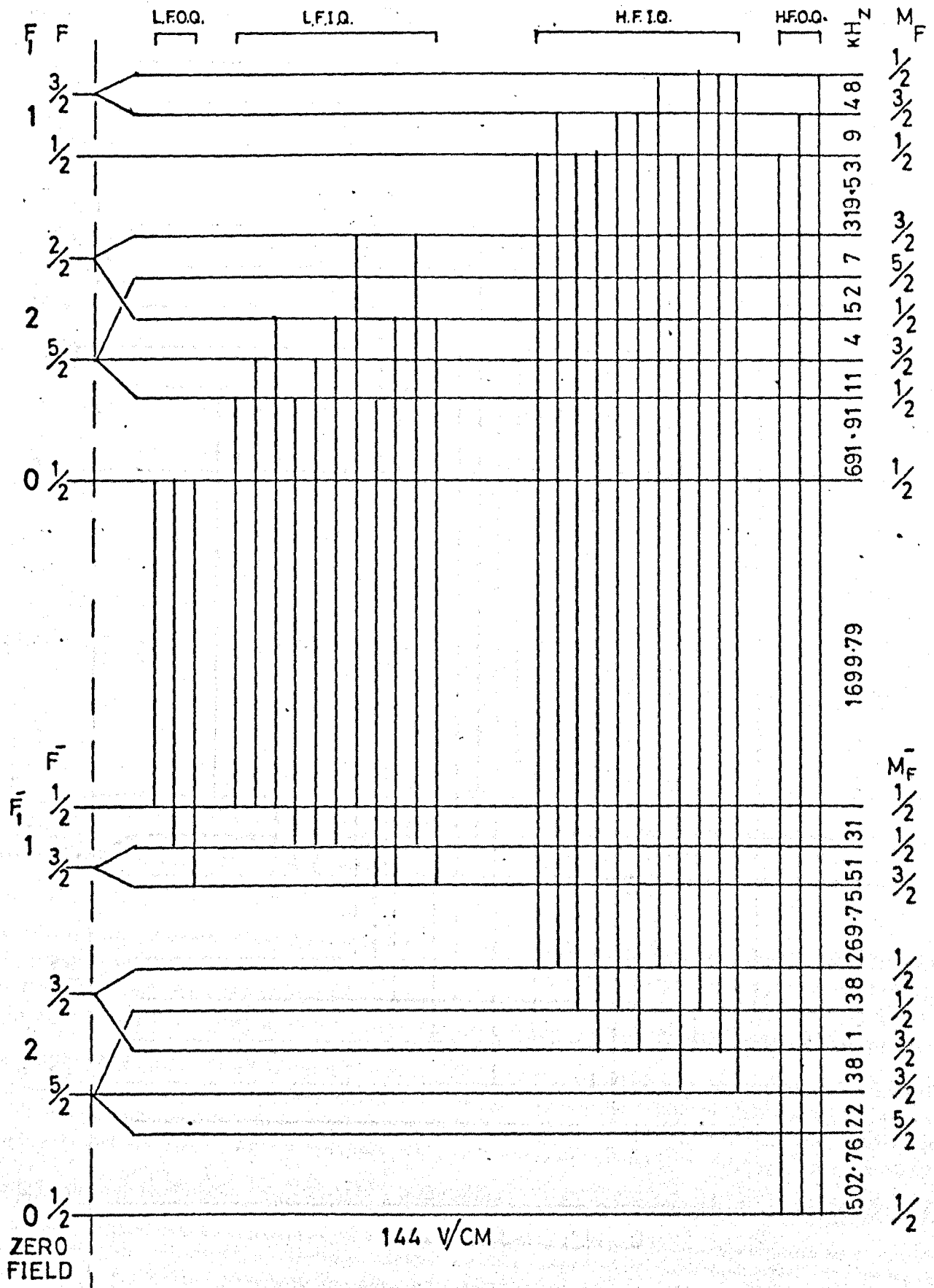


FIG. 3-17 SCHEMATIC DIAGRAM OF ENERGY LEVELS FOR $J=k=1$ INVERSION LINE OF AMMONIA MOLECULE IN WEAK ELECTRIC FIELD (144 V CM) AND $\Delta M = \pm 1$ QUADRUPOLE SATELLITES TRANSITIONS.

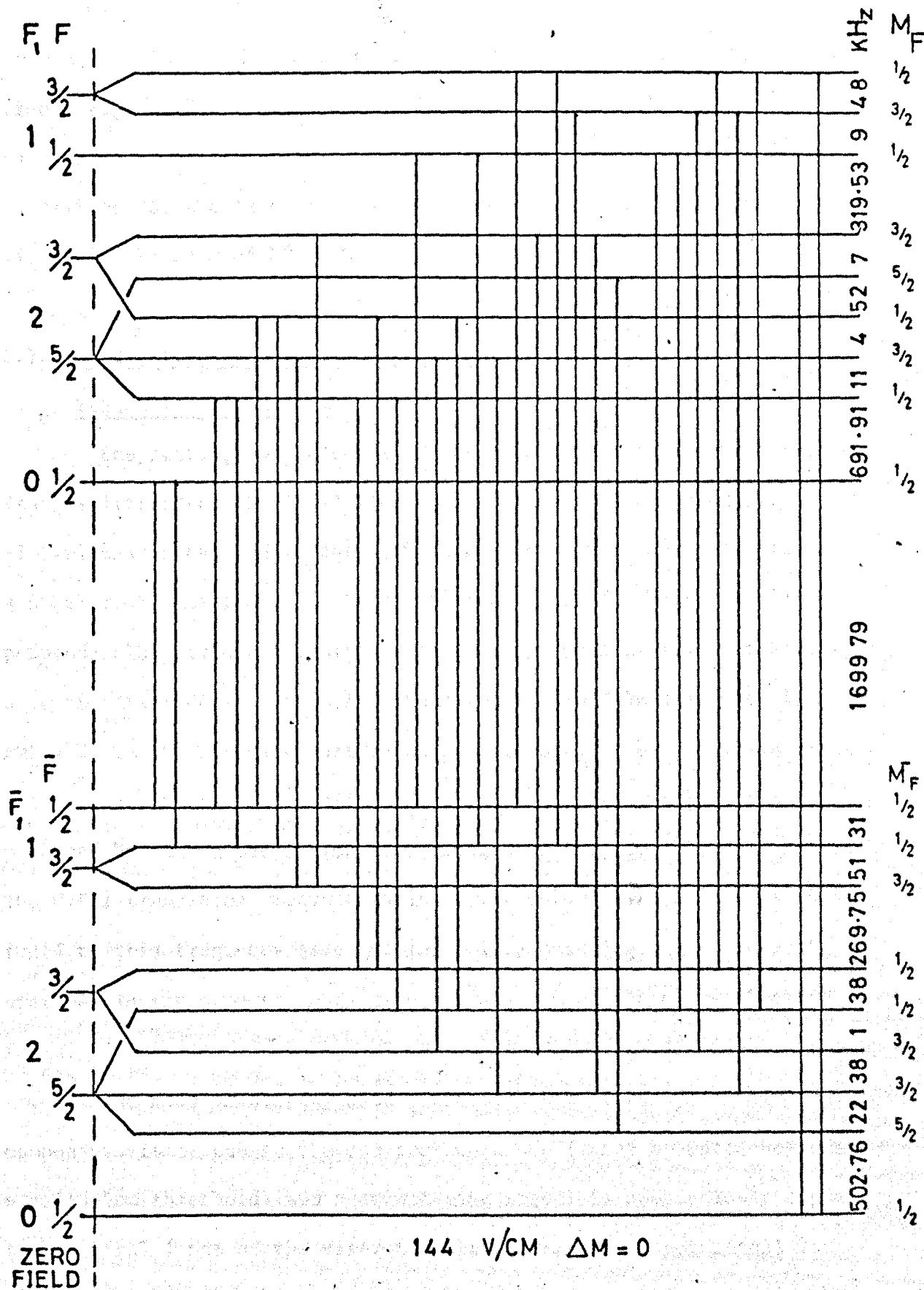


FIG 3-18 SCHEMATIC DIAGRAM OF ENERGY LEVELS FOR $J=K=1$
 INVERSION LINE OF AMMONIA MOLECULE IN WEAK
 ELECTRIC FIELD (144 V/CM) AND $\Delta M = 0$ TRANSITIONS
 (MAIN LINE AND QUADRUPOLE SATELLITES)

the case of $\Delta M_F = \mp 1$, in an electric field of 144 V/cm for the main line. Fig. 3.17 shows the energy levels for the satellites for the same value of electric field. Fig. 3.18 shows the main line and its satellites for the case of parallel Stark and microwave electric fields in the case of $\Delta M_F = 0$.

3.7 Observation of the Stark Effect in the J=K=1 Inversion

Transition of Ammonia

The setting-up procedure of the molecular beam spectrometer for Stark splitting of the J=K=1 line is as follows. The tuning mirror is electrically connected to the stabilized d.c. power supply to produce a Stark field perpendicular to the microwave field. This mutually perpendicular field configuration is the only possibility with this type of open cavity design, and thus the selection rule in this work is $\Delta M_F = \mp 1$. The klystron, acting as a local oscillator (L.O.) is offset in frequency by the intermediate frequency and one of the sidebands produced by 30 MHz modulation of a portion of the L.O. power is set to the J=K=1 transition frequency using a wavemeter. The cavity is then tuned to this frequency (see Section 2.1.5) ensuring that the cavity operates in the simplest mode with one maximum of microwave electric field.

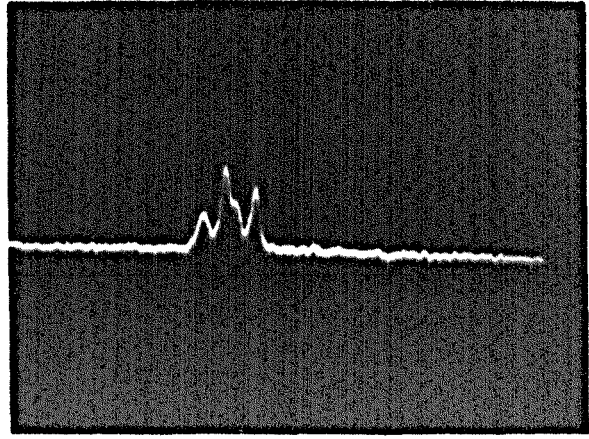
The mode of display used to observe the Stark splitting components is of course the spectroscopic one (maser operated below its oscillation threshold) and a stimulating signal is swept slowly through the spectral lines of the maser transition. If the input signal is sufficiently small, then the output from the maser will reproduce the spectrum of the maser line. In order to observe weak transitions in the spectrum with a satisfactory signal-to-noise ratio, the input signal is often increased so that the most intense spectral lines are saturated.

Fig. 3.19 shows the main inversion line $J=K=1$ of ammonia for the following six values of Stark voltage applied across the cavity: 0, 37, 45.9, 59.3, 77.5, 90 Volt. Since the gap between the mirrors is 0.625cm, then the Stark fields are 0, 59.2, 73.44, 94.88, 124, 144 V/cm. It is clear from the figure that the two zero field components of the main line split into many lines as a result of energy level splitting in the presence of the electric field. The number of components is governed by the number of sub-levels (M_F) and the selection rules. As a result of differential Stark shifts for different components of the main line, the separations between these will only be larger than the resolution of the spectrometer at sufficiently large Stark fields. Thus the spectrometer will resolve more components in the high field than at low field.

From Fig. 3.16, the main line of the $J=K=1$ inversion transition consists of twenty-four components spread over a spectral range of ~181 kHz. But, as a result of the spectrometer resolution and the effect of Stark field on the relative intensities of components, only six components are observed when the Stark field is 144 V/cm, as shown in Fig. 3.19f. As a consequence of the overlap of the components at increasing values of the electric field, the identification of each individual component is impossible. Therefore detailed measurements of the frequency shift for each component, in order to compare with theory, is not possible with the present spectrometer resolution. However, the number of the components from the theoretical and the experimental work can be compared and are found to be in agreement. The theoretical and experimental Figures 3.17 and 3.20 respectively, shows the extent of agreement. Fig. 3.20 shows the outer quadrupole satellite's lines on the low frequency side of the main line, which is the weaker component in the hyperfine structure of the $J=K=1$, at an electric field value of



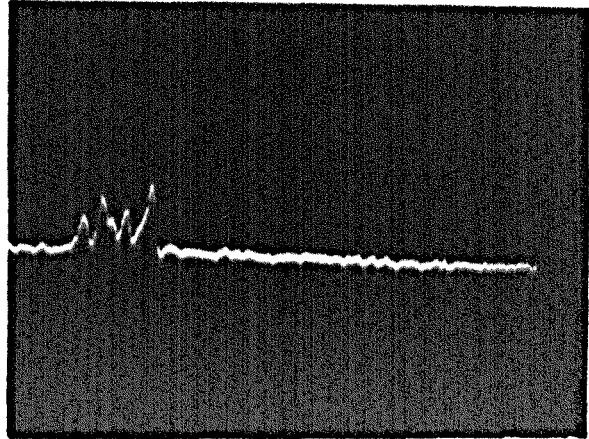
a - zero v/cm



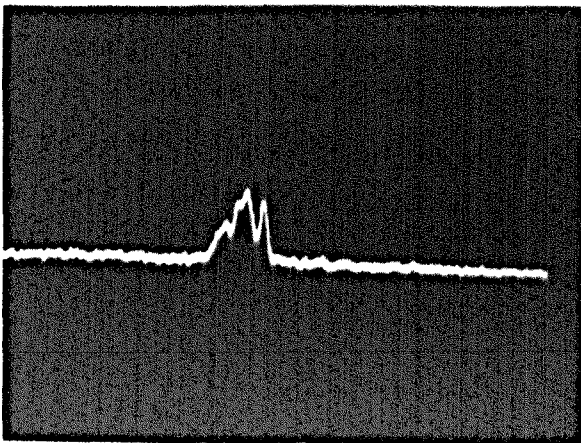
d - 94.88 v/cm



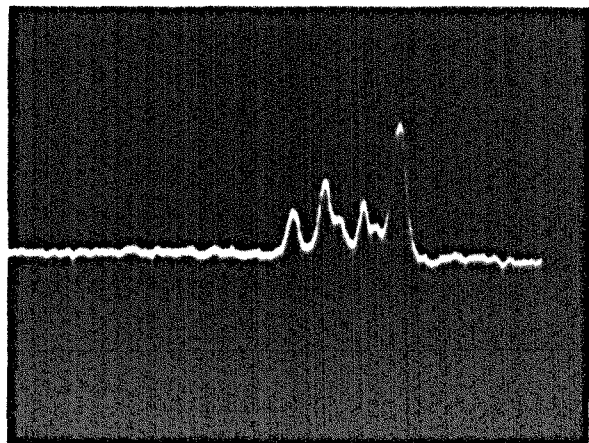
b - 59.2 v/cm



e - 124 v/cm



c - 73.44 v/cm



f - 144 v/cm

Fig. 3.19 STARK EFFECT ON $^{14}\text{NH}_3$ $J=K=1$ TRANSITION
(MAIN LINE)

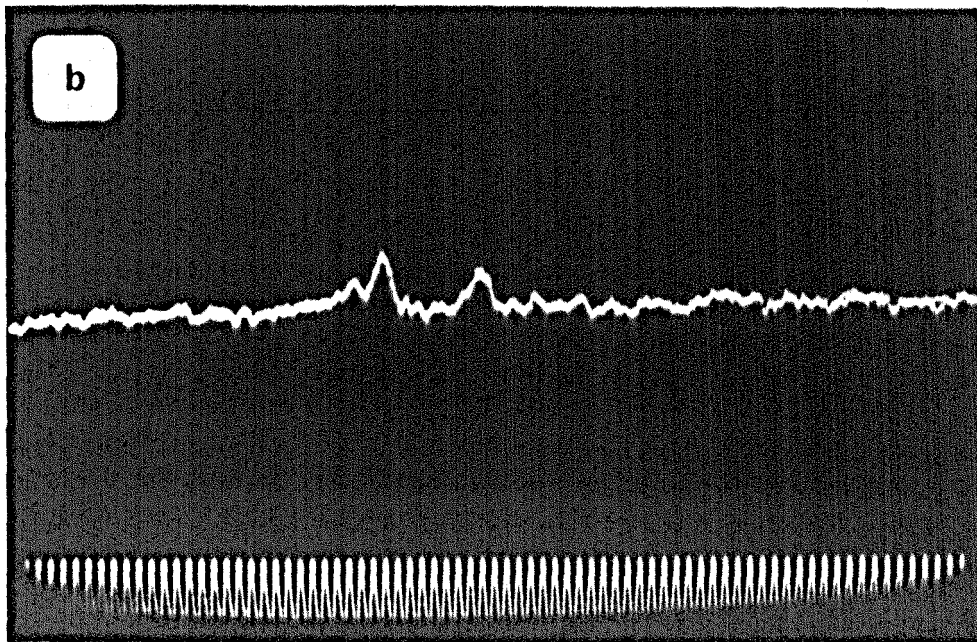
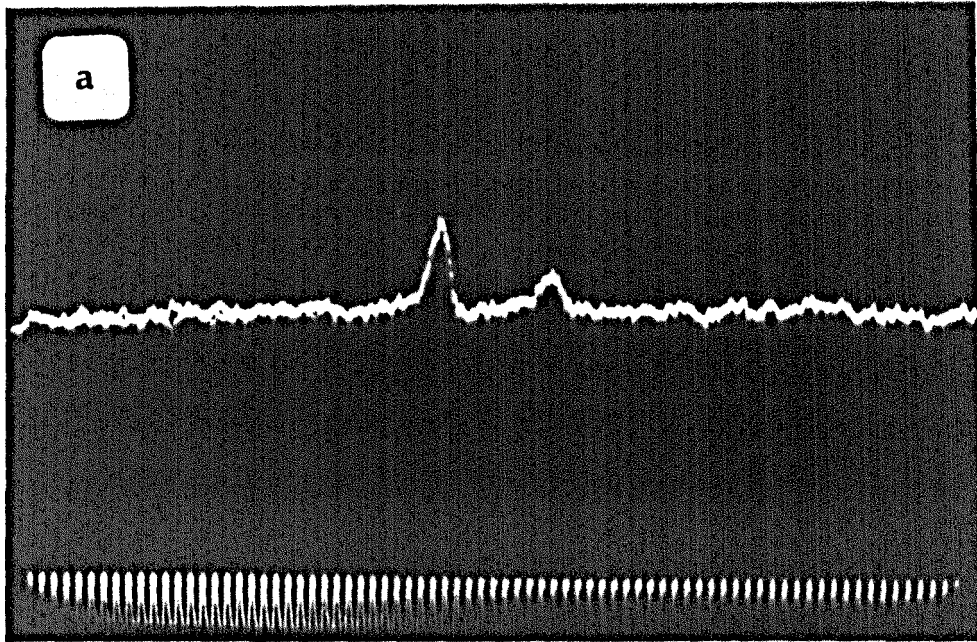


Fig. 3.20 STARK EFFECT ON $^{14}\text{NH}_3$ $J=K=1$ INVERSION
 TRANSITION (OUTER SATELLITES ON THE LOW
 FREQUENCY SIDE OF THE MAIN LINE)

(a) ZERO v/cm

(b) 75.2 v/cm

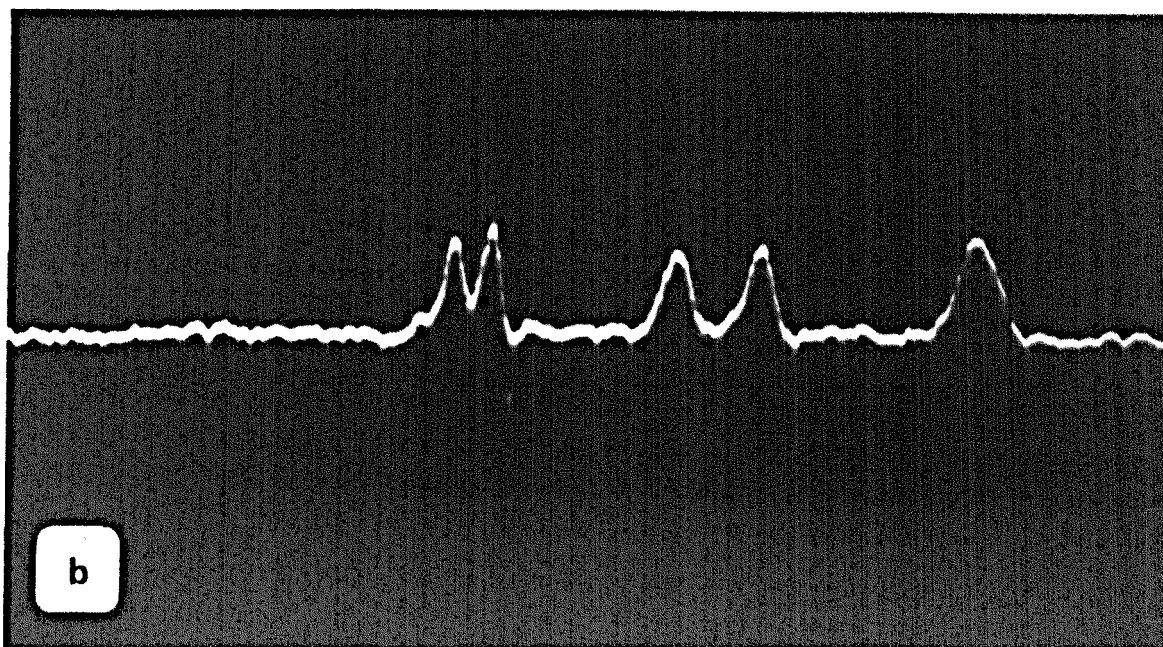
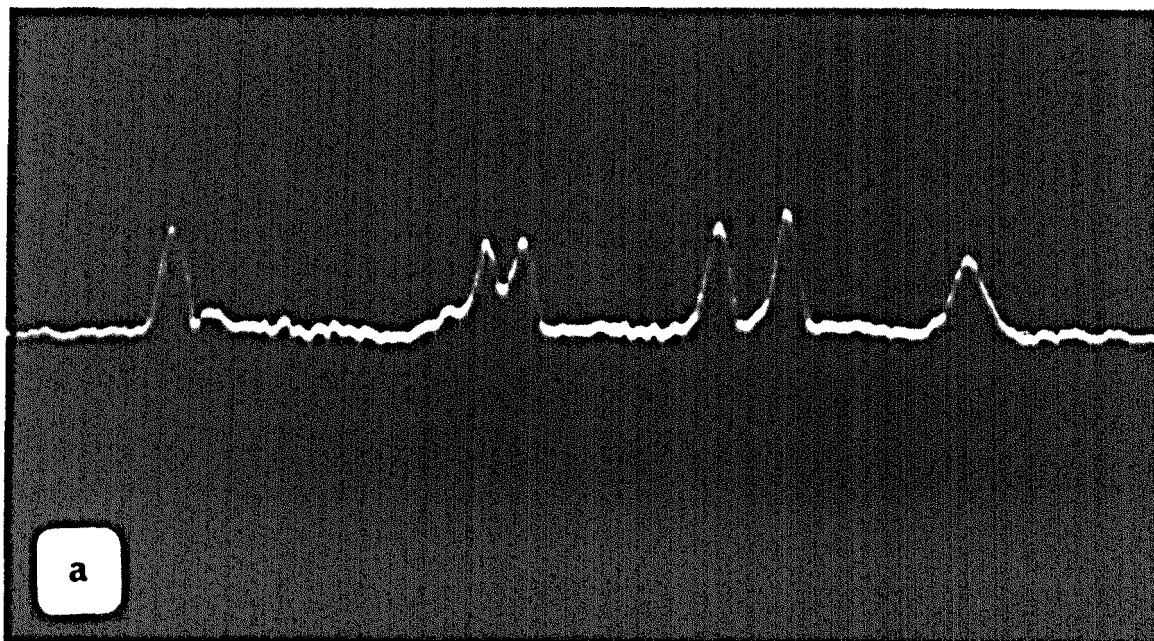


Fig. 3.22 STARK EFFECT ON $^{14}\text{NH}_3$ $J=K=1$ TRANSITION
(240 v/cm)

75.2 V/cm. This group of lines is comprised of three components, in agreement with theory (see Fig. 3.17).

During the observation of the Stark effect, an unusual phenomenon was observed, where the intensity and indeed the number of Stark components were dependent upon the relative polarity of the Stark voltage with respect to the polarity of E.H.T. applied to the state separator electrodes.

Fig. 3.21 illustrates one case of the electric field direction in the cavity and the state separator electrode polarities. In this case the main line components in a Stark field of 240 V/cm, shown in Fig. 3.22a, consists of seven components, while that of Fig. 3.22b for the same line in precisely the same magnitude of Stark field but of reversed polarity across the cavity with unchanged separator E.H.T. or polarity, consists of only six components. Here, the seventh component on the left-hand side of the figure (a) has completely disappeared and the relative intensities of the Stark components has changed.

This phenomenon could possibly arise as a consequence of spatial reorientation of molecules in the weak fringe field between maser cavity and state separator (Strakhovskii et al., 1966). However, this interpretation is hard to reconcile with the further experimental fact that the presence of an earthed metal screen between the state separator and the cavity did not eliminate the effect.

3.8 Operation of the Maser with TEM₁₀₁ Cavity Mode

In 1964(a) Krupnov and Skyvortsov calculated the spectral line shape using the following formula:

$$F(\omega_{12}, \omega_c) = \frac{\Omega^2 E_o^2 \sin^2 \left[\frac{\pi n}{2\Omega} (\omega_{12} - \omega_c) \right]}{[\Omega^2 - (\omega_{12} - \omega_c)^2]^2} \quad 3.7$$

where ω_{12} is the molecular transition frequency, ω_c is the signal frequency, Ω is the frequency of the change in the field amplitude during the flight of a molecule along the spatial distribution of the field $E(z)$, where $z = Vt$; V is the velocity of the molecule and n is the number of variations of the microwave field maxima within the resonator [$n = (\Omega/\pi)t$, where t is the time of flight of molecules through the resonator]. Thus, for $n > 1$ the line is split.

In 1964(b) Krupnov and Skvortsov observed the line splitting on account of the longitudinal Doppler effect in a formaldehyde beam maser at $\lambda = 4\text{mm}$ for $n = 2$ in a Fabry-Perot type resonator. According to Krupnov et al., the frequency separation between the components is $\Delta\nu = n\gamma/L$, where L is the length of the resonator, and the width of each component depends on the total time of interaction between a molecule and the stimulating microwave field. A similar effect was observed by Lainé and Smart (1971) in an ammonia beam maser employing a parallel plate resonator at $\lambda = 1.25\text{cm}$.

The reason for the observation of line splitting in this work was not merely to show the ability of this system to observe this effect even for a weak line of ammonia, but also to observe the beating of beats when the line was split artificially (Section 3.9), as proposed by Lainé and Sweeting (1971b), and to observe biharmonic oscillation (Section 4.7) on the basis of proposals by Krupnov et al. (1964b).

Operation of the maser resonator in a higher order mode (TEM_{101}) (next to the simplest mode) was obtained by a slight increase in resonator spacing to produce two maxima of microwave electric field of opposite phase along the beam axis. The frequency separation between

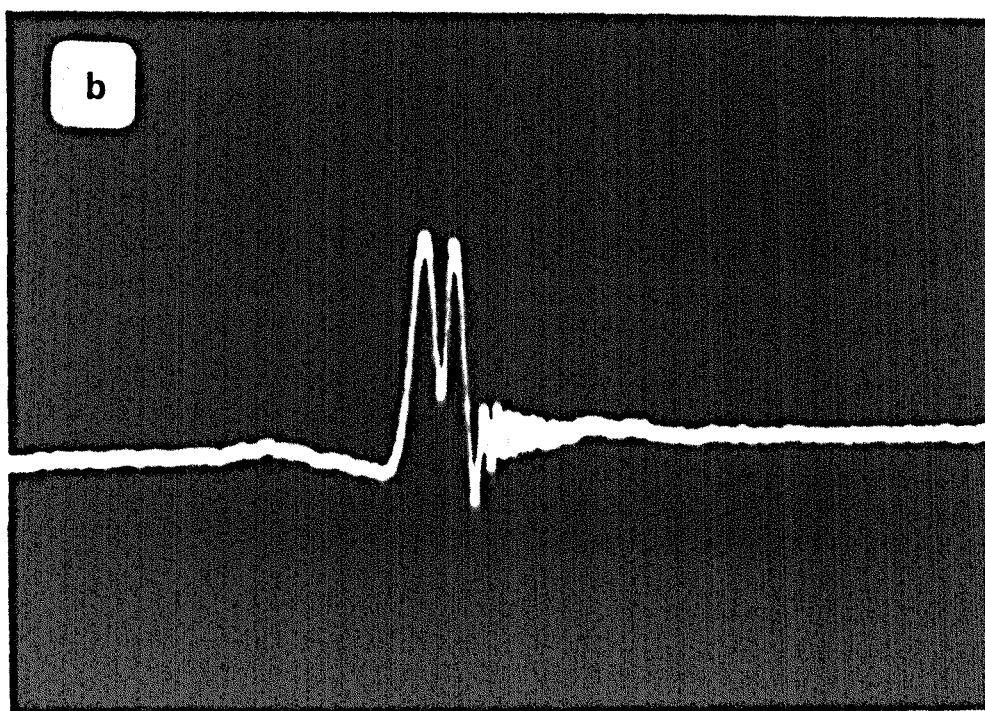
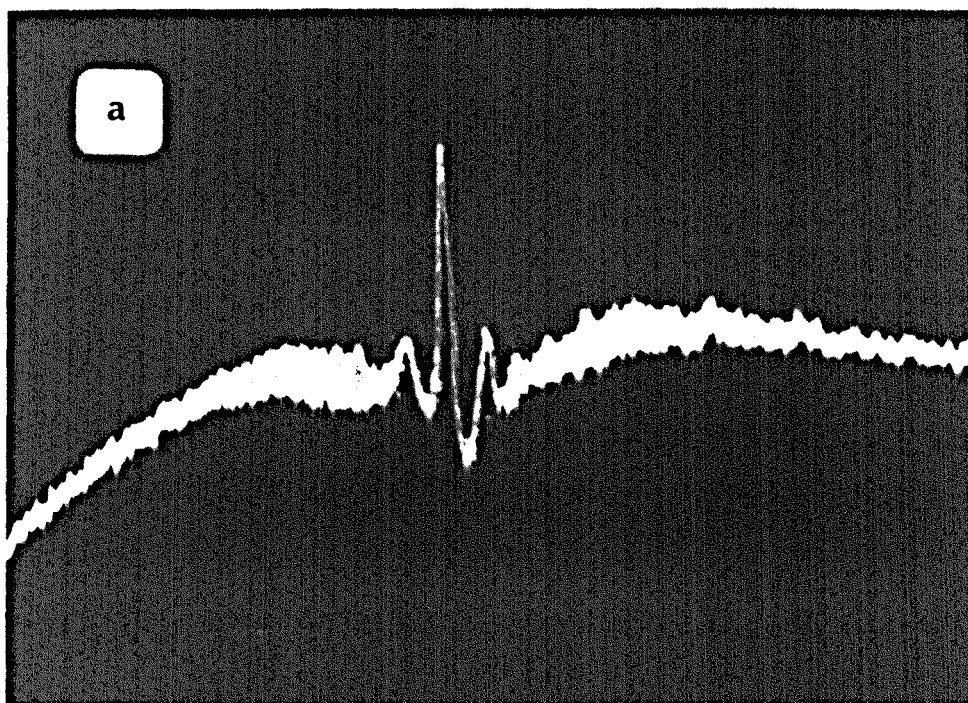


Fig. 3.23 THE $J=K=2$ INVERSION TRANSITION OF AMMONIA
(a) WITH ONE MAXIMA OF MICROWAVE FIELD
(b) WITH TWO MAXIMA OF MICROWAVE FIELD

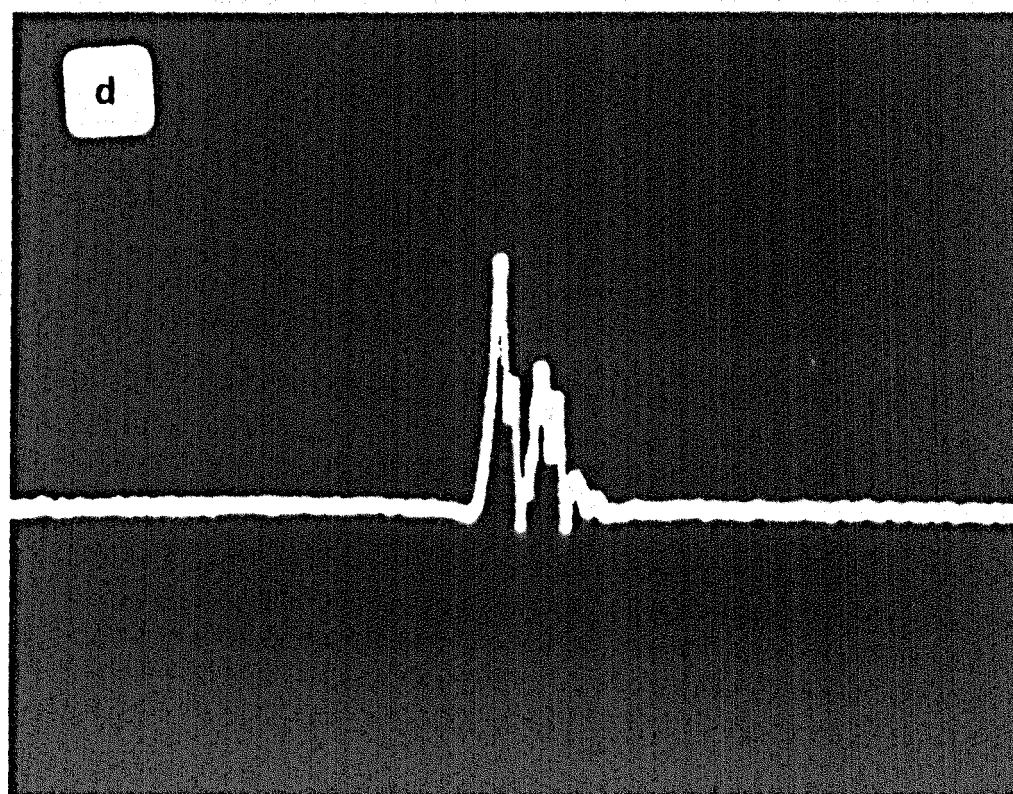
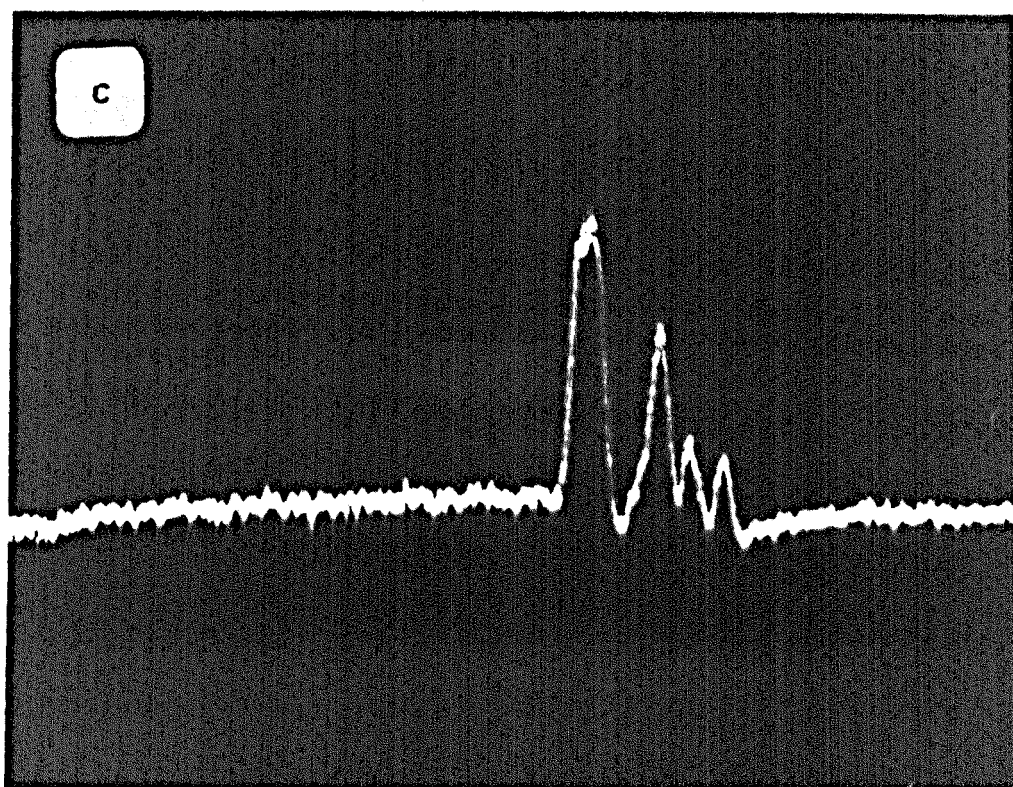


Fig. 3.23 THE $J=K=1$ INVERSION TRANSITION OF AMMONIA
(MAIN LINE)
(c) WITH ONE MAXIMA OF MICROWAVE FIELD
(d) WITH TWO MAXIMA OF MICROWAVE FIELD

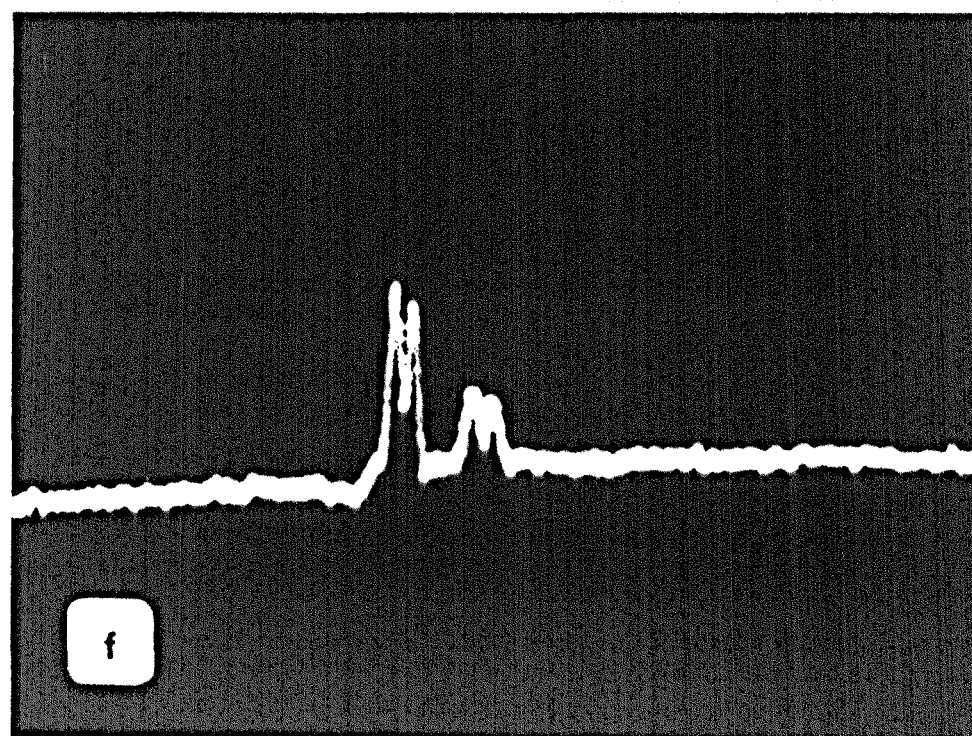
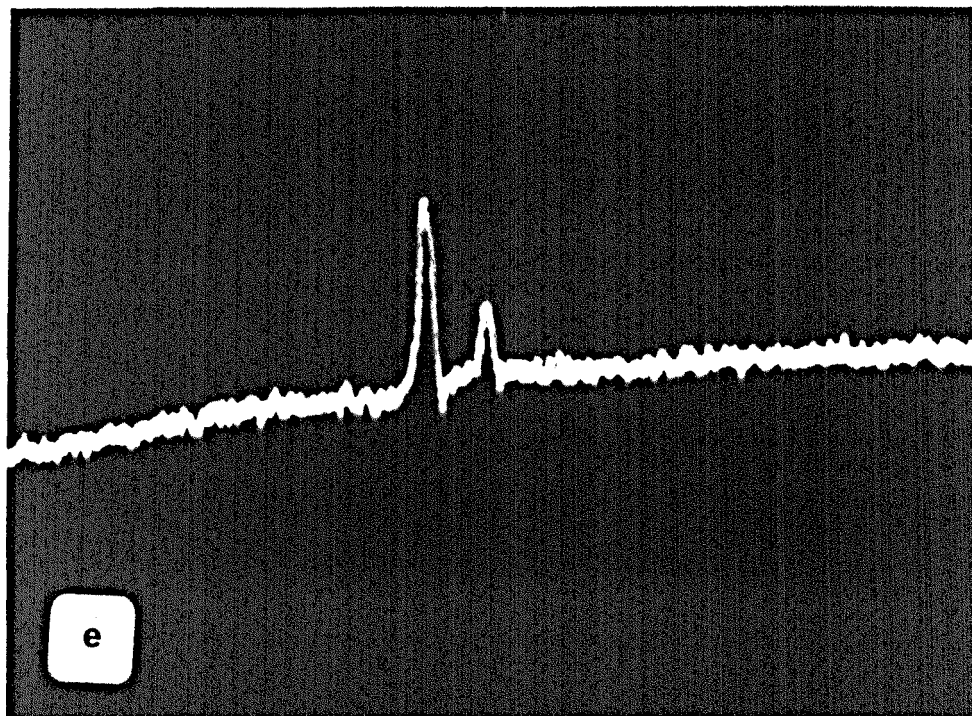


Fig. 3.23 THE $J=k=1$ INVERSION TRANSITION OF AMMONIA
 (OUTER SATELLITES ON THE LOW FREQUENCY SIDE
 OF THE MAIN LINE)
 (e) WITH ONE MAXIMA OF MICROWAVE FIELD
 (f) WITH TWO MAXIMA OF MICROWAVE FIELD

the lowest order mode (TEM_{001}) and the next mode (TEM_{101}) in this cavity was 28 MHz.

Fig. 3.23 shows the photographs of the emission line shape for the lines $J=K=1,2$ with $n = 1$ and $n = 2$, in the case of: (a) the $J=K=2$ main line when the resonator was operated (with respect to the molecular beam axis) with one maximum of electric field; (b) with two maxima of electric field; (c) the $J=K=1$ main line with one maximum of electric field; (d) with two maxima of electric field; (e) the $J=K=1$ outer satellites on the low frequency side of the main line with one maximum; whilst (f) shows the spectrum with two maxima of electric field.

3.9 Observation of a Beating of Beats Effect in both Naturally and Artificially Split Spectral Lines

Bloembergen et al. in 1948, observed an effect which they termed "wiggles" in a nuclear magnetic resonance system. Lainé, in 1966, observed the wiggles phenomenon in an electric dipole system for the first time. The effect followed upon the rapid passage of an exciting signal through the stimulated emission signal from the $J=K=3$ inversion line of ammonia in a beam maser. The exciting signal was frequency swept through the emission line in a time shorter than the mean transit time of molecules through the resonator cavity. Immediately after the passage of the exciting signal, the molecules in the cavity possessed an oscillating net polarisation at the molecular resonance frequency. After that they radiated spontaneously and coherently at a decaying rate, until they finally passed out of the cavity. The decaying ringing signal mixed with the applied exciting signal and produced the wiggles effect as a decaying beam signal of increasing frequency. The decay envelope of the wiggles given by Lainé et al. (1969) is:

$$A = A_0 \exp(-t/t_2)$$

3.8

where A_0 is the initial signal amplitude and A is the signal amplitude at a time t . A photograph of the wiggles which follows the main emission line $J=K=2$ of an ammonia beam maser is shown in Fig. 3.24a.

Under certain circumstances, however, the decay is not exponential and may take the form of an amplitude modulated decay signal known as "beating of beats". In particular, this may occur in a resonant system with closely spaced spectral lines, as it was observed by Gabillard (1951) in a magnetic dipole system, and occurred as a result of intermodulation of two wiggles signals from two closely separated resonance lines. In an electric dipole system, beating of beats was observed by Lainé and Sweeting (1971b) for the naturally split main inversion line $J=K=1$ of ammonia.

Lainé et al. (1971a) proposed that the observation of the beating of beats effect in an electric dipole system is not restricted to naturally split spectral lines. It is possible to observe the effect when a normally single spectral line is artificially split by using the Zeeman or Stark effect. However, in the present work, an artificially split main line of the $J=K=2$ inversion transition of ammonia to produce beating of beats, is achieved using the longitudinal Doppler effect by operation of the maser resonator in the next higher order mode relative to the simplestone (see Section 3.8).

Photographs of the "beating of beats" effect are shown in Fig. 3.24, which show in (b) the beating of beats effect from the naturally split main line of the $J=K=1$ inversion transition of ammonia and in (c) the beating of beats from the Doppler split main line of the $J=K=2$ inversion transition of ammonia.

From measurements of the period of the decaying interference pattern shown in Figure 3.24 (b) and (c), it is possible to calculate

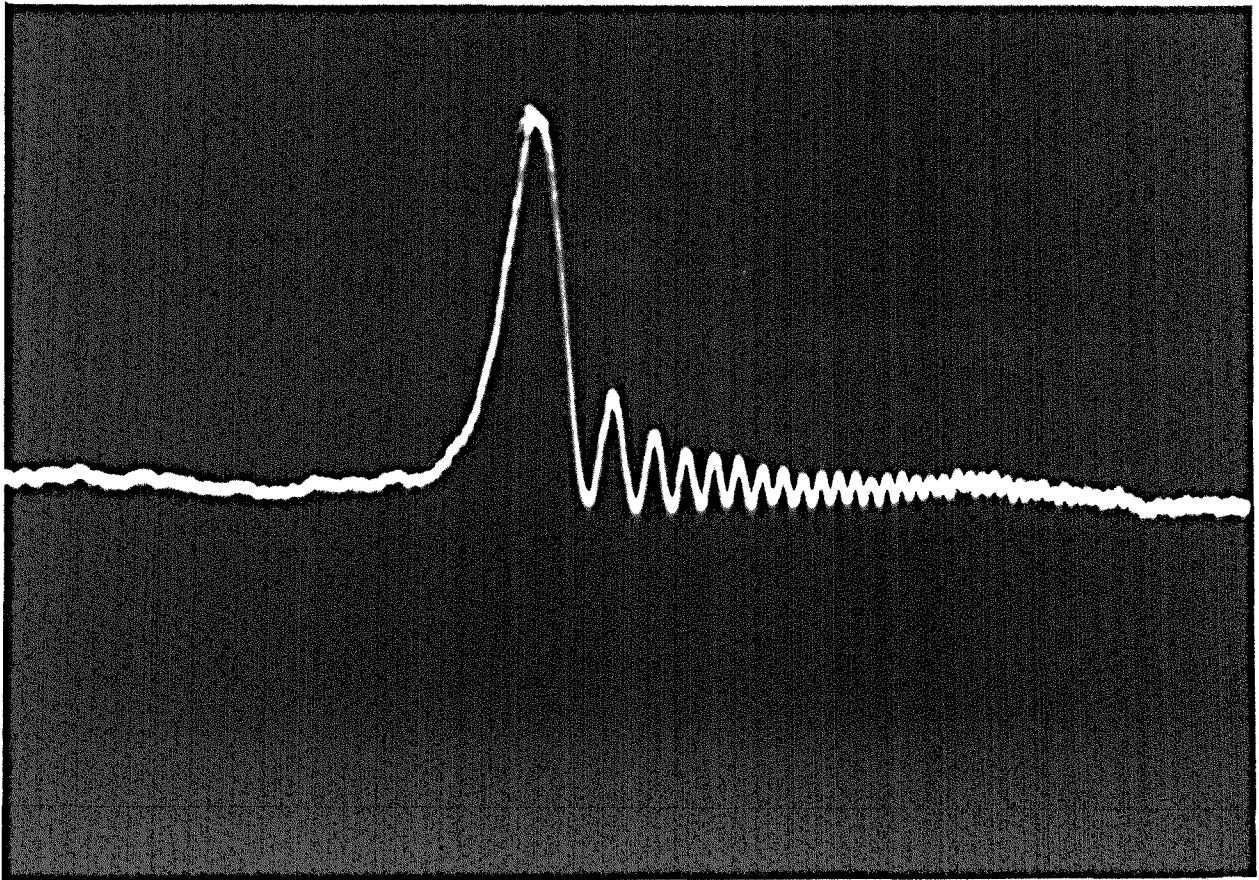


FIG. 3.24a THE 'WIGGLES' EFFECT FOLLOWING THE MAIN EMISSION
LINE OF THE $J=K=2$ INVERSION TRANSITION OF AMMONIA

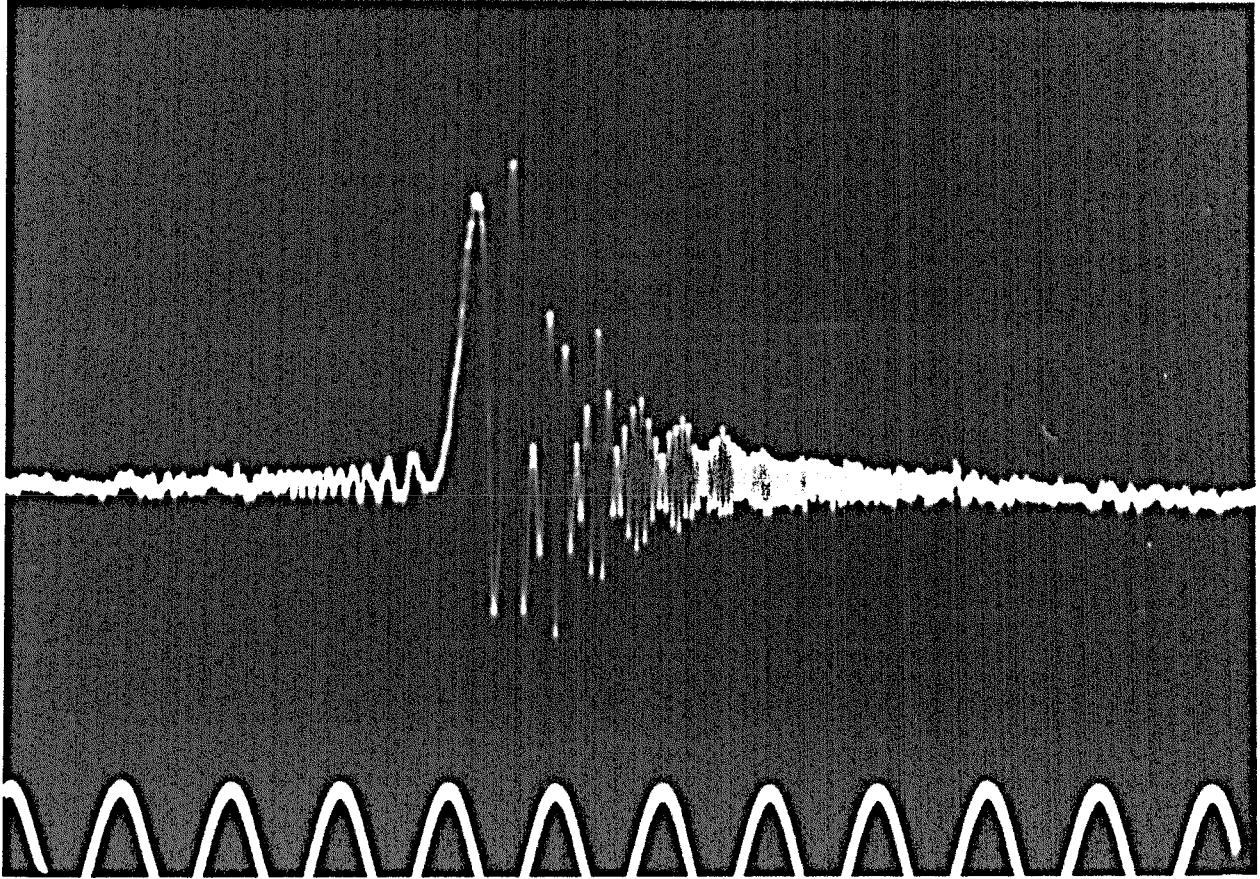


FIG. 3.24b

THE 'BEATING OF BEATS' EFFECT FOLLOWING
THE NATURALLY SPLIT MAIN LINE OF THE
 $J=K=1$ INVERSION TRANSITION OF AMMONIA

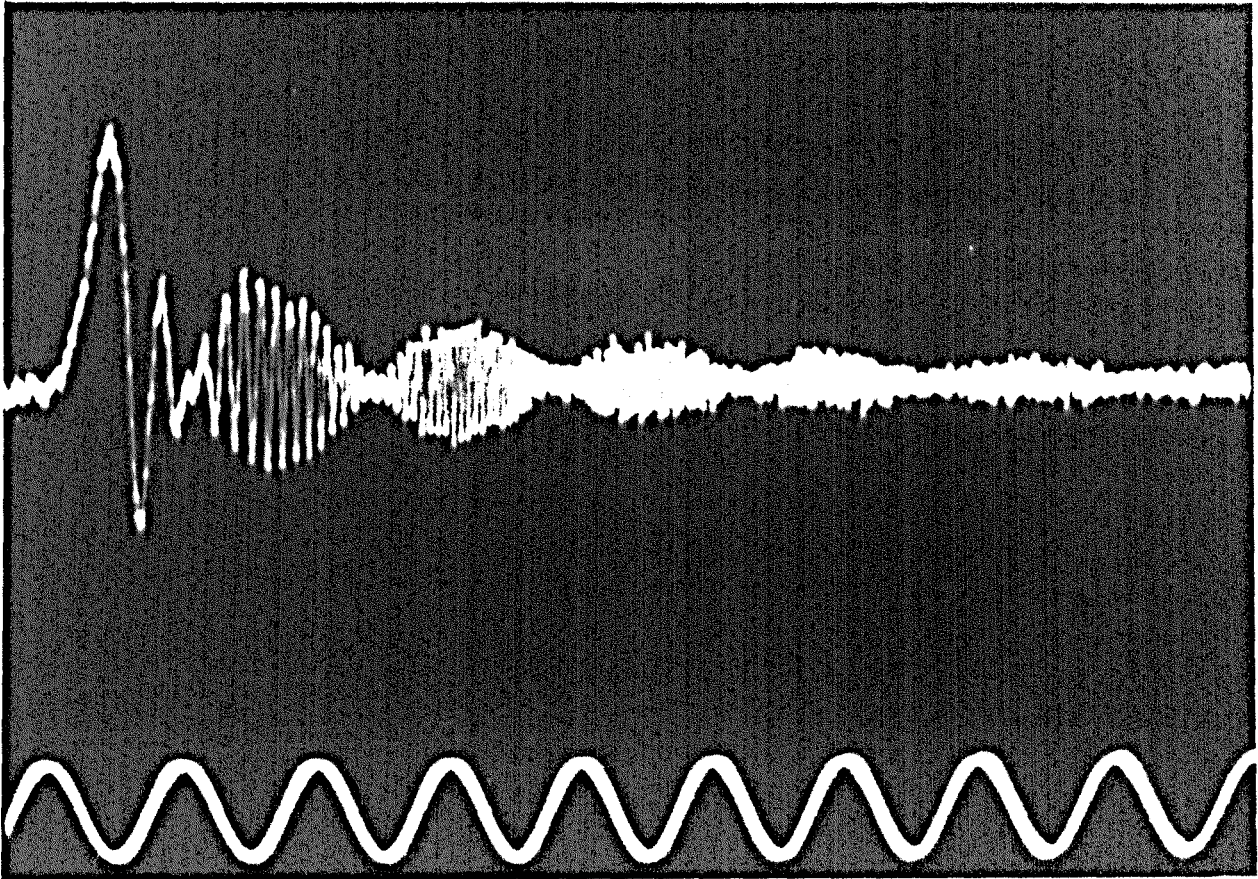


FIG. 3.24c THE 'BEATING OF BEATS' EFFECT FOLLOWING THE LONGITUDINAL DOPPLER SPLIT MAIN LINE OF THE $J=K=2$ INVERSION TRANSITION OF AMMONIA

the frequency separation of the resolved components of the naturally split line $J=K=1$ and Doppler split main line of the $J=K=2$, which are 24.4 kHz and 7.2 kHz respectively. The frequency separation of the resolved components of the $J=K=1$ main line result is in fair agreement with the value of 25.5 kHz recorded by Kukolich (1967).

CHAPTER FOUR

THE MASER AS AN OSCILLATOR

4.1 The Oscillation Frequency

If the power emitted from the molecular beam exceeds the power loss from the maser cavity, the system becomes self-excited and oscillation builds up. Equation 1.22 shows the oscillation condition for the molecular beam maser system. The frequency ω of the oscillation may be written (Oraevskii, 1967):

$$\omega = \omega_L \left[1 - \frac{\omega_L - \omega_0}{\omega_L} \frac{Q_0}{Q_L} \right] \quad 4.1$$

where ω_L is the frequency of the spectral line, ω_0 is the frequency of the resonator, Q_0 is the quality factor of the resonator and Q_L is the quality factor of the spectral line and equal to $\frac{1}{2}\omega_L\tau$, where τ is the time of flight of molecules through the resonator.

As can be seen from Equation 4.1, the oscillation frequency (ω) of a maser depends on the following parameters: the frequency of the spectral line, the natural frequency and Q-factor of the resonator and the width of the spectral line. In the simplest case, for which this equation is valid, the width of the spectral line depends only on the time of flight of molecules through the resonator. Actually, the width of the spectral line in a maser is made up of the spontaneous emission width, the Doppler width and the broadening owing to the finite time of flight of molecules through the resonator. The spontaneous width of an emission line is extremely small in the centimeter range of wavelengths. According to Basov and Prokhorov (1954), it is possible to eliminate the Doppler broadening in a molecular beam by exciting in the cavity the type of mode whose phase velocity in the

the direction of beam propagation is infinite. However, divergent molecules possess velocity components perpendicular to the fundamental wave and introduce a transverse Doppler broadening factor. This can be minimised if the system has a well collimated beam, so that with a suitable maser construction the line width is practically completely determined by the time of flight of the molecules through the cavity.

The actual distribution of the velocity of the molecules in a molecular beam which has been through a state separator differs from the function $(1/\tau')e^{-\tau/\tau'}$ (Skobeltzyn, 1964), where τ is the time a given molecule spends in the cavity and τ' is the average time of flight of the molecules passing through the cavity. Then the distribution of the time of flight of molecules is affected by the voltage on the state separator, which means that the effective line width depends on this voltage. Thus, it is convenient to write Equation 4.1 in the form

$$\omega = \omega_L \left[1 - \frac{\omega_L - \omega_0}{\omega_L} \frac{Q_0}{Q_L} G(U, \gamma_0) \right] \quad 4.2$$

where $G(U, \gamma_0)$ is proportional to the potential on the state separator (U) and to the saturation parameter (γ_0).

In the derivation of the formula (4.2) for the oscillation frequency of a maser, it was assumed that the molecular transition occurs only between two energy levels, so that the emission line consists of only one component of a definite frequency. In practice, however, it is hard to find a spectral line which consists of only one component; the presence of hyperfine interactions in the molecule leads to a splitting of the main transition into a number of hyperfine structure components (see Sections 1.2 and 3.3), and with practically attainable line widths many of these are not resolved. The peak

position (frequency ω_L) of such a line depends on the ratios of the intensities of the individual components and on their frequencies. In the beam which has undergone state selection, the ratios of the intensities of the components are changed, and the peak of the spectral line shifted relative to that of a non state-selected spectral line of the gas. This shift is not a constant quantity, but depends on the voltage of the state selection system, since the ratio of the intensities of the components varies with this voltage (Basov and Oraevskii, 1959). Moreover the different components have different values of matrix element of the dipole moment and show different degrees of saturation. The result is that the shift in question depends on the strength of the field in the resonator, such that, in the final analysis, the oscillation frequency in the maser depends on the intensity of the molecular beam.

Also in the derivation of the oscillation frequency formula, the resonator was represented as an oscillating circuit with lumped parameters. This idealization does not take into account the propagation of the electromagnetic energy along the resonator. Actually, the molecules do not emit uniformly along the length of the resonator, since the probability of emission increases the longer the time the molecule spends in the resonator. This causes a Doppler shift of the frequency of the spectral line. The magnitude and the sign of this shift depends on the intensity of the beam of active molecules (Oraevskii, 1967), since for a small beam intensity, which means weak saturation, the emission of energy from the molecules occurs mainly as they pass out of the resonator, and the flux of electromagnetic energy is directed against the motion of the molecules, which causes a decrease of the frequency. When the saturation is large, the molecules emit their energy in the first part of the resonator, and owing to this the flux of energy is propagated in the direction of motion of the molecules,

and this causes an increase of the oscillation frequency of the maser.

Because of the presence of unresolved hyperfine structure components and the non-uniformity of the radiation of the molecules along the resonator, it is convenient to rewrite Equation 4.2 again, in another form

$$\omega = \omega_L \left[1 - \frac{\omega_L - \omega_0}{\omega_L} \frac{Q_0}{Q_L} G(U, \gamma_0) + \Delta(U, \gamma_0) \right] \quad 4.3$$

where $\Delta(U, \gamma_0)$ is proportional to the ratio of the intensities of the components which varies with the state separator voltage (U).

Therefore, to secure high absolute stability ($\delta d_{\text{abs}} = \left| \frac{\omega_L - \omega}{\omega_L} \right|$) of the oscillation frequency of a maser ($\sim 10^{-10}$ and higher), it is necessary to use two oppositely moving identical beams through the resonator in a symmetrical fashion, and take off the power from the maser exactly in the middle of the resonator, to minimize the frequency shift caused by non-uniformity of the radiation of the molecules along the resonator.

Thus the design of a double beam maser system favours the achievement of the high active beam intensity in the resonator and in addition, improved frequency stability as an oscillator, using a spectral line in which there is no hyperfine structure. A line of this sort is the inversion transition $J=3, K=2$ of $^{14}\text{NH}_3$ or lines of $^{15}\text{NH}_3$. For the first one ($J=3, K=2$) there is no quadrupole hyperfine structure, but only the weaker magnetic hyperfine splitting. The magnetic splitting is small and the frequency shift is of the order of magnitude of one part in 10^{-11} . A disadvantage of this line is its relatively weak intensity (the condition for self oscillation is less well satisfied than for the line $J=K=3$ by a factor of about 135). However, Maroof and Lainé (1974), achieved oscillation on $J=3, K=2$ even without cryopumping.

by using a nozzle source of gas with a gain in beam intensity resulting from rotational cooling after gas expansion.

Thus, if the various perturbations on the oscillation frequency of a maser are eliminated, then the main factor which will now determine the frequency stability of the maser oscillation will be the time of flight of the molecules through the resonator. Under such conditions the frequency stability of the oscillation of the maser will improve with an increase of the time of flight. This can be realized in practice, by increasing the length of the resonator or by decreasing the average speed of the molecules in the beam.

4.2 The Oscillation Amplitude Characteristics (the $J=K=1,2,3$ lines of $^{14}\text{NH}_3$)

The amplitude of oscillation of the maser is often measured by a method of display which involves tracing out the I.F. amplifier bandpass with the I.F. signal derived from the maser oscillator itself. If the local oscillator is swept through a frequency range greater than the amplifier bandpass, then the output signal from the mixer passes through the full range of frequencies accepted by the amplifier. The output from the detector is then a display of the frequency response of the I.F. system, and the height of the response curve is proportional to the maser oscillation amplitude. This display is known as "bandpass display".

The oscillation amplitude characteristics of the maser have been studied using the ammonia inversion lines $J=K=1,2,3$, $J=3,K=2$ in $^{14}\text{NH}_3$ and $J=K=6$ in $^{15}\text{NH}_3$; most of the maser oscillation characteristics studies have been carried out on the line $J=K=3$, which is the strongest inversion line of ammonia. For this line the threshold condition is much more easily satisfied than for other lines, as for example with the

$J=K=1$ transition which is rather weak in intensity in comparison with other lines in the ammonia spectrum. The $J=K=3,2,1$ inversion lines have respective bulk gas intensities of $7.9 \times 10^{-4} \text{cm}^{-1}$, $3.2 \times 10^{-4} \text{cm}^{-1}$ and $1.9 \times 10^{-4} \text{cm}^{-1}$ (Townes and Shawlow, 1955). However, the maser system designed and built for this work (Chapter Two) has oscillated on the $J=K=1$, which has not previously been reported in the open literature using an open resonator. This result gives evidence for the efficiency of the maser system constructed with an open resonator such as that discussed in this thesis.

The oscillation amplitude measurements as a function of various experimental parameters are shown in Figs. 4.3 and 4.4. In Fig. 4.3 the relative oscillation amplitude is plotted against nozzle pressure (nozzle diameter 0.09mm) for various values of state separator voltage, (a) for the inversion line $J=K=1$, (b) $J=K=2$ and (c) $J=K=3$, and in Fig. 4.4, the oscillation amplitude is plotted against state separator voltage for various values of nozzle pressure, for the inversion line (a) $J=K=1$, (b) $J=K=2$ and (c) $J=K=3$. These families of curves give a complete picture of the oscillation behaviour of the maser for a given geometrical arrangement of the maser components.

A peaking of the oscillation amplitude with nozzle pressure is demonstrated for the lines $J=K=1,2,3$ in Fig. 4.3. This oscillation amplitude maximum is due to the collisions of the molecular beam within the state separator itself, rather than with background gas, because the pressure of the chambers appears to remain constant with all values of nozzle pressure up to 760 torr. In Fig. 4.4 the curves corresponding to the tapered state separator shows a saturation behaviour. This is probably a consequence of its small angle of capture, in that when the critical velocity in Equation 1.12 is greater than the transverse velocity (V_y) of the majority of molecules entering the state separator,

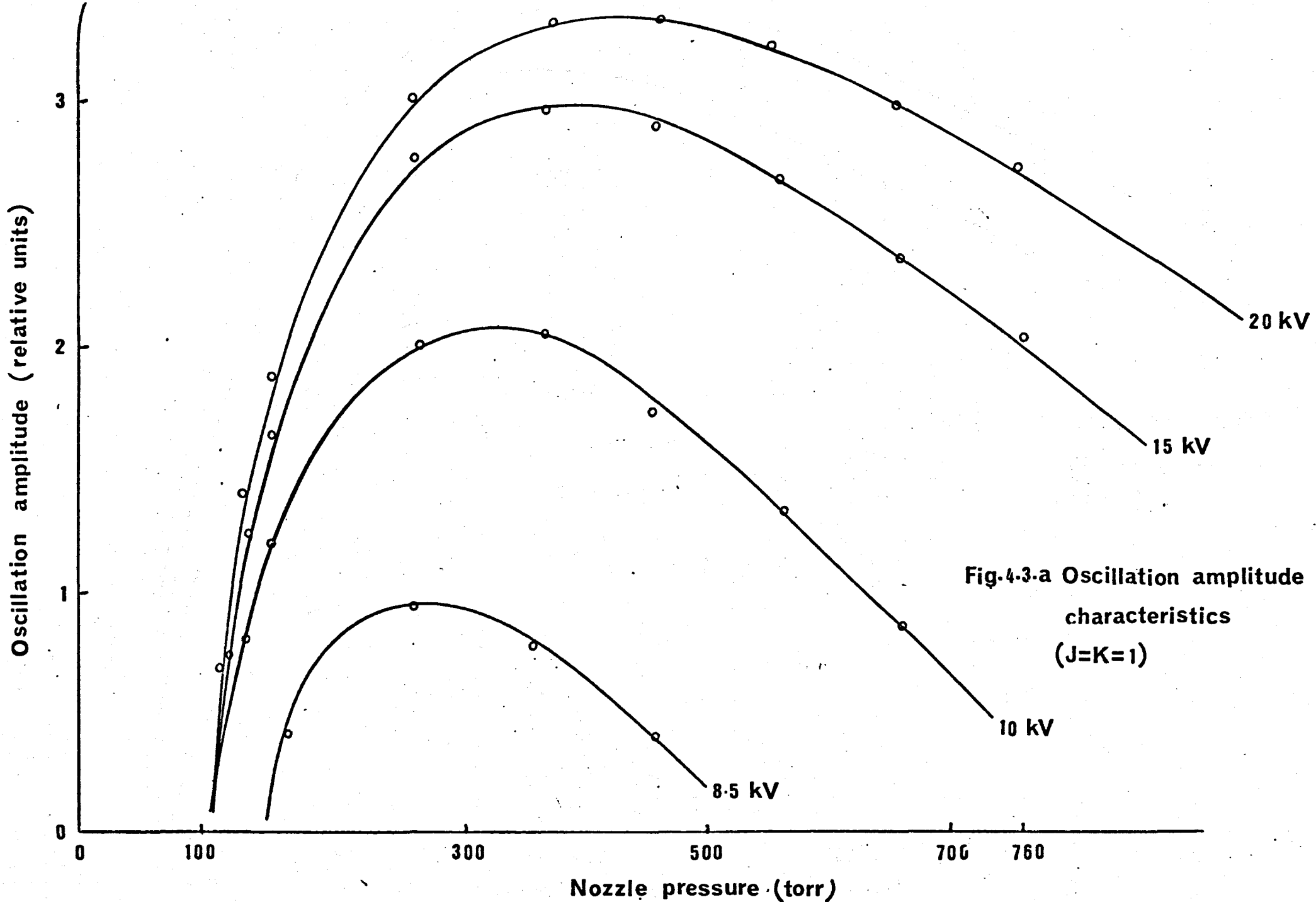


Fig.4-3.a Oscillation amplitude characteristics (J=K=1)

Oscillation amplitude (relative units)

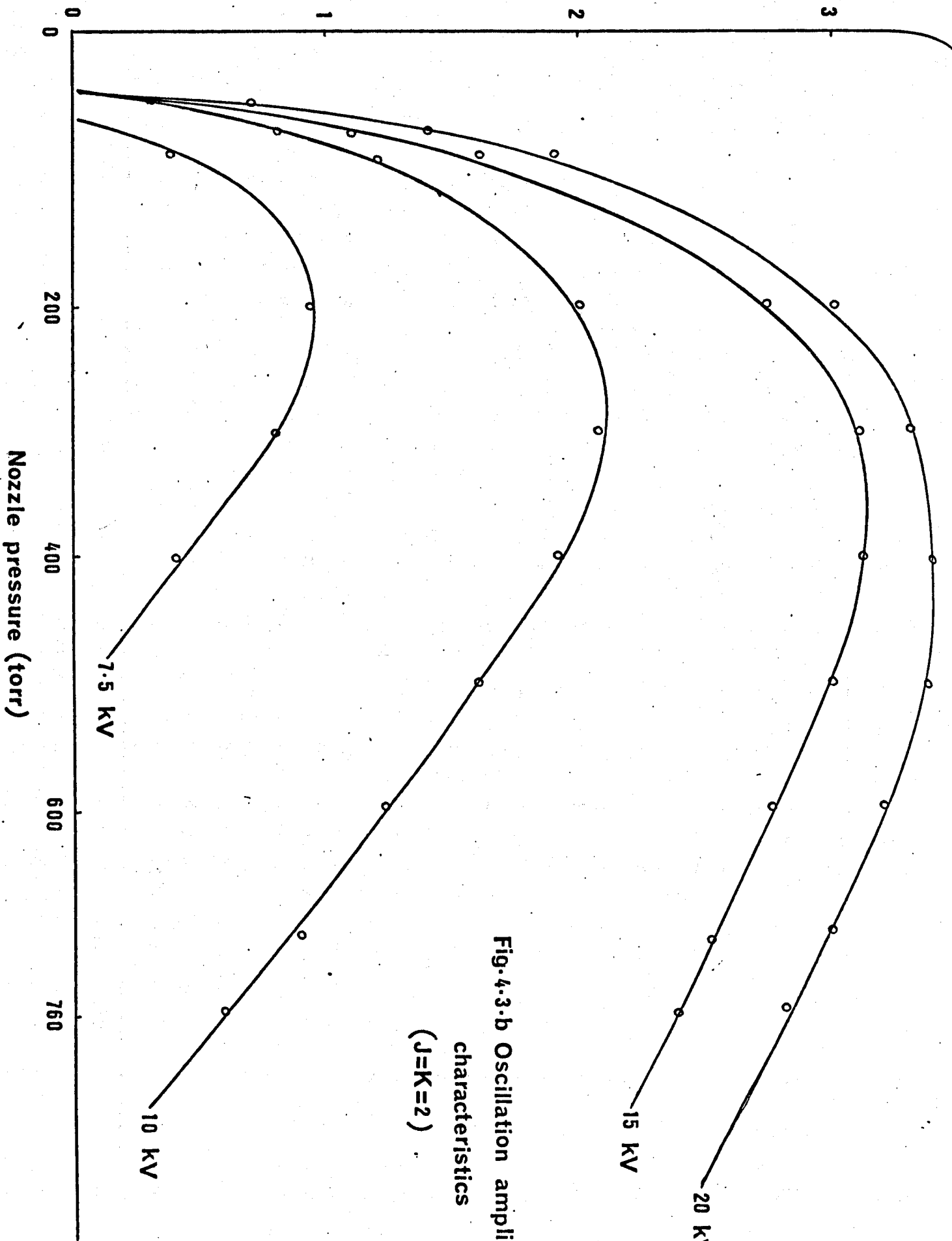


Fig. 4.3-b Oscillation amplitude characteristics (J=K=2)

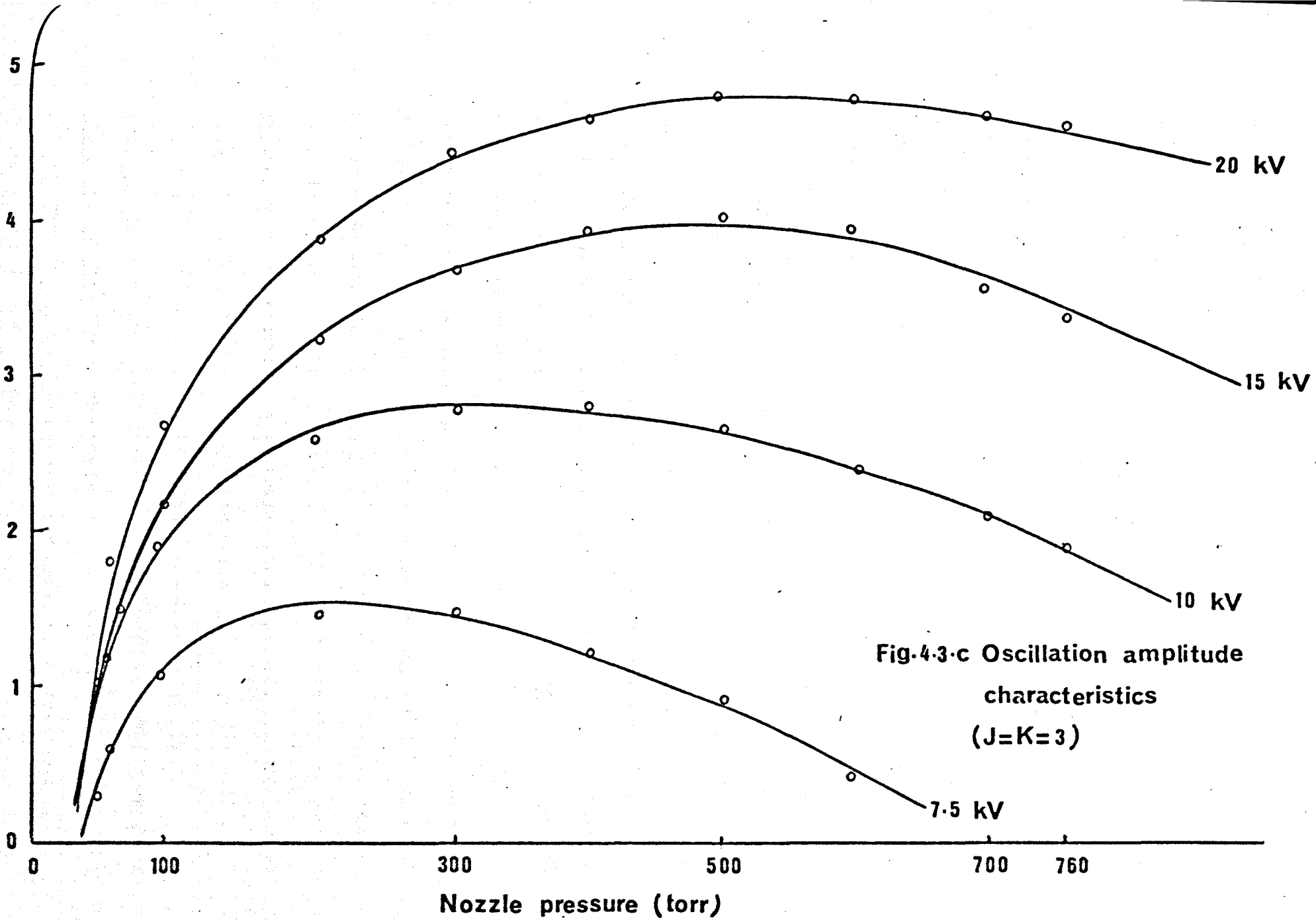


Fig.4.3.c Oscillation amplitude characteristics (J=K=3)

no more molecules are available to be focused as the voltage is increased. A similar saturation behaviour has been noticed when the tapered ladder state separator was used by Becker (1963) and Smart (1973).

As a result of the limited population of the molecules in the upper inversion level for each inversion transition, the state separator voltage for which the onset of the saturation is noticed for each line varies somewhat with the nozzle pressure (Fig. 4.4). The difference in the relative amplitude of oscillation for the curves with different values of state separator voltage for the same line as shown in Fig. 4.3, is presumably due to the presence of scattered molecules both inside the state separator and the cavity.

Also from these figures, it can be seen that the values of the state separator voltage for the three lines ($J=K=1,2,3$) in the same value of nozzle pressure, and the optimum nozzle pressure in the same value of state separator voltage at the maximum oscillation amplitude, are different from one inversion line to another. This difference is as a result of the different population of the molecules in the upper inversion level between the lines $J=K=1,2,3$. For this reason, the optimum state separator voltage and nozzle pressure for different inversion lines in the same maser system, are different to obtain a maximum oscillation amplitude. With the open cavity maser it is important that the cavity be carefully tuned to the centre frequency of the spectral line studied when amplitude measurements are made. Since variation in the quality factor of the cavity will also affect the measured values, the lowest threshold state separator voltages are not reproducible with great accuracy with the open cavity, since the parallelism of the plates is very hard to control. The lowest state separator voltages for oscillation threshold for the

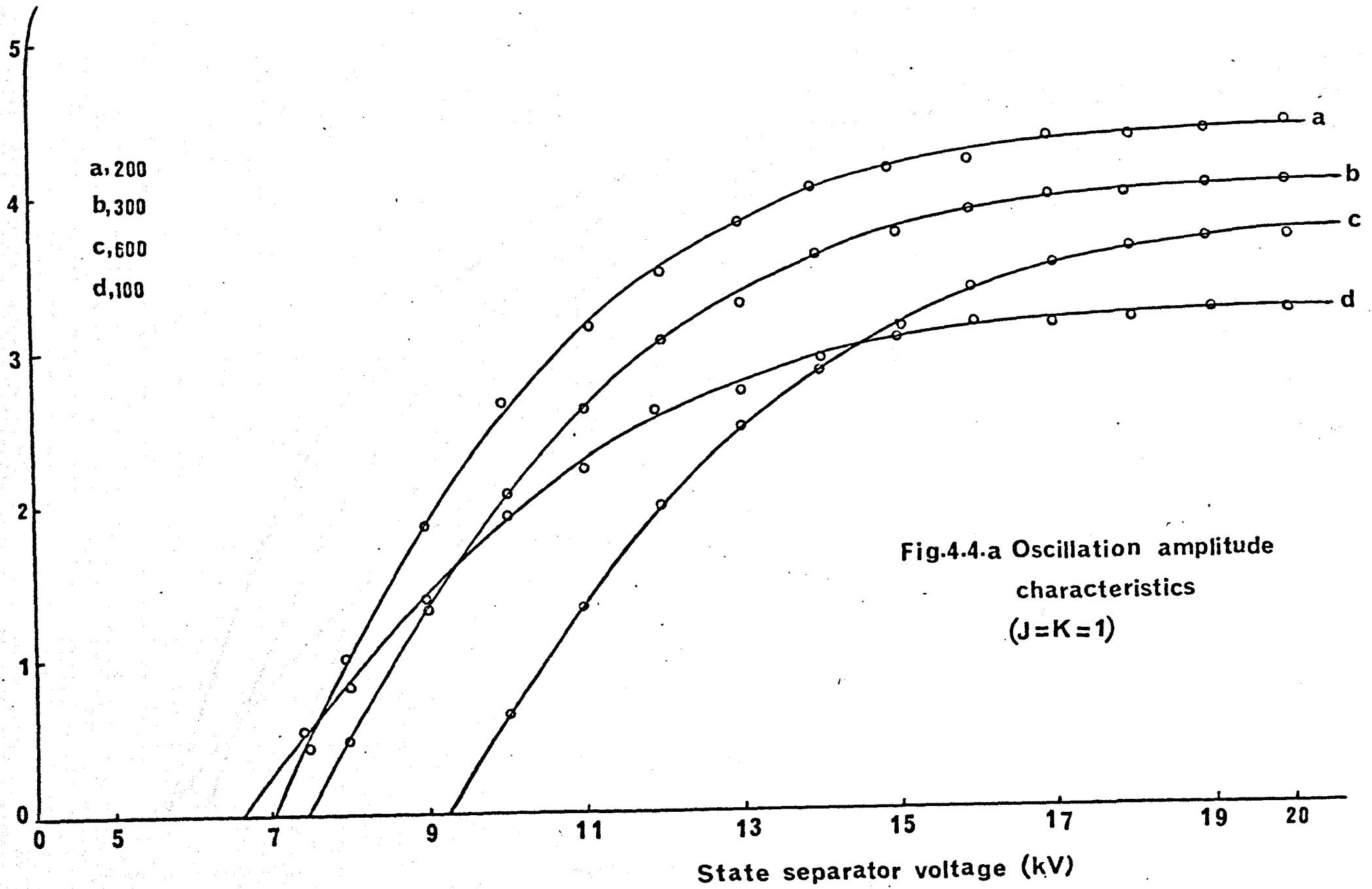


Fig.4.4-a Oscillation amplitude characteristics (J=K=1)

Oscillation amplitude (relative units)

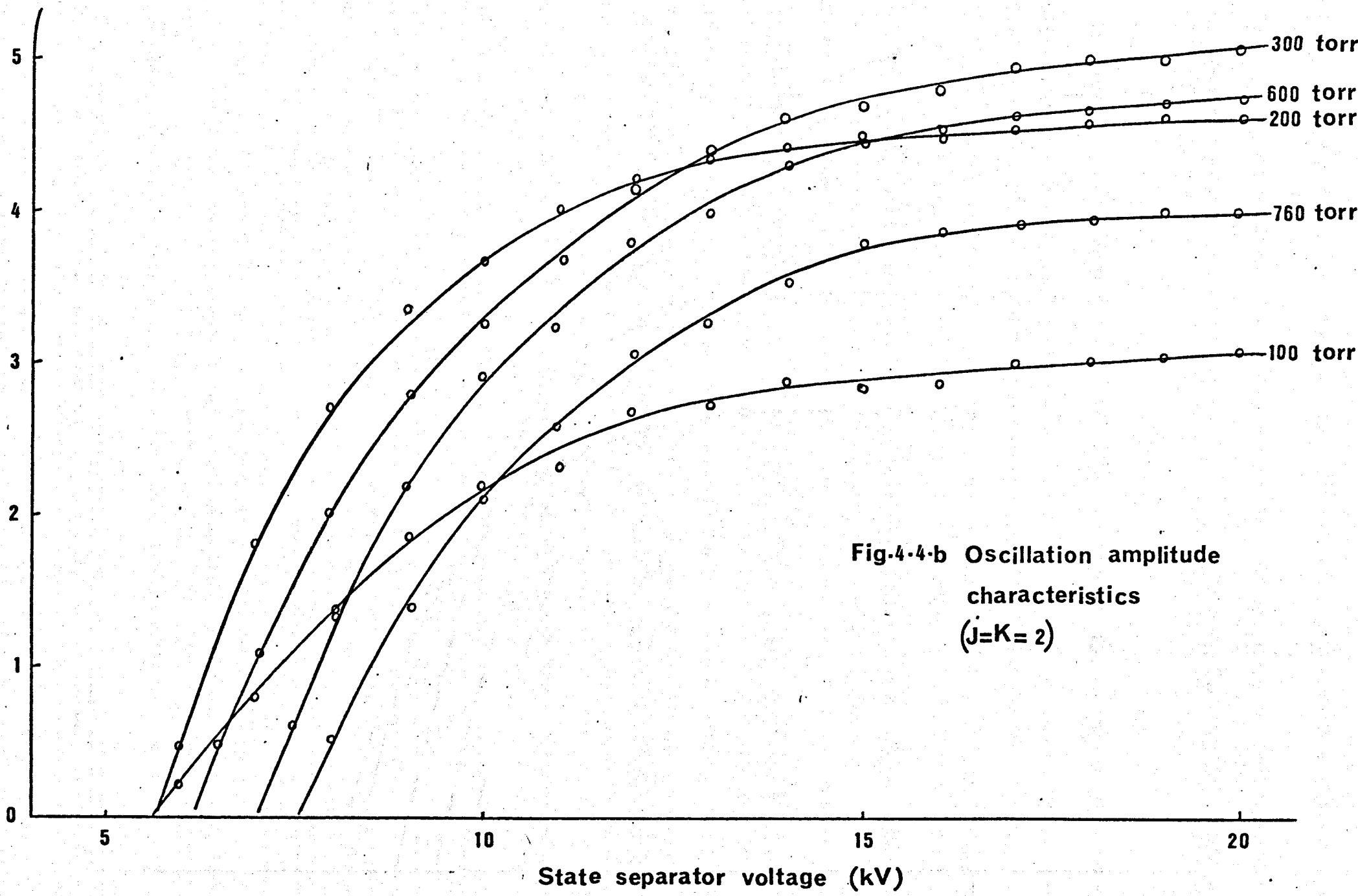
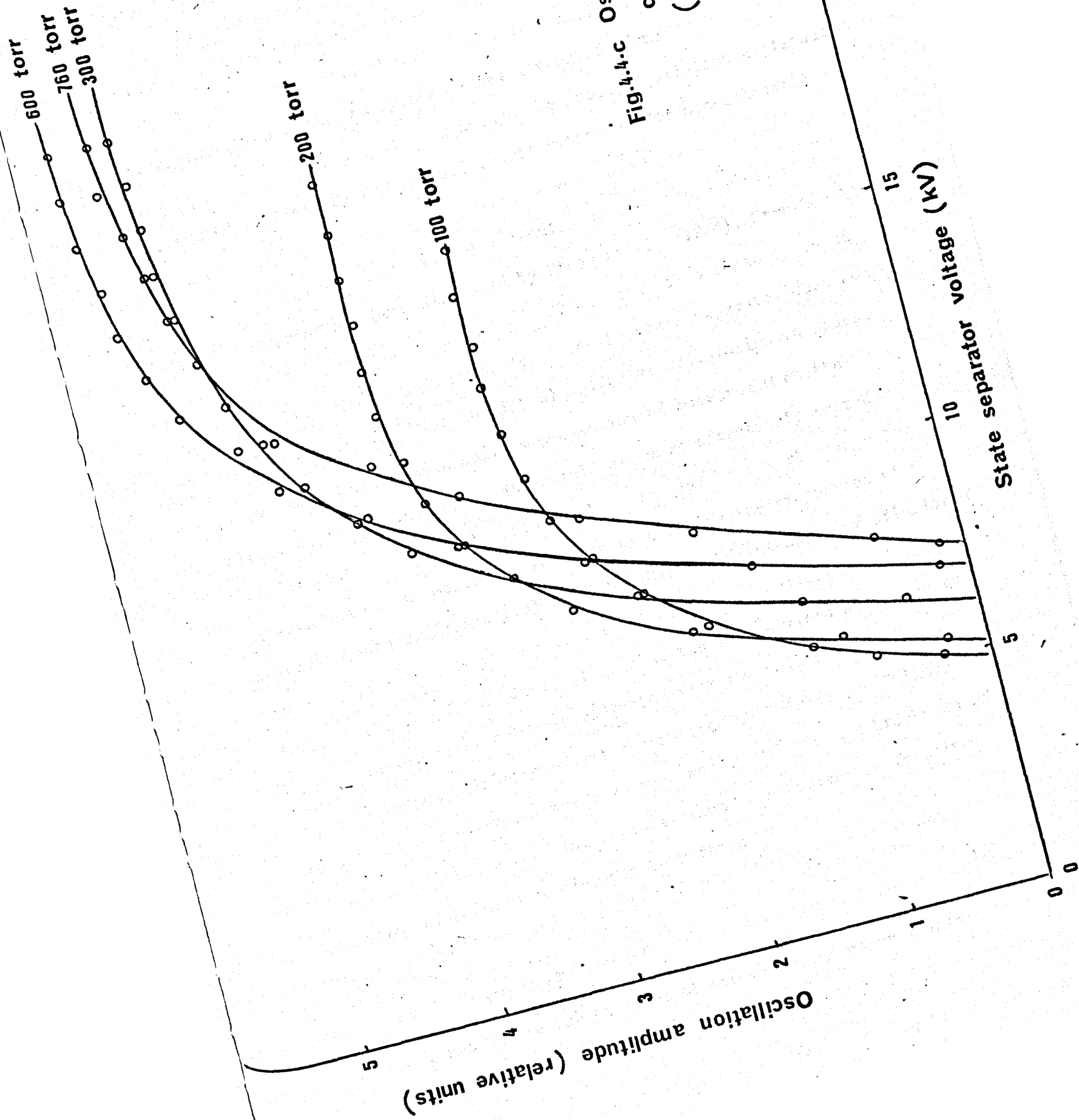


Fig.4-4-b Oscillation amplitude characteristics (J=K=2)

Oscillation amplitude characteristics
($J=K=3$)



$J=K=1,2,3$ respectively were 6.6, 5.5, 5.0 kV.

All the measurements cited so far were obtained in the presence of an earthed electric-conductor screen, to minimize the weak electric fringe field between the maser cavity and the state separator which may be as much as several tens of V/cm. The presence of such a field can change the maser oscillation amplitude (frequency, power) by the spatial reorientation and/or non-adiabatic effects.

Spatial reorientation of molecules by the fringe field of the state separator has been discussed by Basov et al. (1964), Strakhovskii et al. (1966) and Truman and Lainé (1976). This is a consequence of the fact that the beam of molecules from the state separator does not possess an isotropic distribution of molecular orientation in space, since the molecules with maximum projection of momentum M on the direction of the state separator field are more effectively sorted. An additional field in the path of the molecular beam will change the orientation of the molecules in space by changing the proportion of molecules with different projection M . Since the intensity of stimulated emission also depends on the mutual orientation of molecules and the field in the resonator, it is clear that the fringe field will lead to changes in intensity of maser radiation from the molecules.

The non-adiabatic effect was noticed by Shimizu and Shimoda (1961), in the low frequency beam-type maser, which was a breakdown of so-called adiabatic focusing approximation. The adiabatic focusing condition of Shimizu et al., can be written

$$\frac{h}{(W_2 - W_1)^2} \bar{v} \mu_{12} \frac{\partial E}{\partial x} \ll 1 \quad 4.4$$

where W_1 and W_2 are the energies of the lower and upper levels

respectively, \bar{v} is the mean molecular velocity, μ_{12} is the matrix element between the two maser state selectors and $\frac{\partial E}{\partial x}$ is the rate of change of the electric field in the direction of travel of the molecules in the beam. According to Shimizu and Shimoda (1961), Equation 4.4 is always fulfilled in a maser operating in the microwave region. Basov et al. (1964) indicated that the behaviour of a molecule in an inhomogeneous field of several tens of V/cm, is not fully adiabatic. Transitions between the closely spaced Stark sub-levels can occur; this corresponds in classical terms to the inability of the molecule to follow the rapidly changing field direction so that some of the interaction energy is absorbed in changing the molecule's internal state.

In Fig. 4.5 the oscillation amplitude is plotted against the state separator voltage, for the lines $J=K=1,2,3$ with the same value of nozzle pressure (200 torr) in the presence of the fringe field (without a metallic mesh screen). In contrast, the amplitude of maser oscillation in the absence of the fringe field (Fig. 4.4) increases monotonically, as the voltage applied state separator is increased up to the value of the voltage for the state separator for which saturation of the maser oscillation sets in. But in Fig. 4.5 (a,b,c), this monotonic increase of amplitude no longer occurs for all of the three inversion lines studied ($J=K=1,2,3$).

During the investigation of the nozzle diameter on the behaviour of maser operation, it was noticed that there was no effect from the fringe field on the oscillation amplitude without a screen when the nozzle diameter was changed from 0.09mm to the bigger one such as 0.1mm. This result may be explained as a consequence of an increase of the mean molecular velocity \bar{v} (nozzle and vacuum chambers pressure are fixed) to a value that can significantly affect the inequality of

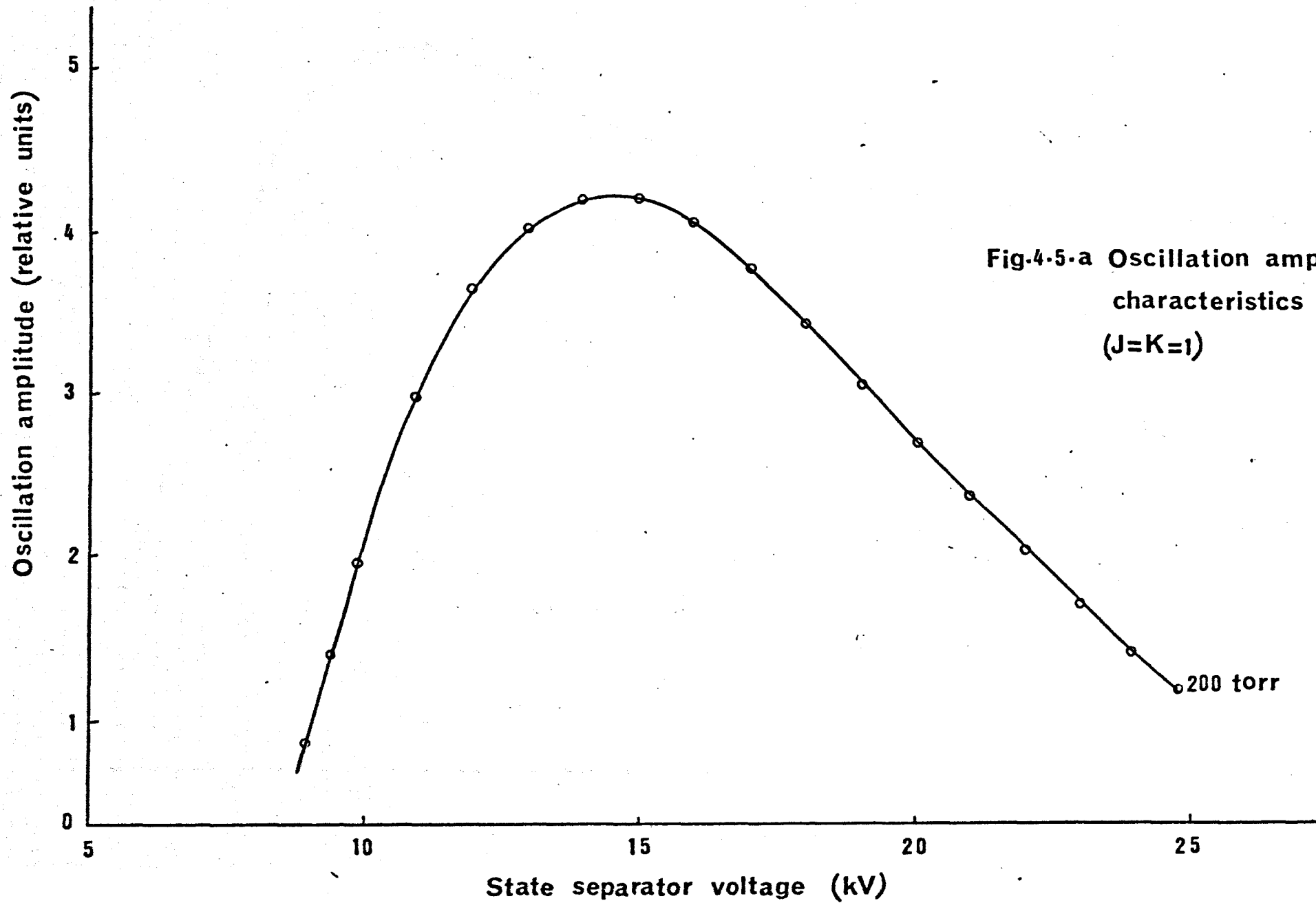
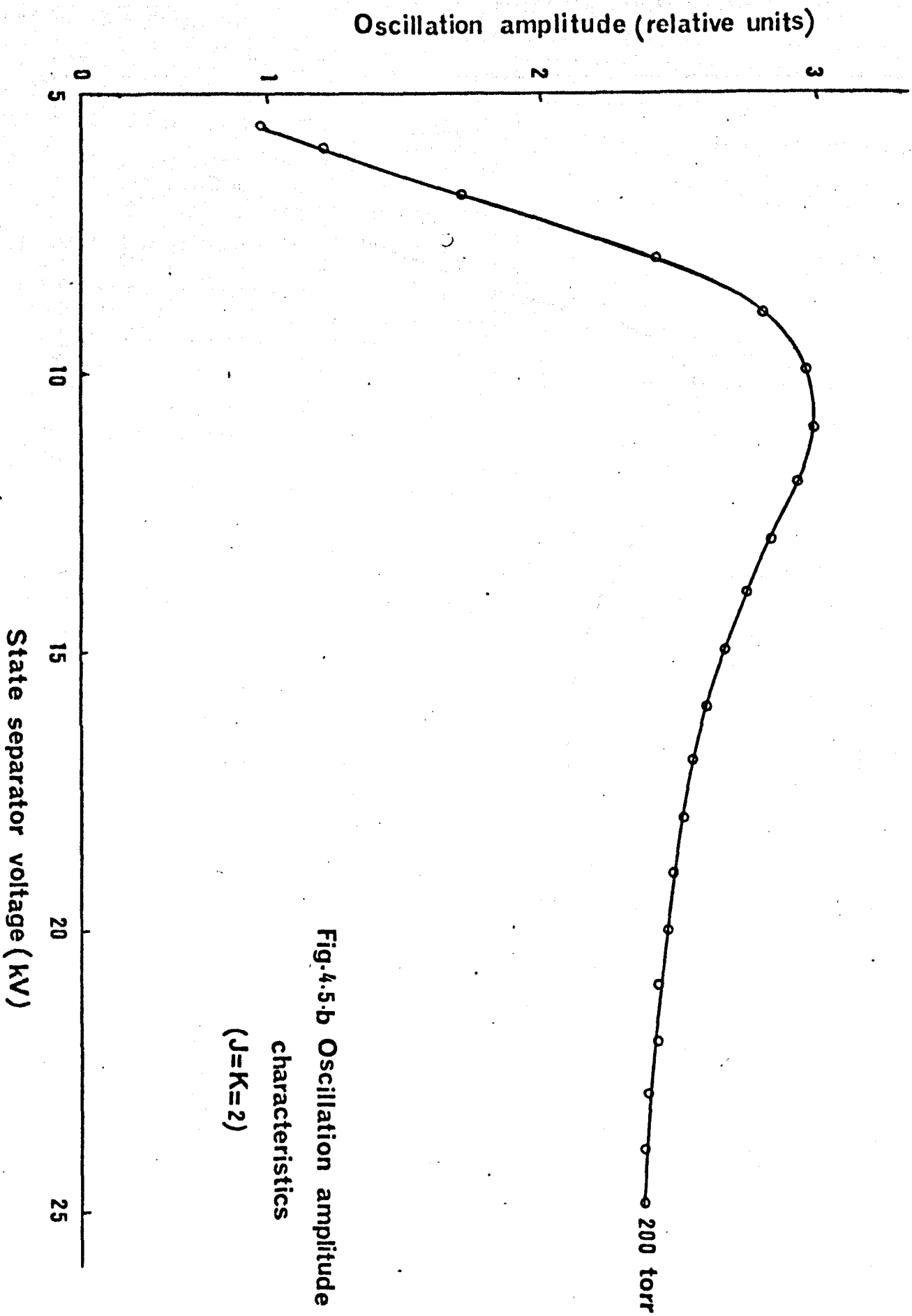
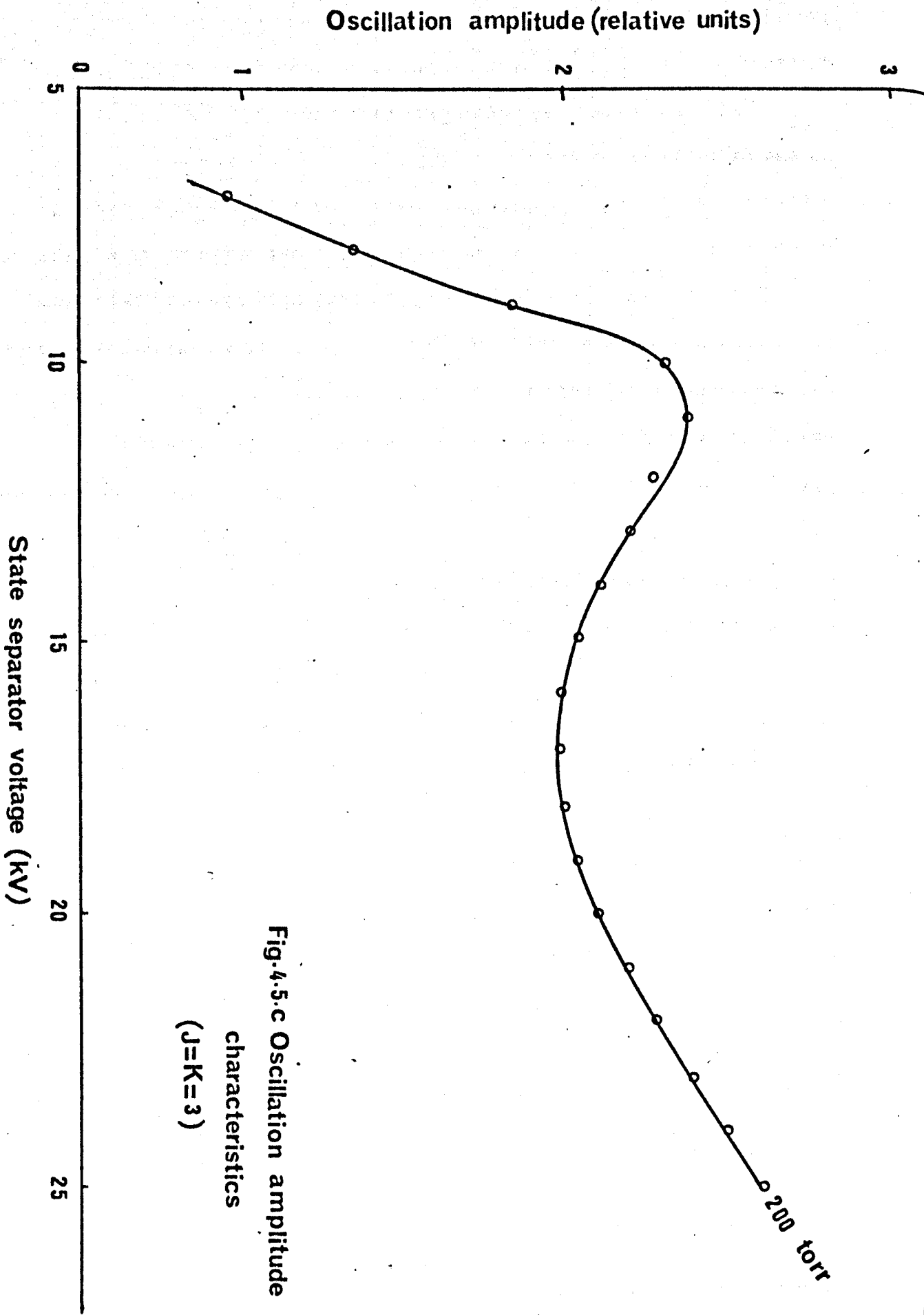


Fig.4-5-a Oscillation amplitude characteristics (J=K=1)

200 torr





the adiabatic focusing condition 4.4. But whether the change in the mean molecular velocity is sufficiently large to affect the inequality of the adiabatic focusing condition 4.4, remains an open question.

4.3 Oscillation in the Next Higher Order Cavity Mode (TEM₁₀₁)

The operation of the open resonator in a higher mode to obtain a line splitting on account of the longitudinal Doppler effect, has been discussed in Section 3.8. Here the observation of the maser oscillation on the two components of the split line, is discussed. The results obtained offer the first unambiguous results for a maser system oscillating with an open parallel plate resonator in a higher mode of operation than the fundamental.

Bonanomi and Herrmann (1956) suggested a method for the precise tuning of a closed resonator ammonia maser, by means of frequency jumps if E_{0ln} types of resonator ($n > 1$) are used, and the cavity is tuned through the split line, the oscillation jumps from oscillating on one component of the split line to the other. When Becker (1966) applied this method, he found the oscillation in his system was only possible on either one or other component by tuning the closed resonator through the centre of the molecular resonance frequency, rather than both. The frequency jump was found to be accompanied by an amplitude jump which showed a hysteresis effect.

Similar amplitude jumps were observed with the open resonator maser, employed in this work, when the system was operated at a state separator voltage or molecular beam flux such that a single oscillation on one or other component of the split line could be supported.

With this mode of operation, biharmonic oscillation was obtained on the two components of the split line of ammonia inversion lines $J=K=2,3$. The state separator voltage necessary to support a

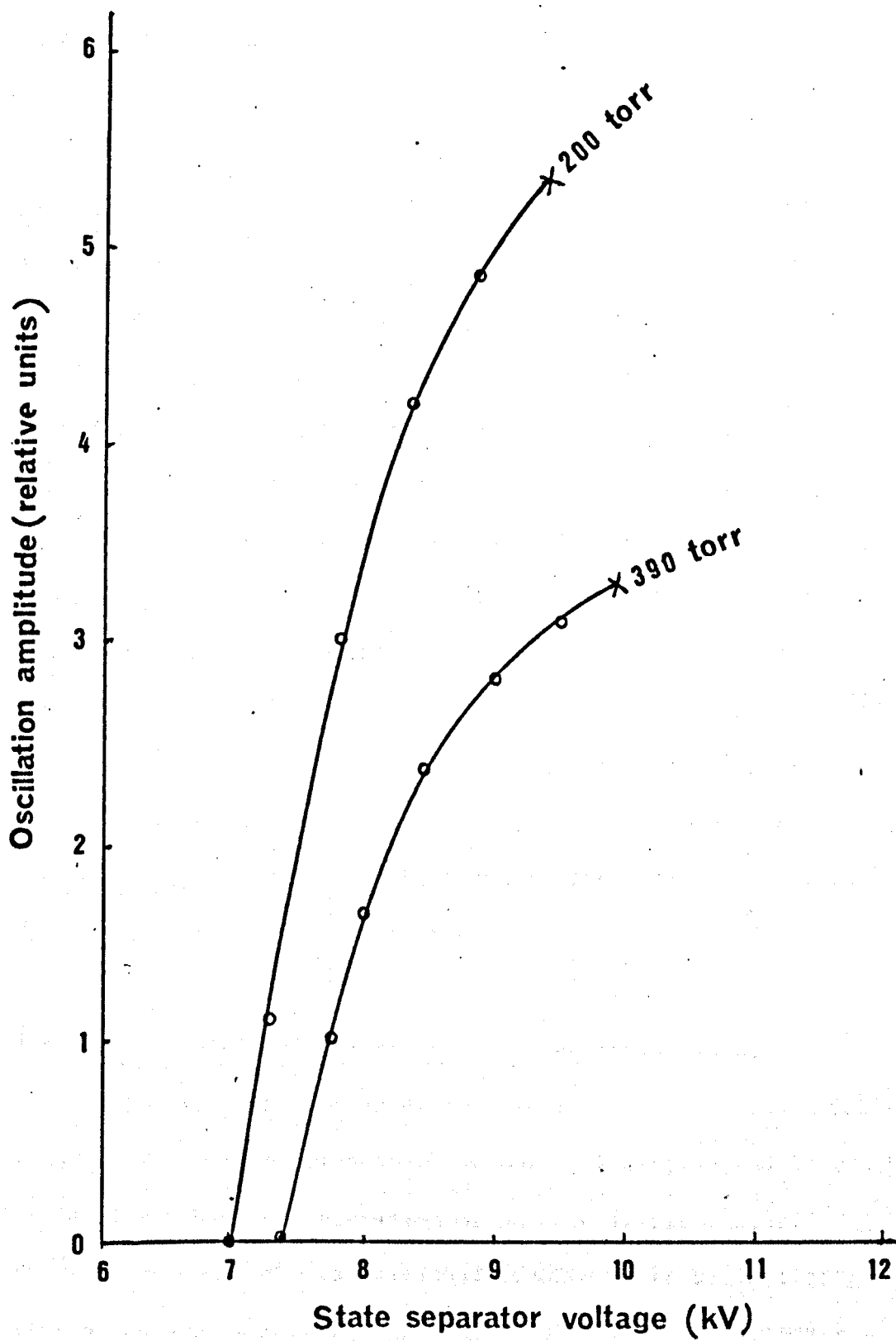


Fig.4.6 Oscillation amplitude characteristics

single oscillation on one component of the split line was 7 kV and biharmonic oscillation set in at a state separator voltage of 9.6 kV with an optimum nozzle pressure in both nozzles of 200 torr. The first and second threshold state separator voltage for the inversion line $J=K=3$, was expected to be less than the threshold of the inversion line $J=K=2$ in this type of operation, since the $J=K=3$ line is the stronger one. However, this was not the case, probably on account of loss of precise mirror parallelism, as a result of tuning from the line $J=K=2$ to the line $J=K=3$ from outside the vacuum chamber by using the mechanical tuning mechanism only.

In Fig. 4.6 the oscillation amplitude for the inversion line $J=K=2$ is plotted against the state separator voltage for two values of nozzle pressure. The point (x) on the end of each curve indicates the onset of oscillation of the second component. This is easily observed because, as soon as the second components starts to oscillate, a beat between the two oscillation frequencies appears on the I.F. bandpass response. The actual value of the beat frequency will be discussed in the following section.

4.4 Biharmonic Oscillation in a Disc Resonator Maser

Between 1963 and 1964, two papers presenting essentially the same results were published by Barchukov, Prokhorov and Savranskiy, concerning biharmonic operation of an ammonia-beam maser. The discussion of the experimental results in these publications were very brief and, therefore, impossible to understand in detail. Barchukov et al. found that if a constant electric field (d.c.) of the order 30 V/cm was applied to the open resonator plates, the frequency beat was 5.4 kHz, and with further increase of the voltage, maser oscillation was cancelled. If a thin wire was inserted between

the plates then the beat frequency was about 600 kHz, whereas under ordinary conditions (which is presumed to mean without d.c. electric field and the thin wire) the frequency of the beat was about 3.8 kHz.

However, Krupnov and Skvortsov (1965), indicated that the biharmonic oscillation observed by Barchukov et al. was probably due to the operation of the maser resonator in high order mode (TEM_{101} or higher). However, Smart (1973) surmised that the maser of Barchukov et al. actually oscillated in the TEM_{001} mode (the lowest order cavity mode). Barchukov et al. indicated that another mode (presumably the TEM_{101}), which had a quality factor of 1000 and frequency separation of 20 MHz from the first, was also present in the cavity. This mode then overlapped with the oscillation frequency of the maser so that some of the oscillation field must have coupled to it.

In a similar experiment by Lainé et al. (1976), a d.c. voltage was applied across the open resonator in the range 0 - 15 Volt, and biharmonic oscillation obtained at frequencies ranging from 250 to 750 Hz (see Section 3.6 for Stark splitting). These showed a similarity to the first part of the Barchukov et al. results. Therefore, it is seen that earlier experimental results were somewhat confused.

In the present experiment (which is a continuation of the work of the Sections 3.8 and 4.3), the open resonator is definitely operated with the TEM_{101} mode (two maxima of electromagnetic field along the molecular beam path). As is noted in Section 4.3, beats on the I.F. bandpass response appeared when the maser system oscillated on the two components of the split line ($J=K=2$ and 3). These beats are shown in Fig. 4.7a, and examination of these in the zero sweep mode of detection show them to be sinusoidal with a frequency of 7.5 kHz (Fig. 4.7b). The state separator threshold voltage for this beat signal is 9.5 kV at a nozzle pressure 200 torr. An analogue frequency meter

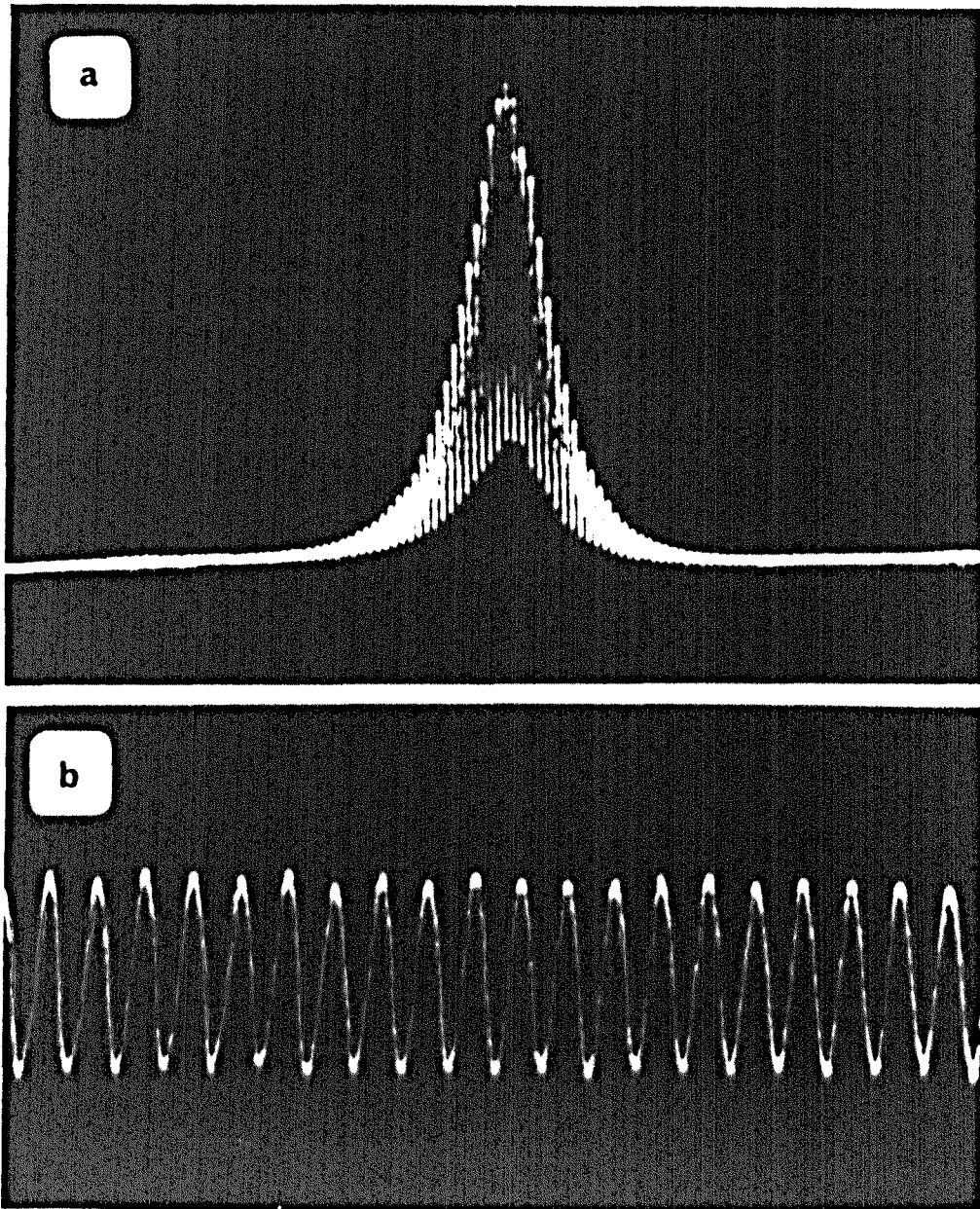


Fig. 4.7 BIHARMONIC OSCILLATION OF THE CENTRAL LINE OF
THE $J=K=2$ INVERSION TRANSITION OF AMMONIA
DISPLAYED IN THE I.F. BANDPASS MODE. BEAT
FREQUENCY 7.5 kHz

(a) WITH SWEEP

(b) WITH ZERO SWEEP

is used for the beat frequency measurement.

An examination of the beat frequency with various maser parameters shows that:

- (a) there was no effect due to the local oscillator power; the beat occurred at all levels;
- (b) no effect was detected by varying the nozzle pressure;
- (c) the beat frequency was strongly affected by the cavity tuning.

It is clear from Section 3.8 that the two components of the split line are observed to have equal amplitude in a spectroscopic mode of display, when the cavity is tuned to the precise transition frequency (Fig. 3.23b). In this case, the beat frequency observed is 7.5 kHz. If the cavity is tuned to the high frequency side (decrease of the mirror spacing) the beat frequency starts at 7.5 kHz and steadily decreases until they disappear at frequency ~ 1.5 kHz (18 kV threshold state separator voltage, Fig. 4.8). The process of cavity detuning during the investigation may well affect the spatial extent of the TEM_{101} mode via a distortion of the microwave amplitude distribution leading to a change in the separation of the two maxima of electromagnetic field in the cavity. This can come about via a deviation of the mirrors from parallelism. According to Krupnov and Skvortsov (1965), imperfect parallelism of the mirrors does not seriously affect the mode and the quality factor of the cavity. However, the position of the field maximum is shifted to correspond with the largest mirror separation. This also affects the coupling, because the microwave field distribution within the cavity changes the location where maximum energy is transferred by molecules to the field when the cavity is used in a beam-type maser. This in turn causes variations in the Doppler frequency shift due to the existence of microwave energy flow from the site of molecular emission to the coupling hole.

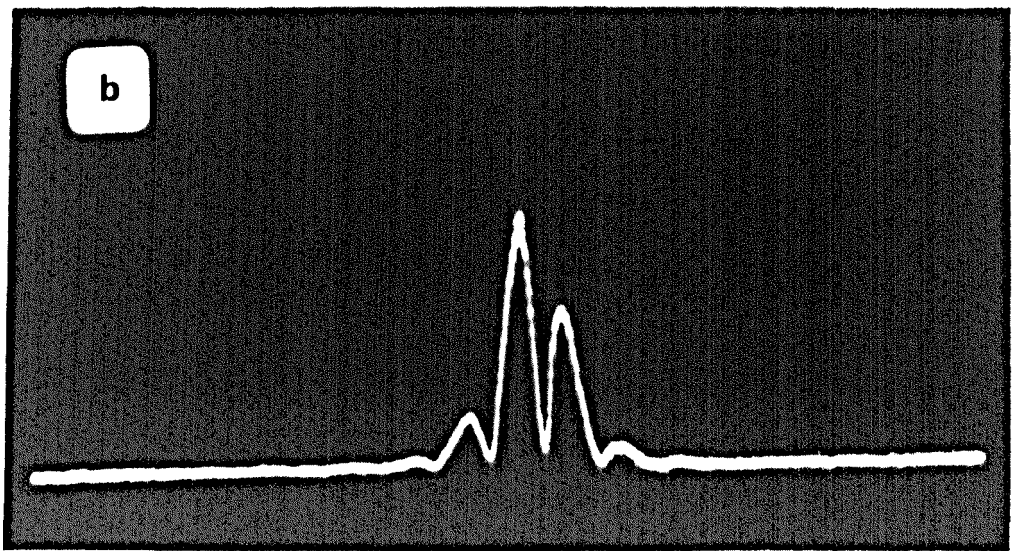
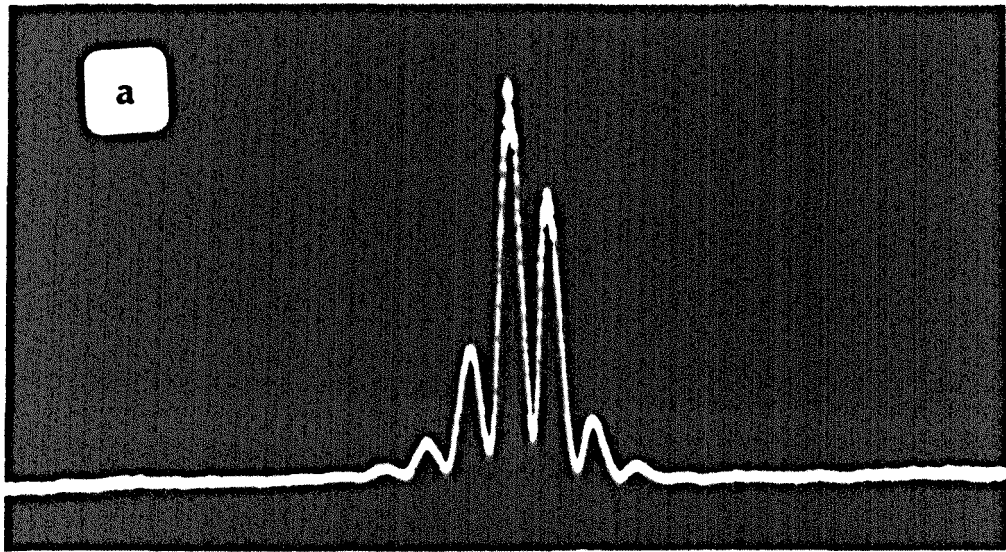


Fig. 4.8 BIHARMONIC OSCILLATION OF THE CENTRAL LINE OF
 THE $J=K=2$ INVERSION TRANSITION OF AMMONIA
 (a) BEAT FREQUENCY 2.5 kHz
 (b) BEAT FREQUENCY 1.5 kHz



Fig. 4.9 THE $J=K=2$ INVERSION TRANSITION OF AMMONIA

Fig. 4.9 shows the spectroscopic mode of display when the cavity is detuned from the molecular resonance frequency, showing a line splitting with components of unequal amplitude. It is when oscillation based on these two components is obtained that a beat frequency in the region between 7.5 to 1.5 kHz results.

Further experiments on self-modulation phenomena with this maser oscillator operated with the ammonia lines $J=K=2,3$ and with the TEM_{001} cavity mode, are possible using a Stark or Zeeman field. The results obtained will now be briefly summarised.

- (a) Self-modulation with all values of the Stark field employed were not observed.
- (b) With a uniform Zeeman field applied in a direction perpendicular to the plane of the mirrors of the maser cavity ($\Delta M = \pm 1$ transitions), beats were observed of similar waveform to those shown in Fig. 4.7 (sinusoidal beats).
- (c) With a further increase in Zeeman field and careful adjustment of the experimental parameters, such as, state separator voltage, nozzle pressure and microwave bridge setting, multiple oscillations are observed similar to those observed by Lainé and Truman (1977a).

In the latter case oscillation was based on the two components $2, \frac{5}{2} \rightarrow 2, \frac{5}{2}$ and $2, \frac{3}{2} \rightarrow 2, \frac{3}{2}$ (see Section 3.3) of the ammonia inversion line $J=K=1$. When the weaker main line component $2, \frac{3}{2} \rightarrow 2, \frac{3}{2}$ oscillated as a result of an increase in the state separator voltage to a value just above the oscillation threshold, beats appeared on the I.F. band-pass response. These beats were sinusoidal with low level of local oscillator power. At higher level of local oscillator power, multiple oscillations occurred as shown in Fig. 4.10.

In the present work the multiple oscillations were highly unstable and were therefore not pursued in further detail.

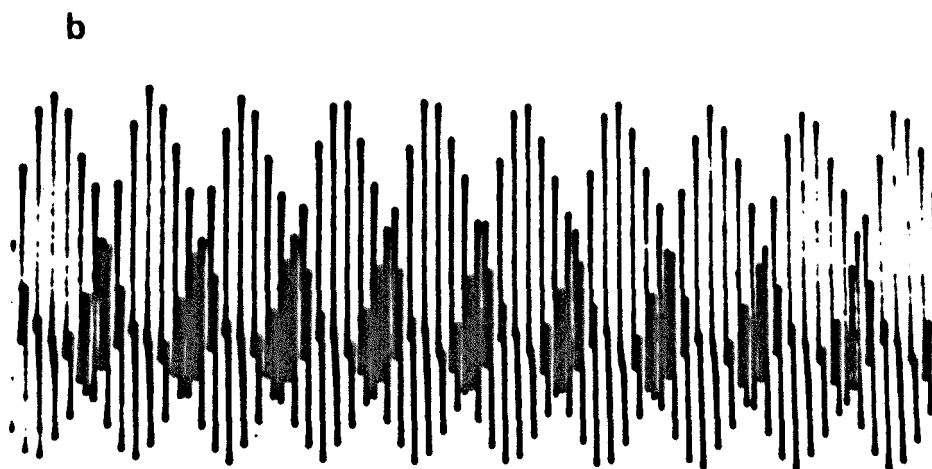
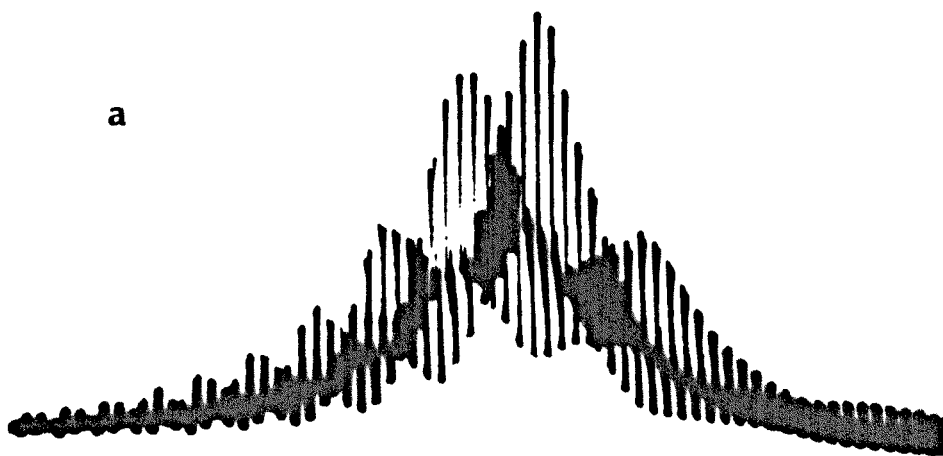


Fig. 4.10 MULTIPLE OSCILLATION DISPLAYED IN THE
I.F. BANDPASS MODE OF THE CENTRAL LINE
OF THE $J=K=1$ INVERSION TRANSITION OF
AMMONIA

(a) WITH SWEEP

(b) WITH ZERO SWEEP

4.5 The Experimental Investigation of the Onset of Oscillation

The mode of display used in this section employs the detection technique which has been described in Section 2.2 and consists of providing a frequency swept stimulating signal to provide a spectroscopic display. The onset of maser oscillation is detected by the appearance of a beat signal of varying frequency, and which goes through zero beat frequency when the external signal is instantaneously at the maser oscillation frequency.

A reduction in the oscillation amplitude at the main line frequency is seen when the signal is swept across the quadrupole satellite frequencies. The quadrupole transitions occur between energy levels which are involved in the main line transitions, and the change in populations of these energy levels induced by the external signal, is detected by a reduction in the main line oscillation amplitude (Shimoda and Wang, 1955). This mode of quenching by population depletion involves excitation at two quite different frequencies.

It is also possible to quench the oscillation by injection of a signal within the linewidth of the maser signal (Lainé, 1967). The external signal is first kept at a low level of power, so that the maser can oscillate freely. At a somewhat higher signal, which is sufficiently strong to induce downward transitions at a rate which cannot be maintained by the following active molecules to sustain maser oscillation, a beat signal between the injected signal and the free maser oscillation appears on either side of the stimulated emission line which now takes the place of the beats in the vicinity of the centre of the molecular resonance.

During the experimental investigation of transient effects by Bardo (1969), the starting time of the oscillation was observed to jitter on the oscilloscope trace, relative to the centre of the

molecular resonance. It was clear that the oscillation was initiated by noise and the point of time at which the oscillation appeared above the noise level of the receiver varied slightly between successive 50 Hz repetitive sweeps.

In this present work, similar results were obtained but with the additional unexpected feature of greatly improved oscillation amplitude stability following an initial period of oscillation growth. This effect was not present in the experiments of Bardo, where a closed resonator was used.

The molecular beam maser system, which has been described in Chapter Two, was set up on the $J=K=3$ inversion transition, and the cavity tuned to the TEM_{001} mode. The emission line that supports oscillation is flanked on both upper and lower frequency sides by magnetic satellites (Fig. 3.7) that are weak relative to the main unresolved composite main line. These satellites cluster over a spectral region of roughly $\pm(50$ to $82)$ kHz (Kukolich, 1967) relative to the emission line centre frequency ν_0 and share both upper and lower energy levels with the oscillating composite main line.

When an external microwave signal E_s of variable frequency ν_s , which is strong relative to the molecular beam maser oscillation signal E_{osc} of frequency ν_{osc} , is scanned through the frequencies of the main line and its magnetic satellites and beyond, the normal beat frequency pattern between E_s and E_{osc} is modified by the combination of those effects noted earlier in this section (observed by Shimoda et al., 1955, Lainé, 1967). The microwave bridge is set at a power level such that the onset of oscillation occurs immediately after scanning through the lower frequency magnetic satellite lines, i.e. the onset of oscillation follows a period of "molecular robbing". In this case the oscillation build-up process may be observed without confusion with magnetic satellite lines.

The ensuing oscillation growth in the maser cavity (tuned to ν_0) may then build up from either noise or a coherent signal at, or near, ν_{osc} . It has been found that under conditions of rapid frequency scanning of an external signal through the main line resonance the molecules within the molecular beam maser cavity are strongly excited to a coherent superposition quantum state (molecular ringing), which decays exponentially with time (Lainé, 1966). This transient signal of frequency ν_0 , together with the frequency-swept exciting signal, also forces maser oscillation. These two forced oscillations then beat together to produce wiggles (see Section 3.9). The onset of free (but phase-locked) maser oscillation is determined by the tail end of the ringing signal and the usual oscillation starting-time jitter may thereby be eliminated.

From this experimental investigation it is noticed that not only does the starting-time jitter, but in addition the amplitude of the settling transient is highly unstable in comparison with the previous results with a closed resonator. This is due to the fact that with the disc resonator maser the linearly polarised electric field vector direction associated with maser oscillation, is not well defined (Lainé et al., 1976), while the closed cavity (TM_{010} circular mode) is well defined in the axial direction of the linearly polarised microwave electric field.

This particular system may be described as "self-primed". The elimination of starting-time jitter is analogous to injection priming of magnetrons (Micronotes, 1966), for which the priming signal was derived from an external microwave source. However, when the rapid-scan experiment is repeated, the effect of self priming is rather dramatic, since it is found that not only is the starting-time jitter eliminated, but the initial portion of the oscillation settling is stabilised in amplitude.

It is evident, therefore, that in this type of maser a frequency scan with an input signal of well defined linear polarisation determines the direction of polarisation of the ringing signal, and thus the direction of electric field vector associated with the initial growth of oscillation as a direct result of priming. It must be pointed out, however, that although the initial amplitude of maser oscillation is amplitude stabilised, a period of decreased amplitude stability has often been observed before steady-state conditions are finally reached, which is taken to be indicative of the transient nature of amplitude stabilisation by what is effectively a pulsed priming signal.

Fig. 4.11 shows the oscillation priming and stabilisation of the oscillation amplitude settling transient by an internally generated molecular ringing signal. The letters on the figure indicate:

- A - centre frequency ν_0 of the saturated emission line ($J=K=3$).
- B - wiggle beats between input signal E_s and ringing signal at ν_0 .
- C - lower frequency magnetic satellite lines of centre frequency 66 kHz (relative to ν_0).
- D - peak of aperiodic oscillation amplitude settling transient.
- E - point of onset of forced oscillation.
- F - onset of oscillation primed by ringing signal.

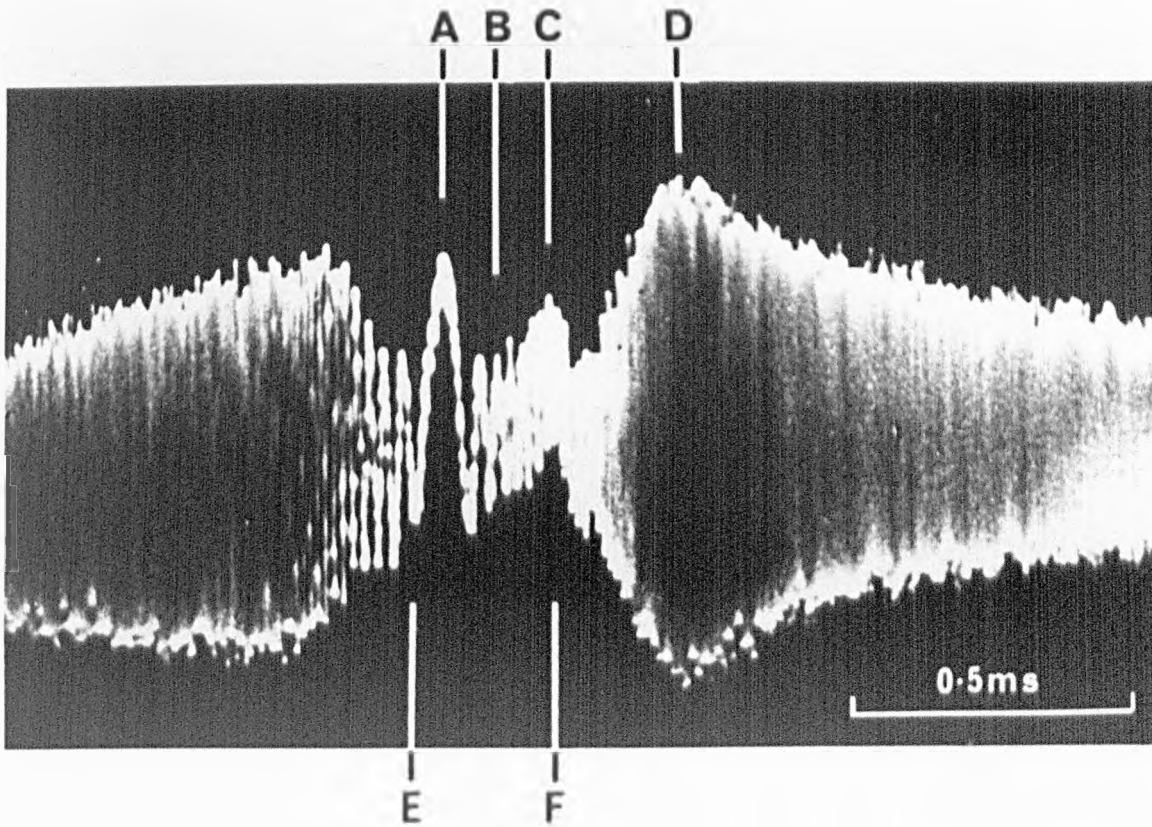


FIG. 4.11 OSCILLOSCOPE TRACE SHOWING
OSCILLATION PRIMING

CHAPTER FIVE

SUGGESTIONS FOR FURTHER WORK

A molecular beam maser employing a Fabry-Perot cavity is normally operated with a mirror separation of $\lambda/2$ or λ . This is in contrast to the use of the cavity in a laser where the longitudinal mode order is very high. In the present work a separation of $\lambda/2$ is used through all the investigations. It should also permit work with λ separation, and perhaps with $3\lambda/2$ or more, when the plane of symmetry of the state separator is aligned with a nodal plane in the centre of the cavity, since two independent molecular beams are employed. Furthermore, the engineering difficulties of obtaining a high filling factor of a large cavity is largely overcome by the use of double independent molecular beams.

One particular aspect of the construction of the present cavity which requires some attention is the tuning mechanism employed. The observation of the low frequency beat down to 1.5 kHz (Section 4.4) which has been attributed to imperfect mirror parallelism, clearly indicates the need to provide mechanisms which permit an accurate and reproducible setting of the cavity.

Some interesting studies of open cavities with other than plane parallel mirrors have been carried out by other investigators. One such cavity which should prove ideal for use in molecular beam maser work is the flat-roof resonator (Yassin and Lainé, 1979). A feature of this resonator is that the radiation field is distributed over an axial region (with respect to the molecular beam) of narrow spatial extent, but which provides a desirably long interaction time of molecules with the cavity radiation field. This type of cavity,

operated in conjunction with a ring state separator, will permit the operation of an ammonia beam maser at higher levels of oscillation, because the ring state separator will of course produce a pencil-like molecular beam of small diameter.

The semi-open type of resonator of Legrand (1975) (Fig. 5.1) should prove an ideal Stark cell for $\Delta M = 0$ transitions (the electromagnetic field parallel to the Stark field). The number of $\Delta M = 0$ Stark components for the inversion transitions of ammonia are less than the $\Delta M = \pm 1$ transitions (see Section 3.7), which should make the weak-field Stark effect accessible to measurement. It is interesting to note at this point that a recent investigation with this resonator by Lainé and Campbell (1979) strongly suggests that this type of resonator should be useful for molecular beam maser spectroscopy work. In particular, this cavity would allow weak field Stark frequency shift measurements for the two components of the outer quadrupole at the low frequency side of the inversion line of ammonia $J=K=1$ (see Section 3.7) which is not possible with the disc resonator since only $\Delta M = \pm 1$ transitions are permitted. However, such measurements will need a klystron signal source with precise frequency control and measurement which was not available for the present work. Furthermore, a more detailed spectroscopic study should give a better understanding of the relations between the Stark components' intensities with respect to the direction of the d.c. field in the cavity and the polarity of the state separator electrodes as noted with this system (Section 3.7). This, with available known techniques and improved frequency control, should permit Stark effect studies to be completed.

The work described in Chapter Four has contributed to a better understanding of the behaviour of open cavity maser oscillators, and

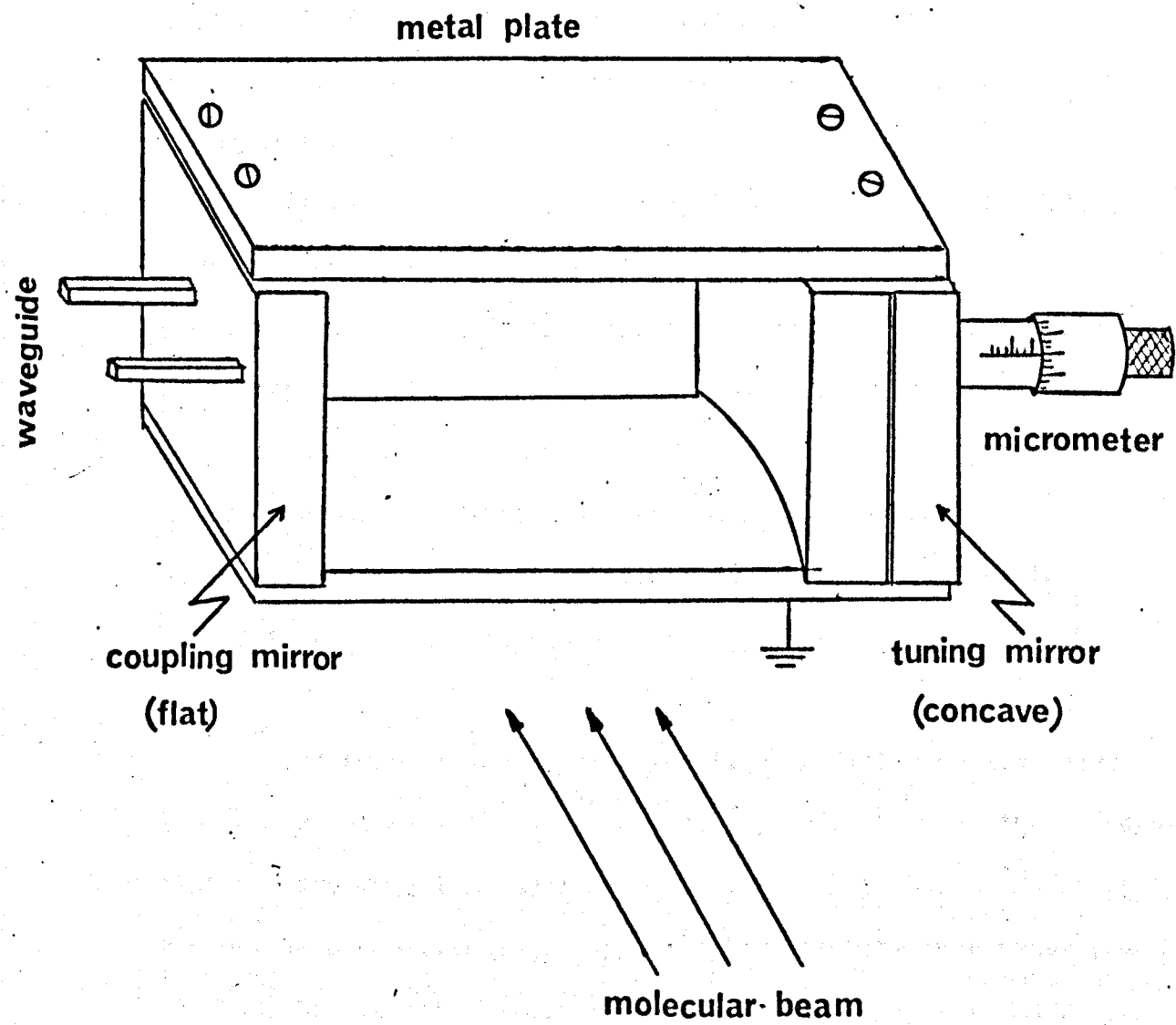


Fig.5.1 Semi-open cavity

a more satisfactory interpretation given for some of the previous results, which had been most confusing. However, the observation of a hysteresis phenomenon between two single frequency oscillations when using the TEM_{101} cavity mode (Section 4.3), suggest that a more detailed study is required with this system so that a detailed comparison can be made with previous observations of Becker (1965) who used the TM_{013} mode of a closed cylindrical cavity.

It is expected that biharmonic oscillation in the TEM_{001} cavity mode should be possible by using Stark field splitting, probably with a higher molecular beam flux with a single maximum of cavity radiation field along the beam axis. This conclusion is supported by the observation of multiple oscillations in an ammonia maser based on the $J=K=1$ line using a microwave Stark field (dynamic Stark effect, Lainé et al., 1977b). Furthermore, biharmonic oscillation has been realised in the present studies using the Zeeman effect.

The observation of high levels of oscillation amplitude in this maser system with the TEM_{101} cavity mode (Section 4.3), indicates that the maser system should also permit work in higher modes ($n > 2$), for which the longitudinal Doppler splitting will be greater than the 7.5 kHz reported here.

APPENDIX ONE

MEASUREMENT OF THE CAVITY QUALITY FACTOR

The loaded quality factor (Q_L) is usually determined by measuring the frequency separation (Δf) between the half-power points on the cavity response curve and using the relation

$$Q_L = \frac{f_o}{\Delta f} \quad \text{App. 1.1}$$

where f_o is the centre frequency of the response.

The microwave arrangement for this measurement is shown in Fig. 5.3. The klystron reflector voltage is swept with a 50 Hz sawtooth waveform, so that the cavity response observed by transmission of microwave power through the cavity, can be displayed on the oscilloscope. The relative frequency determinations are made by a frequency multiplier chain (Micro-Now model 101C), which is used to multiply a tunable crystal oscillator at 5 MHz up to 450 MHz, and then applied to a IN26A crystal (A). One of the harmonics of the 540 MHz signal mixes with klystron power at the same crystal (A), which acts as both multiplier and mixer. In this case, one side of the crystal (A) is fed from the multiplier chain, and the other leads to the input of the radio receiver (Type RA.117) tuned to pick up the beat frequency between the n^{th} -harmonic of the 450 MHz signal and the klystron. As the klystron frequency is swept, the output pip of the receiver is then displayed on the second trace of the twin-beam oscilloscope. By tuning the receiver the pip can be put on the half-power points on the cavity response curve. A measurement of the receiver tuning then gave the relative frequency of each point (F_1 and F_2), which are the only two frequencies required for the determination of Q_L , since

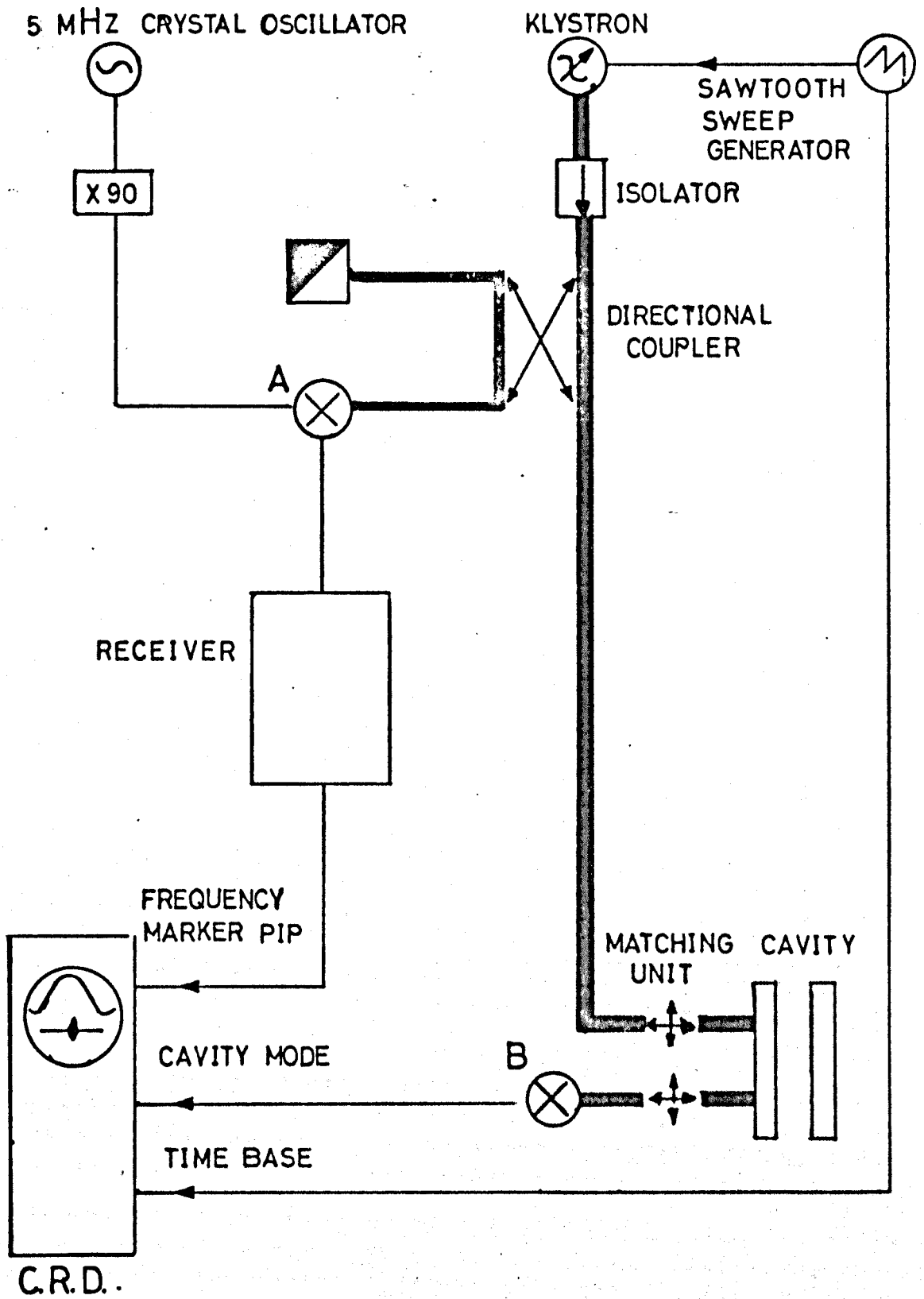


FIG. 5.3 MICROWAVE BRIDGE USED TO MEASURE CAVITY Q.

$$Q_L = \frac{F_1 + F_2}{2(F_2 - F_1)}$$

App. 1.2

The loaded quality factor of the parallel plate resonator, which is used in this thesis work, obtained by this method, is 6000 \pm 400.

BIHARMONIC OPERATION OF A MOLECULAR BEAM MASER EMPLOYING A QUASI-OPTICAL FLAT DISC RESONATOR

A.M. Al-Jumaily[†] and D.C. Lainé

Department of Physics, University of Keele, Keele, Staffordshire, ST5 5BG, U.K.

Abstract Although biharmonic oscillation of a molecular beam maser (MBM) oscillator employing a quasi-optical resonator of the flat disc type has been known for some time, it has not been clear whether this phenomenon had the same physical origin in all experiments reported to date. To clarify this problem, a new MBM has been operated employing a flat disc resonator, and two intense head-on beams of rotationally cooled ammonia gas. In particular, this MBM is found to oscillate on the $J=K=1, 2$ and 3 inversion lines of $^{14}\text{NH}_3$ with biharmonic operation on the last two of these for which the spectral line is known to be split by the longitudinal Doppler effect. These new results, taken with previous ones where line splitting was definitely not present, shows unequivocally that biharmonic oscillation in a flat disc resonator can have at least two different origins.

1. **Introduction.** The operation of a molecular beam maser (MBM) with a disc resonator was first reported by Barchukov *et al* (1963) using the $J=K=3$ inversion line of $^{14}\text{NH}_3$. The oscillation obtained with their maser system revealed an amplitude modulation whose origin was obscure. Subsequent studies of a similar MBM system by Lainé *et al* (1976) also revealed an amplitude modulation whose frequency could be varied from 200 to 800Hz by changes in the system parameters of E.H.T. gas flux, cavity tuning etc. Sometimes the modulation was highly non-sinusoidal. Furthermore, when a low voltage was applied across the cavity plates, the amplitude modulation frequency increased. For example, for an increase of voltage of 0 to 15V, the beat frequency rose from a typical value of 250 to 750Hz, the precise values depending on the prevailing experimental parameters. Similar results with Stark fields were obtained by Barchukov *et al* (1963), although the beat frequency reported in their experiment covered the wider range of 0.6 - 5.4kHz. Despite the difference in beat frequency in these two independent experiments, there were sufficient similarities in MBM behaviour to suggest the possibility of a common origin. The biharmonic oscillation in both experimental situations was tentatively interpreted by Lainé *et al* in terms of two independent circular polarizations which possessed different frequencies. However, Krupnov and Skvortsov (1964) surmised that the origin of the amplitude modulation in the experiment of Barchukov *et al* was due to simultaneous oscillation on both components of a Doppler split spectral line produced by molecules passing through two maxima of the cavity radiation field along the beam axis. This splitting may be understood as a result of the molecules in the beam interacting with both forward and backward travelling waves into which the standing wave field of the resonator may be decomposed. The frequency separation Δf between the maxima of the split line is given by $\Delta f = nv/L$, where n is the number of radiation half-wavelengths along the cavity axis, v the most probable molecular velocity, and L the resonator length (Bonanomi *et al* 1957).

In the experiments of Lainé *et al*, this split line interpretation could not possibly apply since the cavity mode was carefully checked and found to possess only a single maximum value of microwave electric field across any diameter of the discs. Therefore, the question of the results of Barchukov *et al* owing their origin to a Doppler split line or not remained unanswered in the absence of detailed information about their cavity mode. However, the occurrence of such an amplitude modulation effect as proposed by Krupnov and Skvortsov is not at all obvious for an open resonator for at least two reasons. Firstly, in experiments with MBMs operated with closed resonators in a higher order mode,

[†]On study leave from Physics Department, College of Education, University of Baghdad, Iraq.

(TM_{012} , etc.) there is a tendency for mutual phase locking of the two oscillations to occur. Which of these oscillations is dominant depends essentially on cavity tuning. Clearly, such a locking effect is also a definite possibility in an open resonator MBM, which could totally preclude biharmonic oscillation. However, Becker (1966) has observed biharmonic oscillation with a closed resonator operated just above the oscillation threshold. Clearly, suitable conditions may also exist for biharmonic oscillation with an open resonator. Secondly, to sustain oscillation at two different frequencies in an open resonator the MBM will require a larger beam flux than is necessary to support a single oscillation. Whether such an increase in flux can be achieved experimentally is unknown. In an attempt to settle some of these issues an experimental system has been constructed in which the relevant experimental parameters could be carefully monitored and the MBM operated at a sufficiently high beam flux to secure biharmonic operation.

2. Experimental System. The lay-out of the MBM system is shown in Fig. 1.

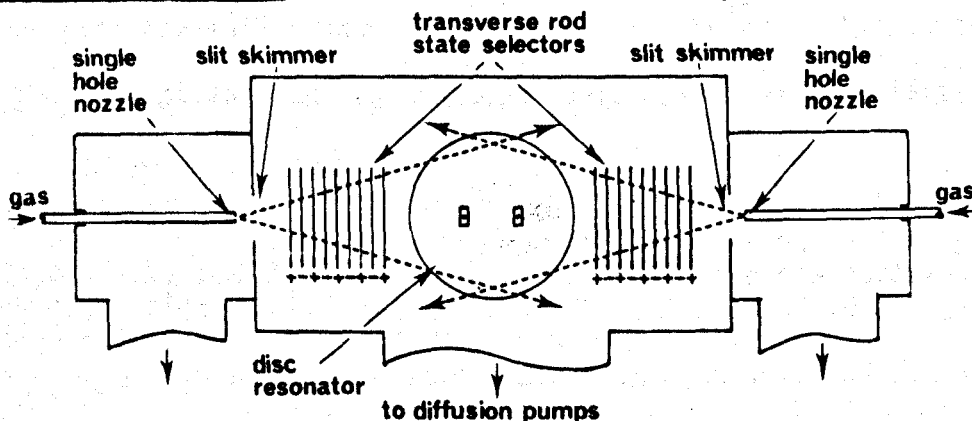


Fig. 1 : Principal components of double beam maser.

The MBM was operated with a disc resonator for which an enhanced molecular flux was provided by the use of two head-on beams. The vacuum system consisted of three chambers, two of which housed independent gas sources and a central chamber which housed the two state selectors and maser cavity. Details of the nozzle system, the state selectors and cavity are briefly given as follows.

(i) The nozzle. The two nozzle systems which produced oppositely directed beams were identical. Each consisted of a single hole of 0.09mm diameter drilled through brass foil of thickness 0.10mm. The optimum gas pressure for operation with a minimum value of EHT for oscillation depended on the spectral line used, but typically lay in the region of 200 to 600 torr with ammonia.

(ii) The state selectors. The two flat beam state selectors were made with two near-parallel ladder-like sets of electrodes placed symmetrically on either side of the molecular beam axis. The length of the electrodes was 86mm and 22 of these were earthed and intermeshed with 21 of opposite polarity. The electrode wire diameter was 1.6mm and adjacent electrodes were separated by 3.15mm, centre to centre. The overall effective focusing length was 134.1mm. The double ladder arrangement was actually tapered to capture a larger solid angle of molecules than would otherwise be possible with parallel ladders. At the focuser entrance the ladder separation was 0.8mm and at the exit 4.8mm. The maximum voltage applied to adjacent electrodes was 30kV. The electrodes were made of mild steel, and chrome plated to prevent tarnishing. The electrode arrays were assembled with machined teflon supports at each end.

(iii) The resonator. The open resonator was of the disc type, and was operated with $\lambda/2$ spacing between plates in either the TEM_{001} or TEM_{101} mode to give a Q value of 6000. The resonator plates of 225mm diameter were made of electrolytic quality copper, 12mm thick to ensure a stable flatness. The coupling holes were placed on a cavity diameter parallel to the molecular beam axis. These holes were of 26mm diameter, of wall thickness 0.63mm and separated by 112.5mm, giving good coupling to both TEM_{001} and TEM_{101} modes. The cavity

could be externally tuned mechanically to the $J=K=1,2$ and 3 lines of ammonia in either of the two modes studied. The cavity was thermally stabilized by an electrical sensor and control system. The waveguide polarization was chosen to couple to a cavity microwave electric field which lay along the molecular beam axis.

The superheterodyne scheme for detection of stimulated emission or oscillation was of the standard type, using a single klystron, (Laine, 1975).

3. Experimental results and discussion. When the cavity was adjusted for TEM₀₀₁, mode operation, with a single maximum of microwave field along the diameter containing the two coupling holes, a normal spectrum was obtained with ammonia (¹⁴NH₃) as the maser medium, with 4kHz resolution. Under these conditions oscillation was obtained using the $J=K=1,2$ and 3 lines. The optimum conditions of nozzle pressure for the lowest value of EHT to reach an oscillation threshold were for $J=K=1$: 200 torr 6.0kV: $J=K=2$: 300 torr, 5.0kV, $J=K=3$: 600 torr, 4.9kV. Operation with the cavity mode TEM₁₀₁ however, caused all the spectral lines to be split by the Doppler effect. Below the oscillation threshold, rapid passage of the stimulating microwave signal through both components of the split line, produced 'beating of beats' with a beat period $\Delta\nu^{-1}$, where $\Delta\nu$ is the frequency separation between the two split line components. The frequency of the 'beating of beats' was measured to be 7.0kHz. Below the oscillation threshold, these beats decay with time on account of (i) the finite transverse relaxation time (T_2) for the resonant molecular system and (ii) the limited bandpass of the I.F. amplifier and associated detection system. A typical trace is shown in Fig. 2a. As the threshold condition for maser oscillation is approached these beats persist for a longer time, until at or above the threshold of oscillation they occur continuously (Fig. 2b). Under these conditions, it is convenient to turn off the stimulating signal and monitor the maser oscillation in the usual I.F. amplifier band-pass display mode. Biharmonic oscillation with the Doppler split line was obtained with both the $J=K=2$ and 3 inversion lines but not with $J=K=1$, which is the weakest of the three transitions. In the case of the $J=K=2$ line, when a single oscillation set in, for example, at a gas pressure of 200 torr and 7.0kV EHT applied to the state selector, biharmonic oscillation on the split line occurred at 9.0kV. Results for the $J=K=3$ line were similar. Biharmonic operation on the $J=K=2$ line is shown in Fig. 3. It was found that for biharmonic oscillation on the split lines, the cavity had to be tuned slightly above the centre frequency of the unsplit spectrum. The biharmonic frequency of 7.5kHz varied only slightly with changes of the nozzle gas pressure and EHT, but rather drastically with cavity tuning. A beat frequency down to a value as low as 1.5kHz was observed as the cavity was progressively detuned.

Whilst the beat frequency of 7.0 to 7.5kHz follows from the expected line splitting, $\Delta\nu \approx nv/L$, taking $v \approx 7.0 \times 10^2 \text{ ms}^{-1}$, the lower beat frequency has not yet been accounted for in a satisfactory way. A beat frequency value of 7.5kHz obtained for the $J=K=3$ inversion line of ¹⁴NH₃ also possessed these anomalous low frequency characteristics. This phenomenon could possibly result from non-parallelism of the cavity plates with detuning.

It has been noted that a small detuning of the cavity from the centre frequency of the split line was necessary to observe biharmonic oscillation, presumably to break a mutual phase-lock condition. Moreover, oscillation amplitude jump and hysteresis effects have also been observed in conjunction with cavity detuning. Such effects were more prominent with the $J=K=3$ line than with $J=K=2$ and biharmonic oscillation was more difficult to observe with $J=K=3$ than with $J=K=2$. These results for a flat disc resonator indicate that a weak mutual interaction exists between oscillating components of the split lines, (with a larger coupling for the $J=K=3$ than for the $J=K=2$), in contrast to the strong coupling which appears to exist in closed cavity resonators which appear to preclude the observation of biharmonic oscillation in all but the most rare circumstances (Becker 1965).

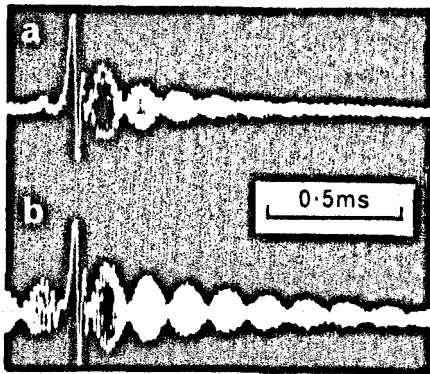


Fig. 2 : 'Beating of beats' following rapid passage of stimulating signal through split $J=K=2$ inversion line of $^{14}\text{NH}_3$ (a) below, (b) above oscillation threshold.

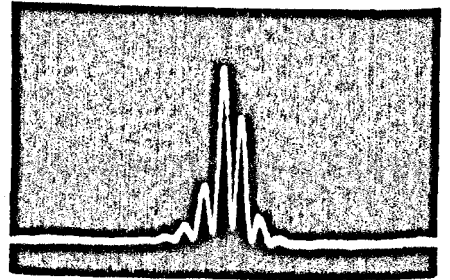


Fig. 3 : Biharmonic oscillation on the Doppler split $J=K=2$ inversion line of $^{14}\text{NH}_3$ observed in I.F. bandpass mode. Modulation frequency $\sim 2.5\text{kHz}$.

Conclusion. Results have been presented which clearly identify biharmonic oscillation in a disc type of open resonator with maser lines split by the longitudinal Doppler effect. Thus, the biharmonic oscillation as observed by Barchukov *et al* (1963) can probably be attributed to the same cause, as proposed by Krupnov and Skvortsov (1965). However, it appears that the form of biharmonic oscillation reported here owes its origin to a different physical cause to that previously obtained by Lainé, *et al* (1976), where a single maximum of microwave electric field along the molecular beam axis was used. However, not all the experimental data is yet understood. Thus further experiments need to be carried out, especially in conjunction with amplitude jumps and an hysteresis phenomenon which are both in evidence when the cavity is tuned across the oscillation frequency.

4. References

- Barchukov, A.I., Prokhorov, A.M. and Savranskii, V.V., (1963), *Radio Engng. Electron. Phys.*, 8, 1564.
- Becker, G., (1966), *Z. angew. Phys.*, 20, 398.
- Bonanomi, J., de Prins, J., *et al*, (1957), *Arch. Sci.* 10, fasc. spec., 187.
- Krupnov, A.F. and Skvortsov, V.A., (1965), *Sov. Phys. - JETP*, 20, 1079.
- Lainé, D.C., (1975), *Advances in Electronics and Electron Physics*, 39, 183.
- Lainé, D.C., Smart, G.D.S. and Corb, A.I., (1976), *Ann. Scient. Univ. Clermont (France)*, No. 59, Phys. 16e Fasc., 37.

REFERENCES

- Al-Amiedy, D.H.H. and Lainé, D.C. (1978) *Phys. Lett.*, 66A, 94.
- Anderson, J.B. and Fenn, J.B. (1965) *Phys. Fluids*, 8, 780.
- Barchukov, A.I. and Prokhorov, A.M. (1961) *Trans. 10th Ampère Soc. Colloq.*, 14, 494.
- Barchukov, A.I., Prokhorov, A.M. and Savranskii, V.V. (1963) *Radio Eng. Electron. Phys. (USSR)*, 8, 385.
- Barchukov, A.I., Prokhorov, A.M. and Savranskii, V.V. (1964) *Quantum Electronics III*, ed. Grivet, P. and Bloembergen, N. (Columbia Univ.).
- Bardo, W.S. (1969) Ph.D. Thesis, University of Keele.
- Basov, N.G. and Oraevskii, A.N. (1958) *Sov. Phys. JETP*, 10, 761.
- Basov, N.G. Oraevskii, A.N., Strakhovskii, G.M. and Tatarenkov, V.M. (1964) *Sov. Phys. JETP*, 18, 1211.
- Basov, N.G. and Prokhorov, A.M. (1954) *Zh. Eksp. Teor. Fiz.*, 27, 431.
- Basov, N.G. and Zeuv, V.S. (1961) *Instrum. Exp. Tech.*, 1, 122.
- Becker, G. (1963) *Z. Angew. Phys.*, 15, 13.
- Becker, G. (1966) *Z. Angew. Phys.*, 20, 398.
- Bloembergen, N., Purcell, E.M. and Pound, R.V. (1948) *Phys. Rev.*, 73, 679.
- Bonanomi, J. and Herrmann, J. (1956) *Helv. Phys. Acta.*, 29, 225.
- Campargue, R. (1964) *Rev. Sci. Instrum.*, 35, 111.
- Checcacci, P.F. and Scheggi, A.M. (1956) *Appl. Optics*, 4, 1529.
- Coles, D.K. and Good, W.E. (1946) *Phys. Rev.*, 70, 979.
- Dakin, T.W., Good, W.E. and Coles, D.K. (1946) *Phys. Rev.*, 70, 560.
- Deckers, J. and Fenn, J.B. (1963) *Rev. Sci. Instrum.*, 34, 96.
- Delucia, F.C. (1969) Ph.D. Thesis, Duke University.
- Dicke, R.H. (1958) *Off. Gaz.*, 734, 526.
- Dugdale, D.E. (1976) University of Keele (private communication).
- Dymanus, A. (1976) *Rev. Sci. Phys. Chem. Ser. Two*, 3 ed. Ramsey, D.A. (Butterworths, London).

- Einstein, A. (1917) Phys. Z. 18, 121.
- Ferguson, R.C. and Wilson, E.B. (1953) Phys. Rev., 90, 338.
- Fluendy, M.A.D. and Lawley, K.P. (1973) "Chemical Applications of Molecular Beam Scattering" (Chapman & Hall, London).
- Fox, A.G. and Li, T. (1960) Bell Syst. Tech. J., 40, 453.
- Gabillard, R.C.R. (1951) Acad. Sci. Paris, 232, 1551.
- Good, W.E. (1946) Phys. Rev., 70, 213.
- Gordon, J.P. (1955) Phys. Rev., 99, 1253.
- Gordon, J.P., Zeiger, H.J. and Townes, C.H. (1954) Phys. Rev., 95, 282.
- Gunther-Mohr, G.R., Townes, C.H. and Van Vleck, J.H. (1954) Phys. Rev., 94, 1191.
- Gunther-Mohr, G.R., White, R.L., Schawlow, A.L., Good, W.E. and Coles, D.K. (1954) Phys. Rev., 94, 1184.
- Harvey, A.F. (1963) "Microwave Engineering" (Academic Press, London).
- Helmer, J.C., Jacobus, F.B. and Sturrock, P.A. (1960) J. Appl. Phys., 31, 458.
- Herzberg, G. (1945) "Infrared and Raman Spectroscopy" (D. van Nostrand Co. Inc., New York).
- Hope, L. (1978) M.Sc. Thesis, University of Keele.
- James, W., Simmons, . and Gordy, W. (1948) Phys. Rev., 73, 713.
- Jauch, J.M. (1947) Phys. Rev., 72, 715.
- Johnson, T.H. (1928) Phys. Rev., 31, 103.
- Kantrowitz, A. and Grey, J. (1951) Rev. Sci. Instr., 22, 328.
- Kistiakowsky, G.B. and Slichter, W.P. (1951) Rev. Sci. Instr., 22, 333.
- Krupnov, A.F. (1959) Izv. Vyssh. Ucheb Zaved Radiofiz., 2, 658.
- Krupnov, A.F. and Skvortsov, V.A. (1964a) Izv. Vyssh. Ucheb Zaved Radiofiz., 7, 991.
- Krupnov, A.F. and Skvortsov, V.A. (1964b) English translation (1965) Sov. Phys. JETP, 20, 1079.
- Krupnov, A.F. and Skvortsov, V.A. (1964c) Sov. Phys. JETP, 18, 1426.

- Kukolich, S.G. (1967) Phys. Rev., 156, 83.
- Lainé, D.C. (1966) Phys. Lett., 23, 557.
- Lainé, D.C. (1967) Electronics Lett., 3, 454.
- Lainé, D.C. (1975) "Advances in Molecular Beam Masers" in 'Advances in Electronics and Electron Physics' (ed. Maton, L.), 39, 183 (Academic Press, New York, San Francisco).
- Lainé, D.C. and Campbell, D.R. (1979), University of Keele (private communication).
- Lainé, D.C., Kakati, D., Uppal, G.S., Smart, G.D.S. and Bardo, W.S. (1969) Phys. Lett., 29A, 376.
- Lainé, D.C. and Smart, G.D.S. (1971) J. Phys. D, 4, L23.
- Lainé, D.C., Smart, G.D.S. and Corb, A.I. (1976) Annales Scientifiques de l'Université de Clermont, No. 59, Physique 16e Fasc., 37.
- Lainé, D.C. and Sweeting, R.C. (1971a) Phys. Lett., 34A, 144.
- Lainé, D.C. and Sweeting, R.C. (1971b) Phys. Lett., 34A, 391.
- Lainé, D.C. and Truman, M.J. (1977a) Annales Scientifiques de l'Université de Clermont, No. 64, Physique 17e Fasc., 129.
- Lainé, D.C. and Truman, M.J. (1977b) Phys. Lett., 62A, 322.
- Legrand, J. (1975) Annales Scientifiques de l'Université de Clermont, (France), No. 59, Physique 16e Fasc., 198.
- Low, W. and Townes, C.H. (1949) Phys. Rev., 76, 1295.
- Marcuse, D. (1962) IRE Trans. Instrum., I-11, 187.
- Maroof, A.K.H. (1975) Ph.D. Thesis, University of Keele.
- Maroof, A.K.H. and Lainé, D.C. (1974) J. Phys. E, 7, 409.
- Maroof, A.K.H. and Lainé, D.C. (1976) J. Phys. D, 9, 175.
- Mednikov, O.I. and Parygin, V.H. (1963) Radio Eng. Electron. Phys., 8, 685.
- Micronotes (1966) "Injection Priming of Magnetrons", Microwave Associates Inc., 4, 2.
- Oraevskii, A.N. (1964) "Molecular Generators" (Nauka, Moscow).
- Oraevskii, A.N. (1967) Sov. Phys. Uspekhi, 10, 45.
- Prokhorov, A.M. (1958) Sov. Phys. JETP, 34, 1140.

- Rodebush, W.H. (1931) Rev. Mod. Phys., 3, 392.
- Schawlow, A.L. and Townes, C.H. (1958) Phys. Rev., 112, 1940.
- Shimizu, T. and Shimoda, K. (1961) J. Phys. Soc. Japan, 16, 777.
- Shimoda, K. and Wang, T.C. (1955) Rev. Sci. Instrum., 26, 1148.
- Shimoda, K., Wang, T.C. and Townes, C.H. (1956) Phys. Rev., 102, 1308.
- Skobel'tsyn, D.V. (1964) "Soviet Maser Research" (Consultants Bureau, New York).
- Smart, G.D.S. (1973) Ph.D. Thesis, University of Keele.
- Strakhovskii, G.M., Tatarenkov, V.M. and Shumyatskii, P.S. (1966) Radio Eng. Electron. Phys., 11, 438.
- Takami, M. and Shimizu, T. (1966) J. Phys. Soc. Japan, 21, 973.
- Townes, C.H. and Schawlow, A.L. (1955) "Microwave Spectroscopy" (McGraw-Hill, New York).
- Truman, M.J. and Laine, D.C. (1976) J. Phys. D. 9, L175.
- Weber, J. (1953) Trans. IRE., PGED-3, 1.
- Yassin, G. and Lainé, D.C. (1979) Actes de "Optique hertzienne et diélectriques", Lille, June 27-30.